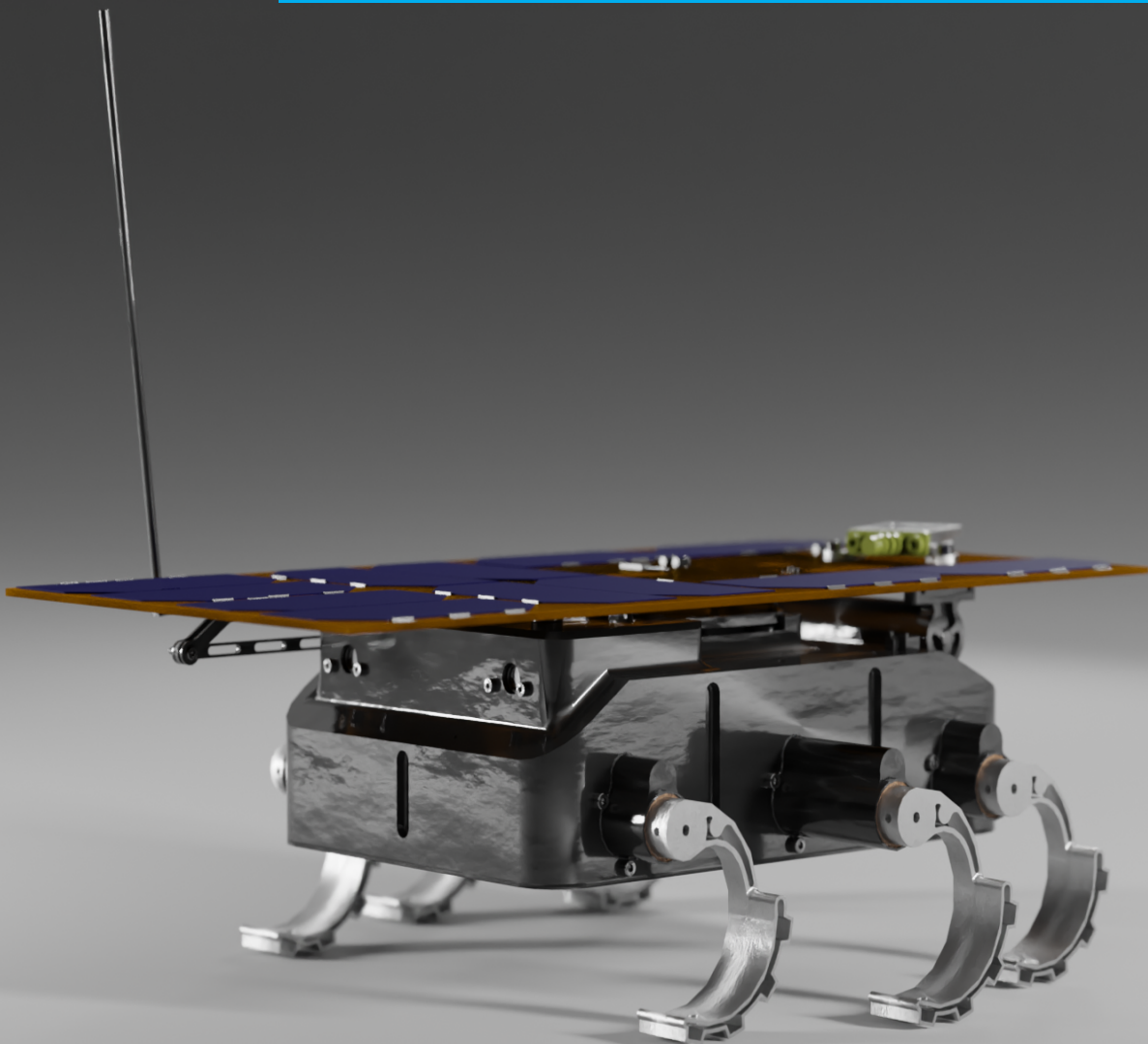


## Department of Precision and Microsystems Engineering

### Improving the Traction of a Legged Lunar Rover: A Biomimetic Approach

E.D.C Solot

Report no : 2022.066  
Coach : Dr.ir. J.F.L. Goosen  
Professor : Dr.ir. J.F.L. Goosen  
Specialisation : Engineering Mechanics  
Type of report : Master Thesis  
Date : 12 October 2022



# Preface

Biomimicry has been a passion of mine since the first moment I ever heard about it. When it came time for me to choose a Master's thesis topic, I desperately wanted to find a way to incorporate it into my project. The Lunar Zebro provided the perfect opportunity to do this. During the process of completing this Master's thesis, I explored new ways of increasing the traction of c-shaped legs on granular and rocky terrain and I discovered solutions that have the potential to change the way these legs are designed in the future. This thesis also highlights the lack of knowledge surrounding this leg and how traction can be increased on the leg. Hopefully, this report can provide a stepping stone to a great many new discoveries.

The process of completing this Master's thesis has been a challenge and an adventure and I am thankful for the opportunity my parents have given me to be able to complete this journey and for their constant support. I am incredibly grateful to Joris, Ines, Ana and Justin for making this year so fun and for being there to celebrate the victories and for their support during the tough times. I would especially like to thank my Supervisor Dr.ir. Hans Goosen, for helping me find a way to incorporate Biomimicry into my thesis, and also for his continuous support and guidance through the process of my Master's thesis and for providing me with valuable feedback when needed. I would also like to thank the rest of the Z-bros team for the bi-monthly feedback sessions where I could bounce around ideas.

*Elke Solot  
Delft, October 2022*



# Abstract

Hexapod robots are becoming increasingly popular for navigating and exploring irregular and inhospitable environments. The Lunar Zebro is such a hexapod robot that has been developed to be the lightest and smallest rover to explore the moon. The purpose of the Lunar Zebro is to navigate the surface of the moon where it will encounter difficult terrains such as regolith (Lunar Soil) and rocks. To date, not much focus has been placed on the design of the Lunar Zebro legs to increase the rover's trafficability on these terrains. Furthermore, the designs of rover wheels are constantly changing, and new lessons are being learnt from each new mission that the guidelines for designing the wheels and legs of rovers are constantly evolving. Using a Biomimicry design framework, the legs of the Lunar Zebro were redesigned using strategies adopted by animals in nature to improve the trafficability of the legs on granular and rocky terrains. Several concepts were created and narrowed down to four final designs (Hair, Web, Paddle and Claw Legs) that were further developed and manufactured. In addition to this, the original leg design and a flat leg with no grousers were developed for testing.

Several different single-leg tests were performed on the legs to measure their sinkage, thrust, rolling resistance and drawbar pull on regolith and rocky surfaces. The results showed that hair has the potential to reduce sinkage on regolith. However, the results from the single-leg tests on regolith also indicated that there is not much difference in the drawbar pull performance of the different legs no matter what features were included on the bottom of the leg or if the leg had grousers or not. In contrast, the results of the experiments performed on rocky surfaces showed that legs with claw-like grousers performed the best.

From there a hybrid leg was designed using the finding of the single-leg tests and this leg was tested on a basic Lunar Zebro prototype against the original Lunar Zebro leg design to determine if the hybrid improves the trafficability of the rover on both regolith and rocky terrains. These tests included testing the drawbar pull of the rover at 100 % slip and measuring the distance travelled by the rover over five steps. The results showed that on regolith terrain, the design of the leg does not have a big impact on the performance of the rover. However, the results showed that on rocky terrain the rover with hybrid legs travelled roughly 10% further over five steps and had a drawbar pull roughly 10% larger than the rover with original legs.

# Contents

<b>Preface</b>	<b>i</b>
<b>Summary</b>	<b>ii</b>
<b>1 Introduction</b>	<b>1</b>
1.1 Background and Context . . . . .	1
1.2 Lunar Environment . . . . .	2
1.3 State of the Art . . . . .	3
1.3.1 Planetary Rovers . . . . .	3
1.3.2 RHex Descendants . . . . .	3
1.3.3 Vehicles that focus on traction . . . . .	4
1.4 Current Leg Design and Configuration . . . . .	5
1.5 Research Question . . . . .	6
1.6 Using Biomimicry to improve the traction of the Lunar Zebro . . . . .	6
<b>2 Terramechanics</b>	<b>7</b>
2.1 Drawbar Pull . . . . .	7
2.2 Bekker Theory . . . . .	7
2.2.1 Pressure-sinkage relationship . . . . .	8
2.2.2 Thrust and Slip . . . . .	8
2.2.3 Resistance . . . . .	9
2.3 Grousers . . . . .	9
2.3.1 Grouser Patterns . . . . .	10
2.4 Gravity . . . . .	11
<b>3 Biomimetic Approach</b>	<b>12</b>
3.1 Biomimicry Design Framework . . . . .	12
3.2 Explore: Distilling Function and Context . . . . .	13
3.3 Discover: How do six-legged creatures locomote? . . . . .	13
3.3.1 General Features . . . . .	13
3.3.2 Gait . . . . .	14
3.3.3 Climbing obstacle . . . . .	14
3.4 Discover: How does Nature Traversing Granulated Terrains . . . . .	15
3.4.1 Minimise Sinkage . . . . .	15
3.4.2 Increase friction . . . . .	17
3.4.3 Adapted Locomotion . . . . .	17
3.5 Discover: How does Nature Traverse Rocky Terrains . . . . .	19
3.5.1 Increase Friction . . . . .	19
3.5.2 Surface irregularities . . . . .	20
3.5.3 Adapted Locomotion . . . . .	21
<b>4 Leg Design and Realisation</b>	<b>22</b>
4.1 Concept Generation . . . . .	22
4.1.1 Parameters and options . . . . .	22
4.1.2 Concept Tree . . . . .	24
4.1.3 Concepts and Concept Selection . . . . .	25
4.1.4 Final Concept Selection . . . . .	30
4.2 Concept Development and Manufacturing . . . . .	30
4.2.1 Hair Leg . . . . .	30
4.2.2 Web Leg . . . . .	32
4.2.3 Paddle Leg . . . . .	34

4.2.4	Claw Leg . . . . .	34
<b>5</b>	<b>Experimental Surfaces</b>	<b>35</b>
5.1	Regolith Surface . . . . .	35
5.1.1	Regolith Simulant . . . . .	35
5.1.2	Testbed Dimensions . . . . .	35
5.1.3	Bearing Capacity in the Transition Zone . . . . .	36
5.1.4	Terzaghi's Soil Bearing Capacity . . . . .	37
5.1.5	Test bed regolith preparation . . . . .	38
5.2	Rocky Surface . . . . .	39
5.2.1	Single Leg Tests . . . . .	39
5.2.2	Rover Tests . . . . .	39
<b>6</b>	<b>Single Leg Experimental Set-up</b>	<b>40</b>
6.1	Measuring Trafficability . . . . .	40
6.2	Test leg . . . . .	41
6.3	Measuring Sinkage . . . . .	42
6.4	Measuring Drawbar Pull . . . . .	42
6.4.1	Thrust . . . . .	43
6.4.2	Rolling Resistance . . . . .	44
6.4.3	Modified Drawbar Pull . . . . .	44
<b>7</b>	<b>Single Leg Results and Analysis</b>	<b>45</b>
7.1	Experimental Data . . . . .	45
7.1.1	Sinkage . . . . .	45
7.1.2	Pivot Thrust . . . . .	47
7.1.3	Drag Thrust . . . . .	48
7.1.4	Rolling Resistance . . . . .	49
7.1.5	Drawbar Pull . . . . .	50
7.2	Comparison of the performance of the different legs . . . . .	51
7.2.1	Regolith . . . . .	51
7.2.2	Rocky Terrain . . . . .	53
<b>8</b>	<b>Rover Experimental Set-up</b>	<b>55</b>
8.1	Hybrid Leg . . . . .	55
8.2	Measuring Trafficability . . . . .	56
8.3	Measuring Drawbar Pull . . . . .	57
8.4	Measuring Distance Travelled . . . . .	57
<b>9</b>	<b>Rover Results and Analysis</b>	<b>58</b>
9.1	Experimental Data . . . . .	58
9.1.1	Drawbar Pull . . . . .	58
9.1.2	Distance Travelled . . . . .	60
9.2	Comparison of the performance of the different legs . . . . .	61
9.2.1	Regolith . . . . .	61
9.2.2	Sandpaper . . . . .	62
<b>10</b>	<b>Conclusion</b>	<b>63</b>
<b>11</b>	<b>Recommendations for Future Work</b>	<b>64</b>
	<b>References</b>	<b>66</b>
<b>A</b>	<b>Lunar Environment</b>	<b>72</b>
A.1	Lunar Conditions . . . . .	72
A.2	Terrain . . . . .	73
A.3	Lunar Regolith . . . . .	74
<b>B</b>	<b>State of the Art</b>	<b>75</b>
B.1	Planetary Rovers . . . . .	75
B.2	RHex and Descendants . . . . .	78

---

B.2.1	The RHex . . . . .	78
B.2.2	SandBot . . . . .	79
B.2.3	Desert RHex . . . . .	79
B.2.4	Whegs . . . . .	80
B.3	Other Vehicles that focus on Traction . . . . .	81
B.3.1	Tractors . . . . .	81
B.3.2	Sand based Vehicles . . . . .	81
<b>C</b>	<b>Terramechanics Supplementary</b>	<b>82</b>
C.1	Terramechanics of C-shaped Legs in very loose soil . . . . .	82
C.1.1	Hybrid model . . . . .	82
C.1.2	Influence of leg shape . . . . .	84
<b>D</b>	<b>Flat Leg Dimensions</b>	<b>85</b>
<b>E</b>	<b>Lunar Zebro Dimensions and Requirements</b>	<b>87</b>
E.1	Dimensions . . . . .	87
E.2	Requirements . . . . .	87
<b>F</b>	<b>Risk Assessment and SDS</b>	<b>88</b>
<b>G</b>	<b>Calculating Ultimate Sinkage</b>	<b>95</b>
<b>H</b>	<b>Terzaghi's shear failure surface calculations</b>	<b>96</b>
<b>I</b>	<b>Ncorr: Step by Step</b>	<b>100</b>
<b>J</b>	<b>Kinovea: Step by step</b>	<b>103</b>
<b>K</b>	<b>Pivot Thrust Results</b>	<b>105</b>
<b>L</b>	<b>Grouser Calculations</b>	<b>106</b>
L.1	Grouser Height . . . . .	106
L.2	Grouser Number . . . . .	107

# Introduction

## 1.1. Background and Context

Man's quest to explore space is in its infancy. From Sputnik, the first satellite in space, to Perseverance, the latest Mars rover, advancements in space exploration have come a long way. Currently, TU Delft is working towards sending the world's smallest and lightest rover to the moon, known as the Lunar Zebro (Figure 1.1b). The Lunar Zebro is a hexapod (six-legged) robot that is based on another robot known as the RHex (Figure 1.1a [1], whose design was in turn inspired by a cockroach. To date, all rovers that have successfully landed on extraterrestrial bodies have been wheeled robots [2]. However, research and investigations have shown that legged robots are more adept at exploring extraterrestrial terrains as legged robots are more capable of navigating irregular terrain and climbing over obstacles [3]. In particular, legged robots have proven to be better than wheeled robots at navigating terrain consisting of granular media as they are able to avoid compaction resistance which is caused by the buildup of substrate material at the front of wheels [3]. Legged robots do not experience this phenomenon as each leg acquires a discrete foothold and then pushes off from that foothold [3]. Since the moon is mostly covered in a layer of regolith, which is a type of granular material consisting of unconsolidated rock fragments, the Lunar Zebro design is ideal for lunar exploration.

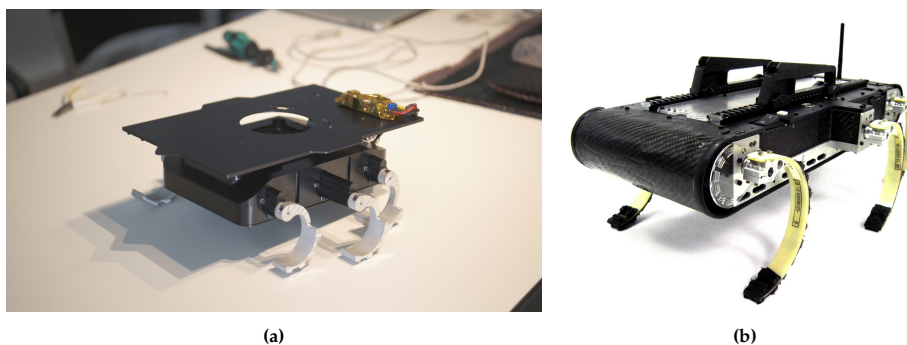
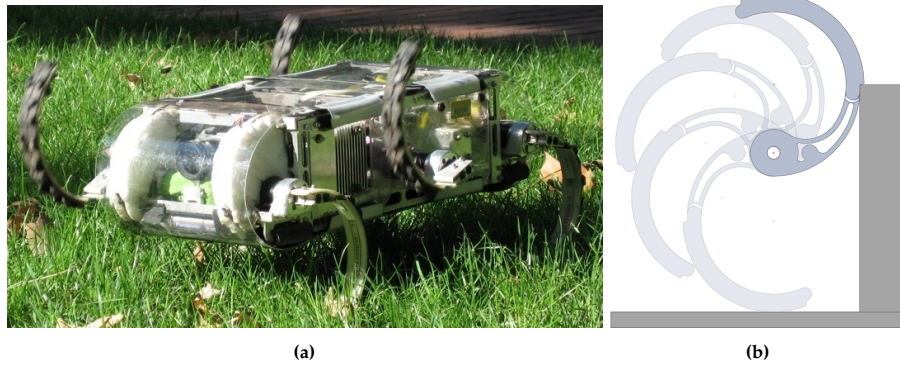


Figure 1.1: (a) The Lunar Zebro [4] (b) Original RHex robot on which the Lunar Zebro is based[5]

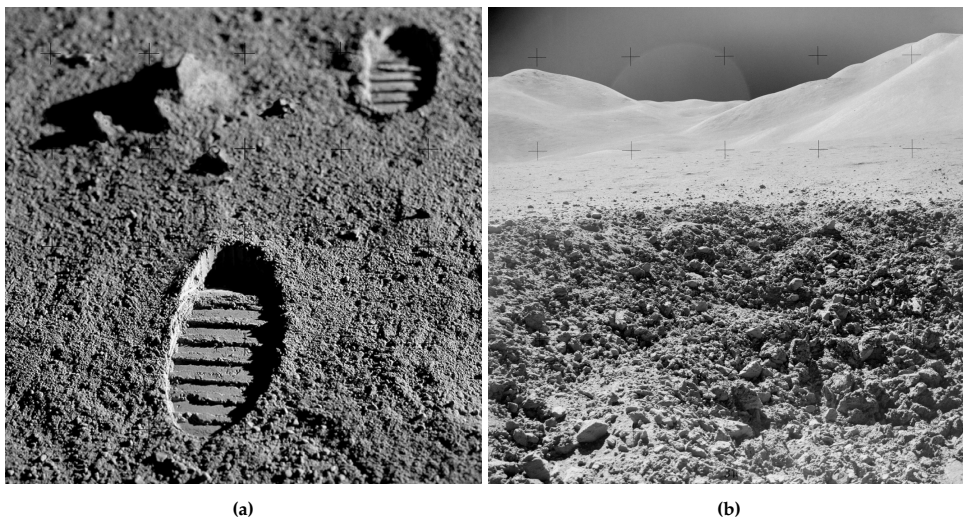
The Lunar Zebro is able to move by rotating the legs in threes with the front and rear legs on the side rotating in sync with the middle leg on the opposite side as seen in Figure 1.2a. When it comes to scaling large objects, the Lunar Zebro will keep rotating its legs until it can find a perch and lift itself up. However, the Lunar Zebro is limited in the maximum height that it is able to climb which is determined by the radius of the legs as seen in Figure 1.2b.



**Figure 1.2:** (a) RHex in motion showing the alternating tripod gait [6]. (b) The climbing height of the Lunar Zebra is affected by the radius of its legs

## 1.2. Lunar Environment

When it comes to the lunar rover, it is very important to take into consideration the environmental conditions that the rover will be exposed to. The lunar environment is very different to that of Earth, with no atmosphere, extreme temperature variations and a terrain that has not yet been fully explored [7] [8]. In addition to this gravity on the moon is about 1/6th the gravity on Earth [8].



**Figure 1.3:** (a) Image showing Lunar Regolith with a moon boot impression [9]. (b) Example of the rocky terrain found on Mars consisting of rock debris [10]

The surface of the Moon is covered in a layer of unconsolidated rock fragments, also known as lunar regolith (Figure 1.3a). The bulk of lunar regolith is made up of particles that are less than 1 cm in size [11] and can be subdivided into 3 categories: *Dust* (<50  $\mu\text{m}$ ), *soil* (<1 mm) and *coarse fine* (1-10 mm) [12]. Analyses of soil samples taken have found that the majority of the regolith is fined-grained, of which dust makes up 40-50% [12]. The only time regolith does not cover the surface of the Moon is at the location of steep-sided crater walls where only bedrock is visible [11]. The surface of the Moon is also riddled with impact craters that vary in size, ranging from a few microns to hundreds of kilometres in diameter [13]. Characteristically, as the diameter of the crater increases, the shallower the depth and the more complex the rims and floor become [13]. These impacts have also resulted in impact fragments that range from massive boulders to powders [7], some examples of these fragments are shown in Figure 1.3b.

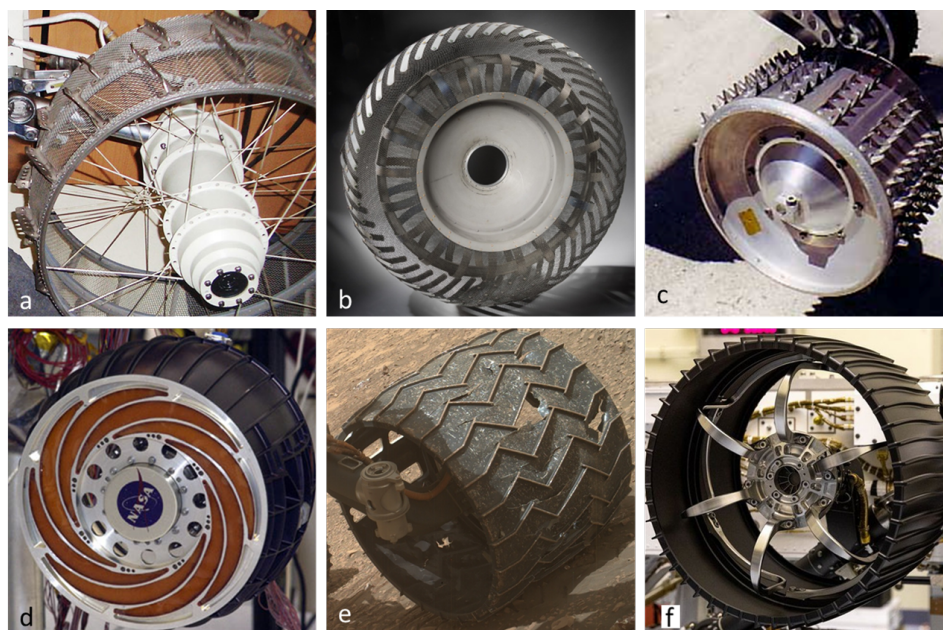
More detailed information concerning the environmental conditions of the Moon can be found in Appendix A



## 1.3. State of the Art

### 1.3.1. Planetary Rovers

Over the past 50 years, many different planetary rovers have been designed with most going on to have successful missions. With each new rover, more and more lessons are being learnt on how to design the wheels of rovers so that they can successfully navigate the difficult terrains and conditions that are present on the Moon and on Mars. Figure 1.4 shows the different designs for six different planetary rovers and what is obvious to note is that the design of rover wheels are constantly changing. This is because with each mission, new lessons are being learnt and discoveries are being made on how to improve the performance of rover wheels.



**Figure 1.4:** Overview of the different wheels used on planetary Rovers: (a) Lunokhod Wheel [14]. (b) Lunar Roving Vehicle (LRV) Wheel [15] (c) Sojourner Wheel [16] (d) Spirit & Opportunity rover Wheel [17]. (e) Curiosity Rover Wheel [18] (f) Perseverance Wheel [19]

More detailed information concerning the state of the art of previous planetary rovers can be found in Appendix B.

### 1.3.2. RHex Descendants

The RHex inspired the development of very similar robots such as the Sandbot and Desert RHex, as shown in the figures below, to be able to walk on Sandy Terrains. Valuable lessons were learnt from these two robots that can be applied to the Lunar Zebro. Experiments performed on the Sandbot showed that the gait (the way the legs are turned) of the robot is very important when walking on Sand. Initially, they assumed that the robot would perform as well as it did on other terrains, however, the SandBot got stuck after a few steps, with the legs spinning uselessly without propelling the robot forward. They then decided to alter the gait of the robot by modifying the speed of the rotation so that the legs would rotate slower when in contact with the ground and then speed up again when in the air [20]. They found that at low frequencies, the penetration depth of the leg was reduced as the leg is able to enter the material more gently allowing the grains to compact to prevent further sinkage [20]. At high frequencies, this behaviour does not occur and the robot displays swimming-like behaviour [20].



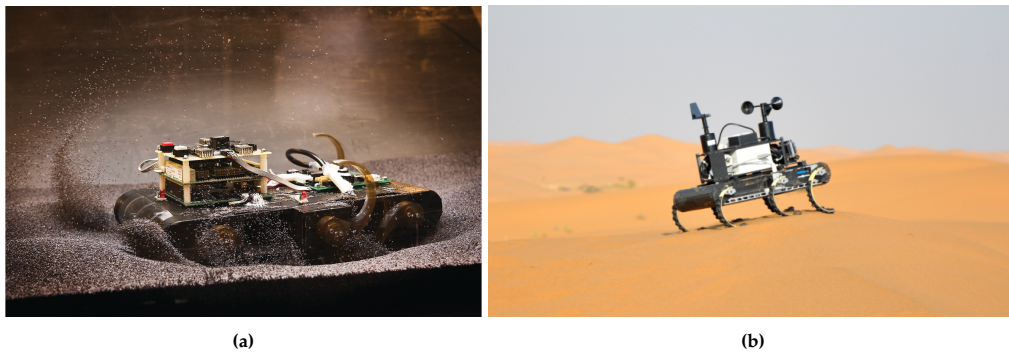


Figure 1.5: (a) SandBot [20]. (b) Desert RHex [21]

For the Desert RHex, one of the aspects that researchers decided to investigate was the impact of increasing the leg width on the performance of the robot. When increasing the width of the legs, they simply doubled the width. It was found that the wide-legged RHex had a specific resistance of 1.1 compared to the specific resistance of 1.3 of the thin-legged RHex [22]. This is evident in the fact that the wide-legged RHex was able to travel further in a single gait cycle than the thin-legged RHex [22]. The difference in specific resistance also means that the wider legs are roughly 20% more efficient than the thinner legs, which increases the range that the robot can travel [22]. When it comes to controlling the RHex while it is walking on the sand, the wide-legs turning performance was greater, making it easier to control [22]. However, it is interesting to note that when ascending a dune with a 30° inclination, the thin-legged robot outperformed the wide-legged robot [22]. The researchers hypothesize that the reason for this is that the thin legs are able to penetrate deeper into the sand and reach more compacted sand underneath [22].

More detailed information concerning the state of the Art of the RHex and its descendants can be found in Appendix B.

### 1.3.3. Vehicles that focus on traction

There are a number of vehicles that have wheels that are designed to traverse difficult terrains such as the wheels of tractors and Sandrails. Tractors normally have large rear wheels which increase the contact area with the ground allowing for increased friction and less slippage [23]. This increased surface area also exerts less pressure on the ground which prevents the tires from sinking into the soil and getting stuck. In addition to this, the rear tires of tractors have very deep treads which increases traction and allows them to navigate difficult and steep terrain [23].



Figure 1.6: (a) Tractor with large wheels and deep treads [24]. (b) Sandrail with front flotation tires and rear paddle tires [25]

Like tractors, the Sandrail has specialized tires that allow it to drive over sandy terrains. It normally uses flotation tires for the front wheels and paddle tires for the rear wheels. Flotation tires are used to "float" over loose soil, meaning they prevent the tire from sinking into the soft terrain [26]. An example

of a flotation tire is shown in Figure 1.6b as the front tires. In contrast, the paddle tires used for the rear wheels are covered in paddles that cover the entire wheel. When driving over loose terrain, the paddles of the wheels are designed to slide into the sand and scoop it up before expelling it which increases the traction of the tire [27]. The more paddles a tire has, the more traction it has, but it also means more torque is required to turn the wheels [27]. The rear tires in Figure 1.6b are an example of paddle tires.

More detailed information concerning these vehicles can be found in Appendix B.

## 1.4. Current Leg Design and Configuration

The Lunar Zebro has been specifically designed to traverse the surface of the moon. Unlike its predecessors, the Lunar Zebro is a hexapod nano-rover which means that the Lunar Zebro has the opportunity to pioneer a new model of rovers for planetary exploration. Right now the focus on the design of the Lunar Zebro has primarily been focused on other aspects of the rover than on trying to improve its trafficability. As it currently stands the design of the Lunar Zebro incorporates six identical c-shaped legs with grousers as shown in Figure 1.7.

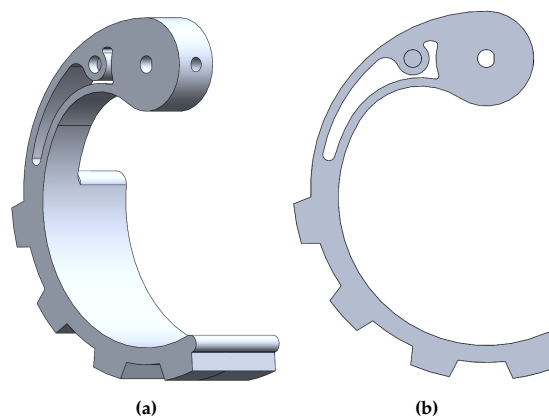


Figure 1.7: Current leg design of the Lunar Zebro

The Lunar Zebro Team considered four different grouser designs for the leg of the Lunar Zebro. These included the Box design which included grousers that were boxed in with a side wall, the Dune design which included a grouser design based on the tread found on beach buggies, the Nanokhod design which had thin straight grousers, and finally the Aldrin design which was based off the moon boots of the Apollo missions and included thick straight grousers. These designs are all down in the Figures below. In the end, the Aldrin design was chosen as the final leg design as the Apollo boots have not changed much across all the Apollo missions.

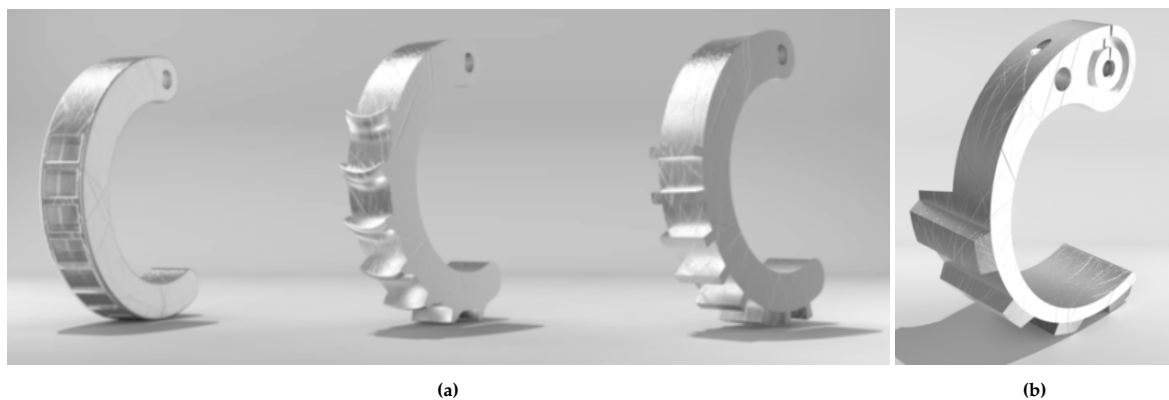


Figure 1.8: (a) Box, Dune and Nanokhod grouser design [28]. (b) Aldrin grouser design [28]

## 1.5. Research Question

The current design of the Lunar Zebro leg was not thoroughly investigated and from previous rovers planetary rovers, RHex descendants and high traction vehicles it can be seen that there are many different features that the Lunar Zebro can include in its leg design to help improve traction. Yet there is no one perfect solution and using biomimetic solutions could provide a whole new range of viable options that could be included in the design of the Lunar Zebro leg that have never been explored. Therefore, the research goal of this paper is to:

*Redesign the legs of the Lunar Zebro for increased Trafficability on Lunar terrains*

This research goal can be broken down into further sub-goals:

1. To generate conceptual designs of the Lunar Zebro leg to improve the trafficability of the rover on both regolith and rocky terrains.
2. Test and compare the trafficability of the newly designed Lunar Zebro legs to the original Lunar Zebro leg on flat regolith and rocky terrains using single-leg tests.
3. Use the results of the single-leg tests to generate a final leg design.
4. Test and compare the trafficability of different legs on a rover prototype on flat regolith and rocky terrains.

## 1.6. Using Biomimicry to improve the traction of the Lunar Zebro

Biomimicry is the design strategy/ problem-solving method used to solve design challenges by learning from and emulating nature's genius [29]. Using the Biomimicry design framework of Explore, Discover, Create and Evaluate [30] set out by *Learn Biomimicry*, the design of the Lunar Zebro leg can be improved upon to help improve the trafficability of the Lunar Zebro on lunar terrains. This framework is further explained in the figure below:

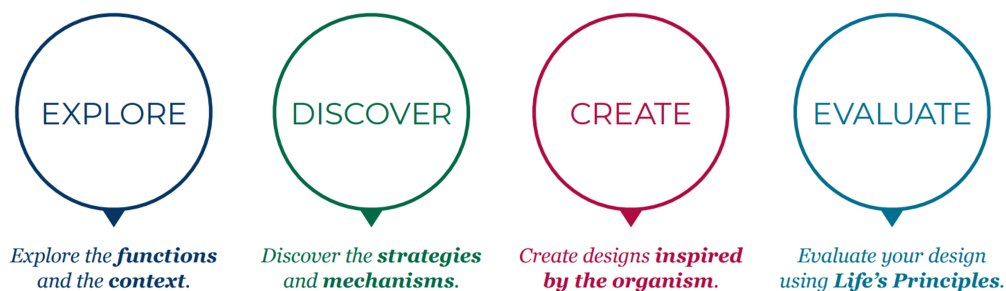


Figure 1.9: Biomimicry Design Framework [30]

# 2

## Terramechanics

In order to understand how the Lunar Zebro is able to move across the Lunar surface, it is first important to understand some of the physics behind it also known as terramechanics. This chapter will also provide some background information on conventional grousers and their patterns.

### 2.1. Drawbar Pull

A good measure of the trafficability of a wheel, or in this case a leg, is to measure its drawbar pull, DP. This is the difference between the horizontal soil thrust,  $H$ , and the sum of all the motion resistances,  $R$ , acting against the wheel. In order for a wheel/leg to be able to navigate a certain terrain, its thrust must be greater than its resistance, in other words, it needs to have a positive drawbar pull [31]. The equation for the drawbar pull is presented below:

$$DP = H - R \quad (2.1)$$

It is possible to predict the drawbar pull of a wheel using Bekker Theory. This theory is explained in the upcoming sections.

### 2.2. Bekker Theory

In the 1950s Bekker and other researchers developed terramechanics theory to describe the tractive performance of large vehicles on granular media such as soil [32]. Bekker theory describes a set of semi-empirical equations that are based on a pressure-sinkage model [32][33]. A visual representation of this theory is shown below

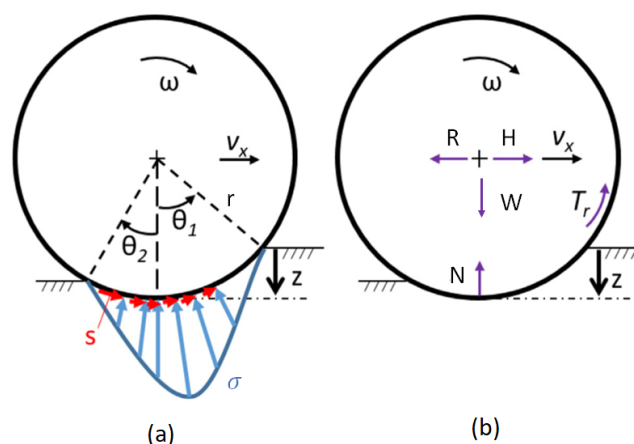


Figure 2.1: (a) Wheel-soil stresses: normal stress ( $\sigma$ ) and shear stress ( $s$ ) [34] (b) Resulting interaction forces [34]

### 2.2.1. Pressure-sinkage relationship

When driving on granular media such as soil, the wheel supports the weight of the vehicle, which in turn subjects a load onto the surface of the terrain and leads to soil deformation. This deformation causes the wheel to sink into the soil which Bekker investigated and derived a relationship between the pressure and sinkage. Bekker based his model on the Bernstein–Goriatchkin model 2.2 below:

$$\sigma = kz^n \quad (2.2)$$

Where  $\sigma$  is the normal stress (i.e. ground contact pressure),  $k$  is the soil deformation modulus,  $z$  is the depth, and  $n$  is the exponent of soil deformation.

Bekker expanded upon the Bernstein–Goriatchkin model by separating the soil deformation modulus,  $k$ , into two moduli  $k_c$  and  $k_\phi$ . Where  $k_c$  is the modulus of the soil deformation due to soil cohesion, and  $k_\phi$  is the modulus of the soil deformation due to friction in the soil. The modified equation is shown below:

$$\sigma = \left( \frac{k_c}{b} + k_\phi \right) z^n \quad (2.3)$$

Where  $b$  is the width of the wheel and  $k$  in equation 2.2 is now a function of  $k_c$ ,  $k_\phi$  and  $b$ . These models show that the pressure scales exponentially with depth.

### 2.2.2. Thrust and Slip

Soil thrust is the resulting force from the soil when wheels, or legs, push on the soil and it provides the traction needed for vehicles to traverse granular media. The thrust is dependent on the maximum shear strength,  $\tau_{max}$ , of the soil as shown in the equations below, which in turn is dependent on the ground contact pressure of the wheel,  $\sigma$ .

$$\tau_{max} = C_0 + \sigma \tan \phi \quad (2.4)$$

Where  $C_0$  is the soil cohesion, and  $\phi$  is the internal friction angle of the soil. The maximum soil thrust occurs when there is zero slip and can be calculated using the Bernstein-Bekker equation 2.5 below:

$$H_0 = A\tau_{max} = A(C_0 + \sigma \tan \phi) = AC_0 + W \tan \phi \quad (2.5)$$

Where  $A$  is the contact area of the wheel,  $W$  is the vehicle's weigh.

However, soil thrust is affected by slip, which is when there is a difference between a vehicle's translational velocity and the wheel's/leg's rotational velocity. The slip ratio can be defined as follows:

$$s = 1 - \frac{V}{r\omega} = 1 - \frac{V}{V_t} \quad (2.6)$$

Where  $r$  is the radius of the wheel,  $\omega$  is the angular speed,  $V$  is the translational velocity and  $V_t$  is the rotational velocity of the wheel. Therefore, the soil thrust, when slippage occurs, is defined as:

$$H = H_0 \left( 1 - e^{-\frac{sl}{\kappa}} \right) \quad (2.7)$$

Where  $s$  is the slip ratio,  $l$  is the ground contact length, and  $\kappa$  is the shear deformation slip modulus.

### 2.2.3. Resistance

Working against thrust is the resistance caused by soil compaction which in turn is dependent on sinkage  $z_0$ . Using equation 2.3, Bekker was able to derive an equation for static sinkage as shown in equation 2.8 below:

$$z_0 = \left( \frac{3W}{b(3-n) \left( \frac{k_c}{b} + k_\phi \right) \sqrt{D}} \right)^{2/(2n+1)} \quad (2.8)$$

where  $D$  is the wheel diameter.

The compaction resistance,  $R_c$ , is highly dependent on the pressure-sinkage relationship and it describes the work done by the wheel on the soil in the vertical direction. Bekker describes the compaction resistance as follows:

$$R_c = \left( \frac{k}{n+1} \right) z_0^{n+1} \quad (2.9)$$

From the above two equations 2.8 and 2.9 it can be seen that sinkage is dependent on the width of the wheel,  $b$ , which means that the larger the width of the wheel the less the wheel will sink into the soil. In turn, this means that the compaction resistance of the wheel decreases. This is also true for legged vehicles.

Another form of resistance that a wheel/leg encounters is gravitational resistance,  $R_g$  when navigating slopes. This resistance can be described as follows:

$$R_g = W \sin \theta \quad (2.10)$$

where  $\theta$  describes the angle of the slope.

Lastly, bulldozing is also another type of resistance that occurs with wheels. Bulldozing occurs when loose soil is pushed in front of the wheels which counteracts the direction of motion. This effect only occurs for the front wheels of a vehicle as the rear wheels follow the more compacted tracks of the front wheel. However, this effect does not occur for legged vehicles as the leg lifts instead of rolls continuously and therefore this effect [31] will not be discussed in more detail in this section.

As a result, the total motion resistance of the leg of the Lunar Zebro is the sum of the individual resistances described above. Therefore the motion resistance can be described as:

$$R = R_c + R_g + R_{other} \quad (2.11)$$

## 2.3. Grousers

When traversing granular media, wheels and legs can easily lose traction which results in slip and sinkage. The use of features such as grousers, lugs and cleats has proven to improve the tractive capabilities of wheels on light-weight vehicles [35]. Studies by Bauer et al. [36] found that increasing the number of grousers on a wheel improves traction, while Sutoh et al. [37] found that there is a limit to the number of grousers a wheel should have as the spacing between consecutive grousers becomes too small. Both studies showed that increasing the number of grousers provided higher traction gains than those provided by increasing the radius of the wheel by the height of the wheel. In addition to this, Ding et al. [38] found that the height of the grousers also affected the wheel's tractive performance.

Inotsume et al. [35] describe a set of equations (2.12 and 2.13) that can be used to determine the ideal height of the grouser,  $\hat{h}$ , and the ideal number of grousers,  $n_g$  for a wheel. Where the ideal grouser height can be calculated using the following relationship:

$$\phi < \frac{1}{1-s} \left( \sqrt{(1+\hat{h})^2 - (1-\hat{z})^2} - \sqrt{1 - (1-\hat{z})^2} \right) \quad (2.12)$$

Where  $\phi$  is the angle between two successive grousers,  $s$  is the slip ratio,  $\hat{h}$  is the normalized height of the grouser, and  $\hat{z}$  is the normalized sinkage of the wheel. A visual representation can be found in Figure 2.2. The detailed derivation for this inequality can be found in [37].

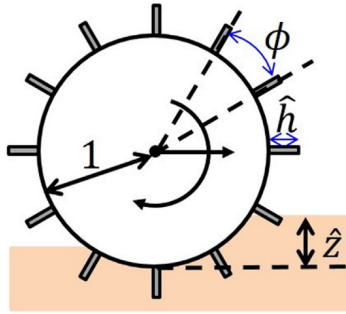


Figure 2.2: Parameters needed for grouser design. Note the dimensions are normalized to the radius of the wheel [35]

For a fixed grouser height,  $\hat{h}$ , the grouser count,  $n_g$  can be found using the following formula:

$$n_g > \frac{2\pi(1-s)}{\sqrt{(1+\hat{h})^2 - (1-\hat{z})^2} - \sqrt{1 - (1-\hat{z})^2}} \quad (2.13)$$

### 2.3.1. Grouser Patterns

Another factor relating to grouser design that influences performance is the type of pattern used. As briefly discussed in Chapter B, NASA used a variety of different grouser patterns including straight, W/chevron pattern and straight with end-caps. Recently a study by Nagaoka et al. [39] investigated the effects of different grouser patterns (shown in Figure 2.3) on traction performance on flat, sandy terrain and they found that the slanted shape performed the best out of all the patterns. While Inotsume et al. [35] found that V-shaped grousers performed the best on flat terrain and that parallel grousers performed better when ascending steep slopes. Additionally, they found that end-caps decreased drawbar-pull but helped improve performance when traversing cross-slope and sloped ascents.

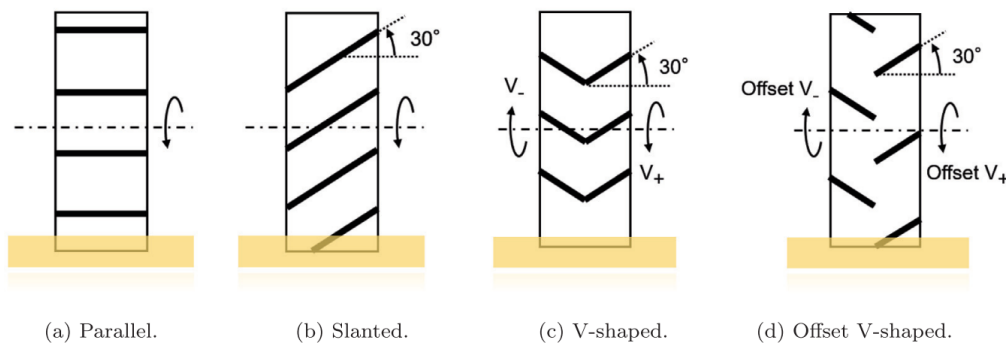


Figure 2.3: Grouser patterns [39]



## 2.4. Gravity

Another aspect that needs to be taken into consideration is the effect that lunar gravity has on wheel-soil interactions. One of the most influential parameters that affect the performance of a wheel is its sinkage and slip. The overall sinkage of a vehicle can be divided into two parts, static sinkage,  $z_0$ , and dynamic sinkage,  $z_d$ . There are two factors that effect sinkage and slip in low gravities: (1) Reduced Normal Load (RNL), which is when the soil experiences a lighter load from the wheel as a result of gravity and (2) Reduced Bearing Capacity (RBC), which is the reduction in the confinement stress of soil resulting in a diminished capacity for the soil to bear weight [40]. A study by Jiang et al. [41] found that under extraterrestrial conditions, a wheel experiences more slippage and sinkage than on Earth and that RBC plays a dominant role in the sinkage and slippage of a wheel; while RNL is less important. In addition to this, they found that wheels that have grousers have a larger dynamic sinkage than flat plain wheels. Lastly, they also found that wheels are able to perform more efficiently in extraterrestrial environments.

Addition information regarding the terramechanics of C-shaped in legs in very loose soil can be found in Appendix C

# 3

## Biomimetic Approach

Improving the tractive capabilities of a wheel or leg has usually been done using conventional grouser designs and patterns. This chapter will use a Biomimetic design framework to find new ways to improve the tractive capabilities of the Lunar Zebro. Lessons can be learnt from six-legged creatures and the way they walk. In addition to this, there are several animals including reptiles, mammals and insects whose habitats are similar to the terrains found on the moon and who are able to move across them with relevant ease and who can provide inspiration for new designs. This chapter explains the Biomimicry design framework and applies it to the research goal of this report.

### 3.1. Biomimicry Design Framework

*Learn Biomimicry* has set out a design framework [30] to help solve design challenges by learning from and emulating nature's genius. This framework can be broken down into the 4 steps listed in the figure below:

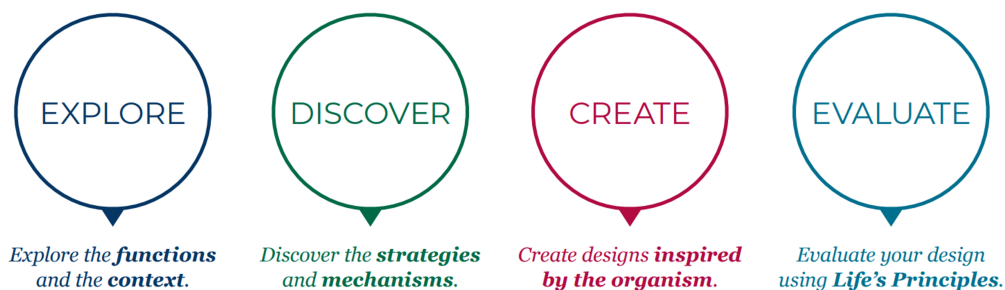


Figure 3.1: Biomimicry Design Framework [30]

The first step is to break down the design problem into its core functions and context. This is done by reframing the design problem into a verb and then identifying the context in which the problem is taking place, in other words, under what conditions does the solution need to work. The next step is to use these functions and contexts to discover natural models and abstract their working design principles to understand how and why the principles work. With this new knowledge, it is then possible to create new designs that are applicable to the original design problem. The last step is to evaluate the design using Life's principles as shown in Figure 3.2.

Evaluating the designs against Life's principles is not largely applicable to the Lunar Zebro leg. Therefore, in this report, the generated leg designs will not be evaluated against these principles. Instead, the generated concepts will be evaluated and narrowed down using a pros and cons list. The final concepts will then be developed and experimentally tested to determine their performance.

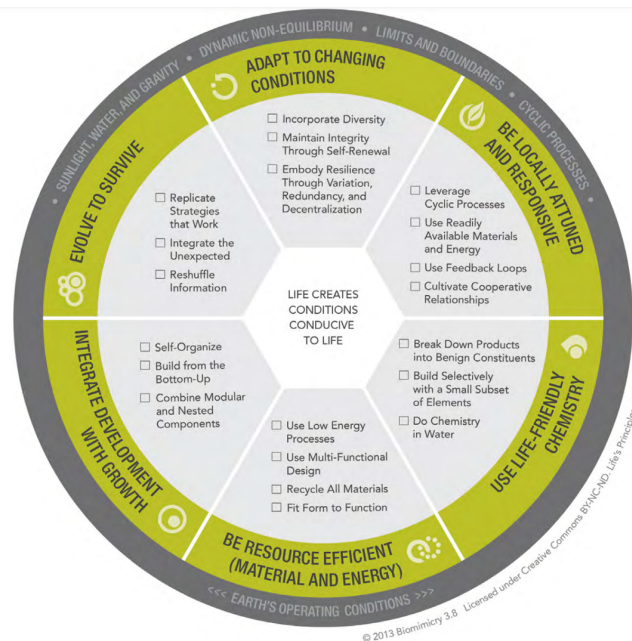


Figure 3.2: Life's Principles [42]

## 3.2. Explore: Distilling Function and Context

The design problem that is trying to be solved is to redesign the legs of the Lunar Zebra to improve the trafficability of the rover on Lunar terrain. This problem can be broken down into several functions and contexts as listed and explained below:

1. **How do six-legged creatures locomote:** The Lunar Zebra is a six-legged robot whose purpose is to locomote across the surface of the moon, therefore valuable lessons can be learnt from the way six-legged creates locomote.
2. **How does nature traverse granulated terrains:** The primary terrain that the Lunar Zebra needs to navigate is lunar regolith which is a type of granular terrain. Therefore, learning how creatures in nature navigate granular terrains such as sand and soil could be insightful.
3. **How does nature traverse rocky terrains:** The Lunar Zebra also may encounter rocky terrains, therefore, like with the granular terrain, it would be beneficial to learn how creatures navigate rocky terrains.

## 3.3. Discover: How do six-legged creatures locomote?

The RHex was inspired by the cockroach, in terms of the number of legs and its tripod gait. However, there may be more that can be learnt from the cockroach and other insects and the way they move.

### 3.3.1. General Features

Insects have 3 pairs of legs: front, middle and hind legs. Each pair of these legs performs a different function that aids with walking. For the purpose of this analysis, the cockroach will be used as an example although all insects generally display the same characteristics. Starting from the back, the hind legs are adapted to provide the cockroach with the necessary forces to propel itself forward [43][44]. As a result, the hind legs are the largest and most powerful set of legs of an insect [43]. The front legs are used to make more complex movements. They are able to reach forward, which aids with turning and climbing, and they are also used to generate braking forces [43][44]. Insects use a tripod gait so the middle legs are used to balance the lateral forces of the front and back legs on the opposite side [43]. The middle legs also provide a mixture of propulsive and braking forces[44]. Quadruped animals that evolved legs independently from insects also display specializations between their rear and front legs, with the rear legs providing the power for locomotion while the front legs provide the

searching movement and braking forces [43]. All of the RHex robots and lunar robots have ignored these principles of different leg pairs so all their legs/wheels are identical.



Figure 3.3: Image of a Cockroach showing the different types of legs it has [45]

### 3.3.2. Gait

As mentioned previously insects rely on a tripod gait to rapidly navigate any terrain. Ramdya et al [46] set out to test if the tripod gait is the most efficient gait for hexapod insects using a model based on the *Drosophila melanogaster*, which is a type of fly. Their results show that the tripod gait is indeed the best gait to use when climbing or walking on flat ground when the feet of the insect include adhesive pads which all insects have. However, when these adhesive pads are covered, the best gait for walking on flat ground is a bipod gait, while a tripod gait is still best for climbing. To verify the result of the bipod gait, Ramdya et al covered the adhesive pads of a *Drosophila* and they found that the animal did start to exhibit a bipod-like gait.

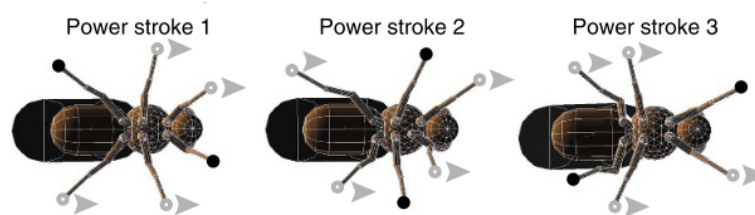


Figure 3.4: Bipod Gait of the *Drosophila melanogaster* [46]

### 3.3.3. Climbing obstacle

When it comes to climbing obstacles, Watson et al. [47] investigated the climbing strategies used by *Blaberus discoidalis*, also known as deathhead cockroaches. They found when these cockroaches encounter relatively small obstacles, the cockroach is able to climb over the obstacle with relatively little change in their leg movement or motor activity. When navigating relatively large obstacles, the cockroach displayed a variety of behaviours including head-butting the obstacle, elevating its body, lifting up its front legs and rearing up. These behaviours are illustrated in Figure 3.5. The rearing-up behaviour was most commonly used and requires the cockroach to alter the orientation of its middle legs to allow the front part of its body to pitch up allowing the front legs to be closer to the top of the obstacle.

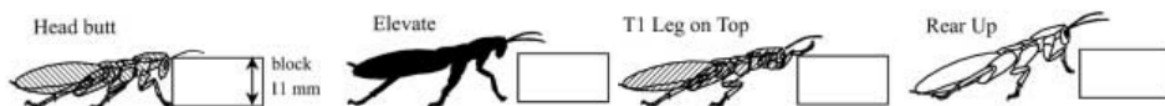


Figure 3.5: Climbing strategies of a cockroach modified from [47]

### 3.4. Discover: How does Nature Traversing Granulated Terrains

Regolith covers the majority of the surface of the moon. Regolith is a type of granular media, so in this section animals who have evolved several adaptations that allow them to survive and navigate granular media, such as sandy or snowy terrains, will be explored. Some animals display similar characteristics although their species evolved parallel to one another. These features and their working principles are broken down in the ACCREx <sup>1</sup> tree below.

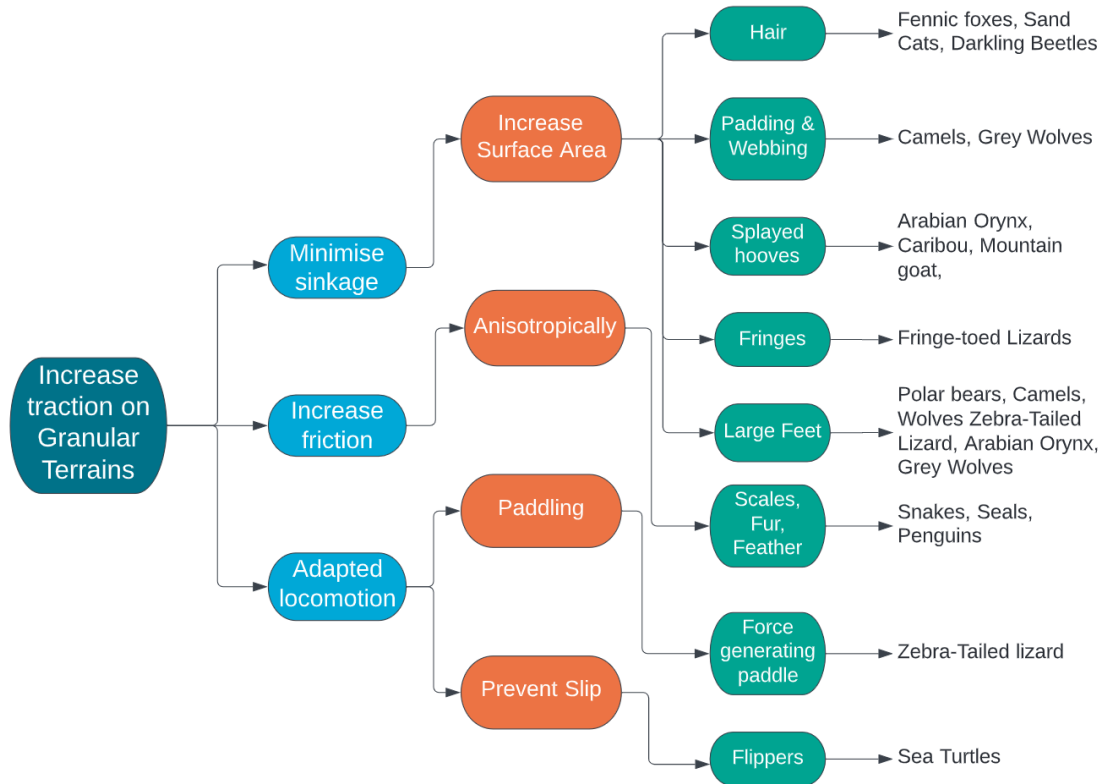


Figure 3.6: ACCREx Tree showing all the features and adaptations animals display to be able to traverse Granulated Terrains

#### 3.4.1. Minimise Sinkage

Like with wheels, minimizing sinkage is very important when it comes to animals walking across granular material. By minimising sinkage, these animals have to expend less energy in order to cross it. In nature, minimising energy expenditure is key to survival.

##### Increased Surface Area

When it comes to walking on sandy or snowy surfaces, having a large contact area with the ground is a common trait that has developed across many species, whether the animal has a foot, paw or hoof. An increased contact area with the ground allows the animal to exert a small pressure on the ground which in turn prevents them from sinking into the ground.

##### *Hair:*

Many desert-dwelling animals such as the Fennec fox, Sand cat, and Darkling beetle have developed hair or bristles on the underside of their feet (Figure 3.7b) [51]. Some sources speculate that the fur aids with preventing the feet from sinking into the loose sand as the animal walks by increasing the surface area of the animal's feet [52]. While others suggest that the hair aids with braking as the foot pushes back into the sand [51].

<sup>1</sup>The ACCREx tree falls under the ACCREx design method [48] which stands for Abstraction, Categorization, Reflection, Reformulation, and Extension of search results. In this case, the ACCREx method has been used to show the working principles used by animals to solve the design problem.



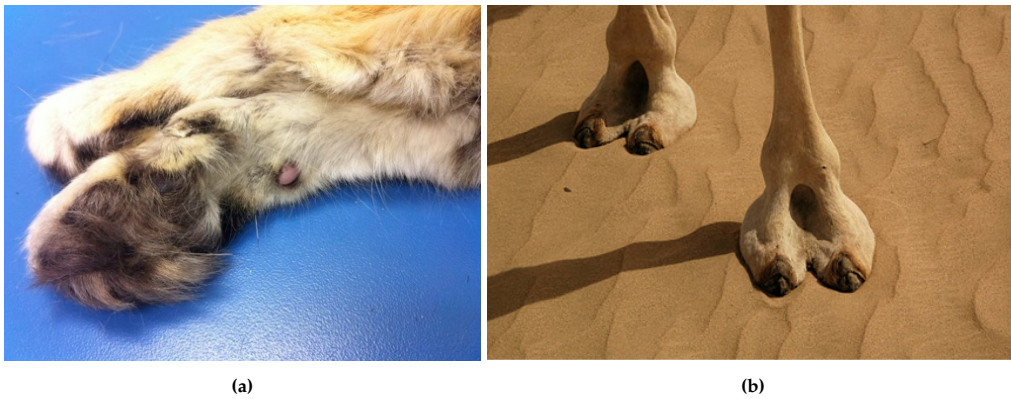


Figure 3.7: (a) Sand cat paw displaying the fur which covers the bottom of the paw [49] (b) Camel Feet [50].

***Padding and Webbing:***

The feet of a camel are very broad with two toes that have a pad that spreads even more when the camel's foot makes contact with the ground thereby increasing the foot's surface area in contact with the ground [53]. In between these two toes, there is webbing that further prevents the camel from sinking into the sand [53]. Similarly, the Grey wolf has adapted similar features to the camel with large paws including webbing in between their toes, however, this allows them to walk over snow instead of sand [54].

***Splayed hooves:***

Many animals in the Bovidae family who live in sandy or snowy terrains, such as the Arabian Orynx, and the Caribou, have large splayed hooves which they use to increase their ground contact area, thereby preventing them from sinking into the sand or snow[55] [56][57].



Figure 3.8: (a) Hind leg of a fringe-toed Lizard[58] (b) Caribou splayed hoof[59]

***Fringes:***

The Fringe-toed Lizard has developed a unique feature to aid with traction when traversing sandy terrains. This lizard has developed elongated scales on its hind legs that look like a fringe (Figure 3.8a) which helps to increase the surface area of the leg which is in contact with the ground [60].

***Large Feet:***

A common trait seen in most animals mentioned previously, is that they have large feet, paws or hooves, whether they live in sandy or snowy terrains. As mentioned previously this is to increase the surface area and prevent sinkage.

### 3.4.2. Increase friction

Increasing friction aids with generating the tractive forces needed for an animal to propel itself forward or to provide a braking mechanism to prevent the animal from slipping.

#### Anisotropically

##### *Scales, Furs and Feathers:*

Snakes rely on their scales to produce anisotropic friction to help propel themselves forwards on sandy terrains [61]. Their scales consist of micro-patterns that form an array of v-shaped feather trailing edges that point towards the tail of the snake [61]. In a similar way, the stiff furs and feathers of seals and penguins are also orientated in such a way to allow them to produce anisotropic friction which allows them to glide forward over ice and snow while providing a braking mechanism when sliding backwards [51].

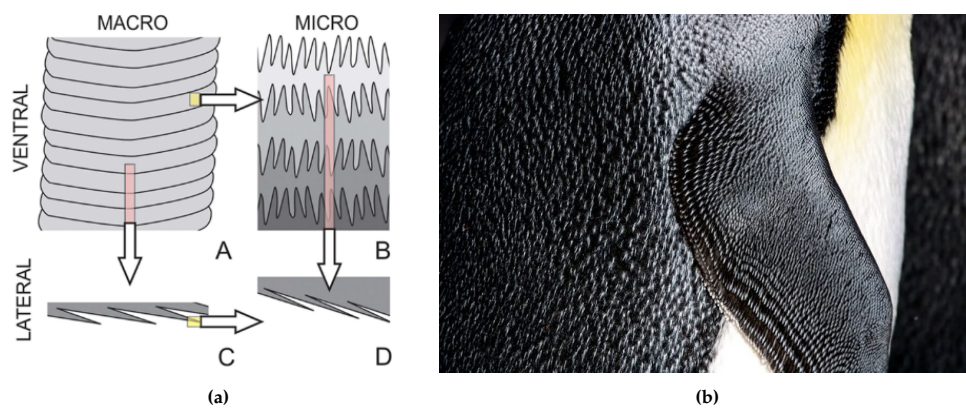


Figure 3.9: (a) Snake scales [61] (b) Penguin Feathers [62]

### 3.4.3. Adapted Locomotion

The animals in this subsection have adapted the way they walk, i.e. the way they move their limbs, to help them navigate granular terrain in a more efficient manner.

#### Padding

##### *Force-generating paddle:*

The Zebra-Tailed Lizard is found to be the most efficient animal at crossing sandy terrains (Figure 3.10a). The Zebra-Tailed Lizard has incredibly large hind feet with elongated toes (especially when compared to its front feet) [63]. These hind feet act as a "dissipative, force generating paddle" which allows the lizard to generate sufficient lift and thrust to lift the weight of the lizard off the ground and propel it forward [63]. Any dissipation of energy must be compensated by greater mechanical work from the hind-leg muscles [63].

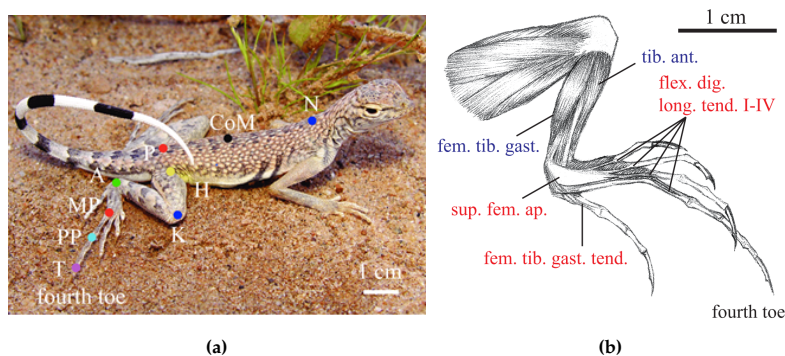


Figure 3.10: (a) Zebra-tailed Lizard [63]. (b) Hind leg of a Zebra-tailed Lizard [63]



**Prevent slip****Flippers:**

Another animal that has proven to be successful at navigating sandy terrains is the sea turtle. Sea turtles crawl over sand, which means they rest most of their body weight on the sand while moving. They propel themselves forward by inserting and anchoring their front flippers into the sand, which they then use to push themselves up and forward [64]. The back flippers remain planter above the surface of the sand and are mostly used to lift the body off the sand [65]. During this type of locomotion, there is no slip between the flippers and the sand. This is because when the flipper is planted in the sand, the sand behind the flipper solidifies [65]. The sea turtle then bends its wrist propelling the rest of its body forwards while maintaining the solidified material behind the flipper [64]. In order to be able to push themselves forward without slipping, the forward thrust must be below the yield force of the sand [65].

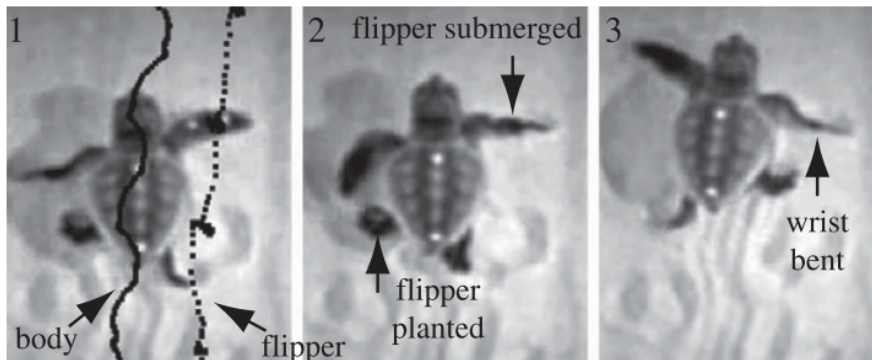


Figure 3.11: Hatchling turtle locomotion on Sand [65]

### 3.5. Discover: How does Nature Traverse Rocky Terrains

Just like some animals have adapted features that allow them to walk over granular media, so have other animals evolved features that allow them to navigate rocky terrains (which is also a terrain on the Moon). Some of these features will be discussed in the upcoming subsections. These features and their working principles are broken down in the ACCREx tree below.

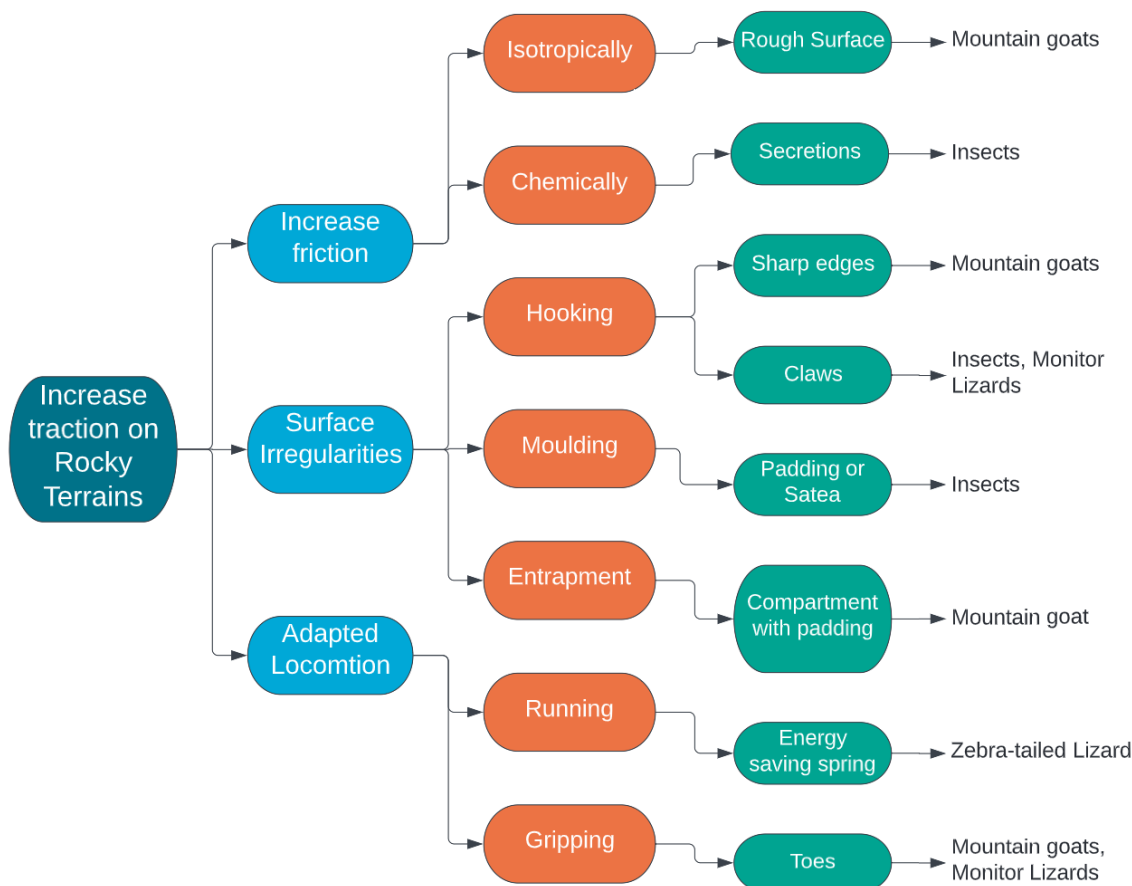


Figure 3.12: ACCREx Tree showing all the features and adaptations animals display to be able to traverse Rocky Terrains

#### 3.5.1. Increase Friction

##### Isotropically

##### *Rough Surface*

One of the most proficient animals at climbing rock terrains, no matter how steep, is the Mountain Goat. This animal relies on a number of adaptations to be able to navigate these terrains, with one of them being that the bottom of the padding in their hooves is very rough [66]. Unlike snakes, seals and penguins, the rough pads of the Mountain goat allow the Mountain Goat to generate friction isotropically, meaning it generates friction in all directions.

##### Chemically

##### *Secretions*

Insects generate friction by secreting a chemical adhesive which allows the pads and setae on the feet of the insects to stick to the surface they are walking on [67]. It was found that if the volume of the secretion was reduced then the ability of the insects to adhere to surfaces also decreased [67].

### 3.5.2. Surface irregularities

#### Hooking

##### *Sharp Edged Hooves*

The hooves of the Mountain Goat also consist of a very sharp and hard outer rim, which allows the Mountain goat to hook/wedge its hooves onto any irregularities in the rock surface [66].



Figure 3.13: (a) Hoof of a Mountain Goat (b) Claw Morphology of the *Varanus glauerti* [68]

#### Claws

Monitor lizards are particularly good at navigating difficult terrains owing to their claws. Depending on their habitat, different taxa of monitor lizards have developed different claw morphologies. In particular, the *Varanus glauerti*, an escarpment monitor Lizard, has adapted claws which are suitable for climbing large, sandstone rocks faces. Their claws were found to be the highest and shortest of all the taxa [68]. Claws help the lizard to climb as the tip of the claw is able to interlock with any irregularities in the rock face and the lizard is able to pull itself up [68]. The height of the claw provides a mechanical advantage as it is able to support the reaction forces as the lizard clings to the rock face [68]. Their claws are also significantly shorter than other monitor lizard taxa and one of the possible reasons for this is that the claws are not able to penetrate the surface of the rock and must therefore interlock with grain-size particles when climbing. If their claws were long, the lizard's centre of mass would be projected away from its supports, which would increase the likelihood of toppling [68]. Similarly, many insects have also developed claws to help them climb and navigate rough surfaces.

#### Moulding

##### *Padding or Setae*

Insects do not solely rely on their claws to climb rough surfaces. They also rely on smooth pads or hair pads (Setae) found on the bottom of their feet. When the protrusions are too large for the claws to hook onto, the pads are able to mould to any protrusions on the surface [69]. This also aids with distributing the chemical secretions for adhesion which was mentioned earlier [67].

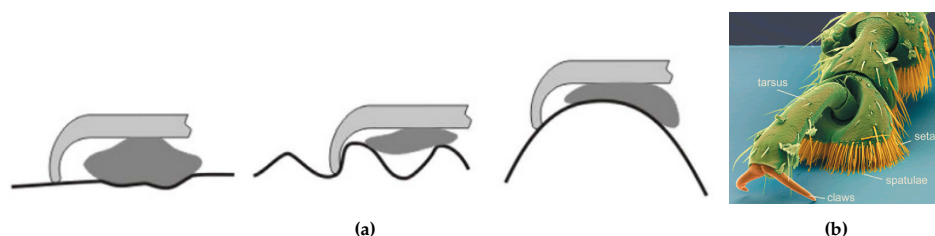


Figure 3.14: (a) Attachment abilities of insect claws and adhesive pads [69]. (b) Claws and Setae of a chrysomelid beetle [67]

**Entrapment***Compartment with Padding*

The Mountain Goat uses the combination of the hard outer rim and soft, central pad to help them walk across rocky terrains. When they are walking any irregularities in the ground surface pushes into the soft pad of the hoof causing the pad to indent and conform to the shape of the bump [66]. This bump is entrapped by the soft pad and hard edge that encompasses it. As a result, the hoof is locked in place and is no longer able to slide [66].

**3.5.3. Adapted Locomotion****Gripping***Toes*

The hooves of the Mountain goat also consist of two independent toes as shown in Figure 3.13a below. These toes are able to spread apart or grip together which further enhances the grip of the hoof [66]. Similarly, Monitor Lizard's feet consist of five independent toes which allows them to individually place each toe to find surface irregularities and grip them together to help them walk and climb over rocky terrain.

**Running***Energy Saving Spring*

The Zebra-Tailed Lizard is as adept at running on rocky terrain as it is on granular terrain. That is because its hind foot also acts as an "energy saving spring" allowing the lizard to store and reuse energy while running thereby reducing the energy expenditure of the lizard while running [63].

# 4

## Leg Design and Realisation

In this chapter, several conceptual designs are proposed based on the features found in Chapter 3. From there the pros and cons of each design is determined and used to narrow down the conceptual designs to a select few. These designs are then further developed.

### 4.1. Concept Generation

Several strategies were used to help aid with generating concepts. These include creating a table listing several parameters and their options. Some of these options are eliminated due to their incompatibility with the design of the Lunar Zebro. From there a Concept tree is created, to easily visualize which parameters and their options can be combined to create final concepts. These concepts are visualised and described in detail and their pros and cons are listed.

#### 4.1.1. Parameters and options

In Table 4.1 below, several parameters are given and their options are listed. These parameters are key to help generate concepts as it gives an overview of the different options available and how different parameters can be combined to give a final concept. In this table five parameters are discussed relating to the design of the leg:

1. **Number of Toes:** In nature the number of digits (toes/fingers) animals have varies from species to species. In general, this number ranges from 1 large digit such as the hoof of a horse, to 5 digits like humans. The leg of the Zebro can also be divided into digits/toes. This number will depend on the other parameters and the features that need to be included.
2. **Toe Division Type:** It is possible to create toes on the leg of the Zebro in a number of different ways. Gaps can be cut into the leg, thereby dividing the leg into the desired number of toes. The shape of the leg can be modified into a section of a sphere and split to create the toes. Lastly, the leg can be modified to include a folded design that can open or close when actuated.
3. **Location of features:** A number of additional features can be included in the design of the leg to help improve the trafficability of the leg of the Zebro. These locations are limited to the side walls of the leg, the bottom, the front and back tips of the leg, and in between the gaps of the toes.
4. **Sandy features:** In Chapter 3, Figure 3.6, a number of biological features and strategies were found that can be applied to the legs of the Zebro.
5. **Rocky features:** In Chapter 3, Figure 3.12, a number of biological features and strategies were found that can be applied to the legs of the Zebro.

Table 4.1: Parameters and Options

Parameter	Options				
Number of toes	1 	2,3,4... 			
Toe Division Type	Gap 	Sphere Section with Split 		Fold 	
Location of features	Sides 	Bottom 	Front Tip 	Back tip 	Gap 
Sandy features	Hair/fur 	Fringes 	Scales 	Pads 	Webbing 
	Splayed Hooves 	Paddling 	Flippers 		
Rocky features	Claws 	Compartment with padding 	Sharp edges 	Rough surface 	Pads 
	Chemical Secretions 	Energy Saving spring 			

## Reductions

Several reductions can be made to reduce the number of options, as some of the options are not compatible with the design of the Lunar Zebro or because they are either impracticable to implement or outside the scope of this project.

These reductions include:

- *Sphere section with split*: In this design, only the inner edges of the toes would be in contact with the ground. This means high strain and wear would occur at that edge of the toe and any additional features that would be incorporated into the design would need to be placed at the edge of the toes and if placed elsewhere these features would not have the proper contact with the ground to be effective.
- *Fold*: This design would require complex mechanisms to be implemented into the design of the Zebro to actuate the folding mechanism. In addition, this design is limited to 2 toes.
- *Splayed hooves*: The design of the leg of the Lunar Zebro, makes it difficult to incorporate splayed toe features into the design of the leg beyond simply incorporating toes.
- *Paddling and Flippers*: To implement these strategies, the walking motion of the Zebro would have to be altered.
- *Chemical Secretions*: The environmental conditions that the Lunar Zebro will experience on the moon, such as the extreme conditions and dusty environment, make it difficult to use chemical secretions as a method of adhesion to rocky surfaces.
- *Energy-Saving Spring*: To make the legs into energy-saving springs would either require complex mechanical mechanisms or to create a compliant mechanism. While this is something that could potentially be beneficial to the Lunar Zebro, it is less relevant to trafficability and considered outside the scope of this project.

### 4.1.2. Concept Tree

With the reductions made to Table 4.1, it is now possible to visualise how these options can be combined to create a range of conceptual designs. This is shown in Figure 4.1 below:

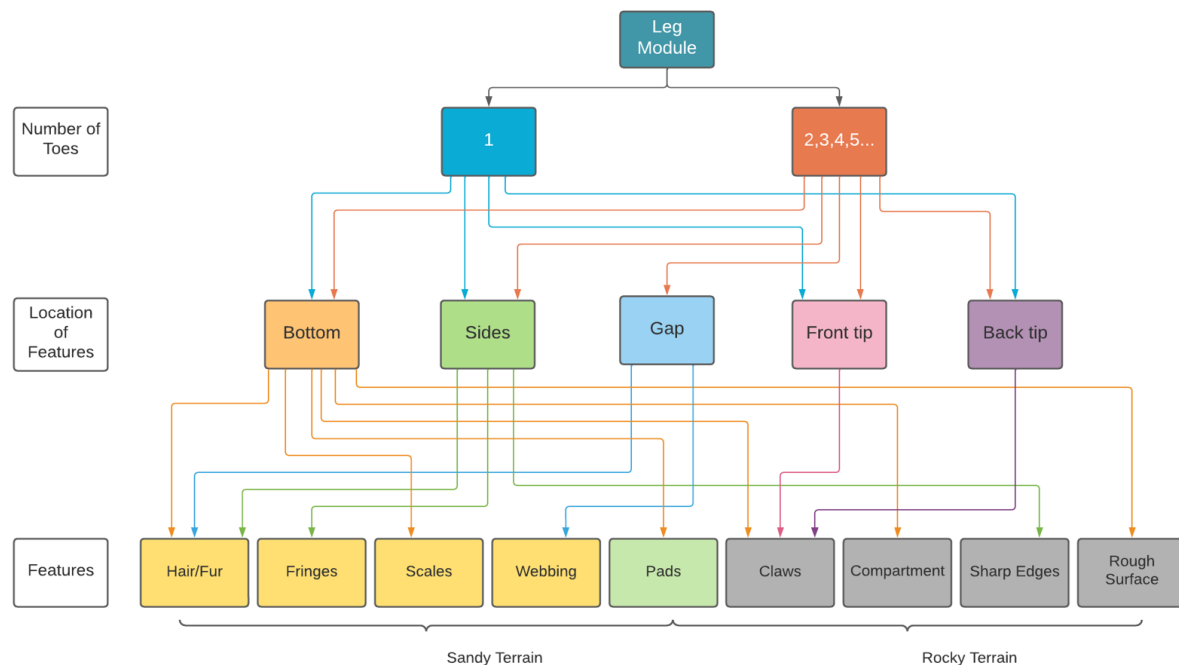


Figure 4.1: Concept Tree showing the possible combinations of all the options

While it is possible to combine several of the biological features such as adding hair and claws to the bottom of the feet, this report will focus on testing individual features to better measure how these features individual contribute to the trafficability of the legs.



### 4.1.3. Concepts and Concept Selection

Using the Concept Tree in Figure 4.1, several conceptual designs were created for each of the biological features listed. These concepts are found in Tables 4.3 to 4.6 and are described in detail. The pros and cons are then listed for each of the concepts and scored using the Score Conditions listed in Table 4.2 below.

Table 4.2: Rating Score

Score	Condition
3	Highly favourable
2	Favourable
1	Mildly favourable
0	Neutral
-1	Mildly unfavourable
-2	Unfavourable
-3	Highly Unfavourable

There are several criteria that were crucial to consider when listing the pros and cons of each concept. They are as follows:

1. Ability to prevent sinkage: This criterion especially applies to concepts generated using features that animals use in granular terrain.
2. Increase friction: Animals in both granular and Rocky Terrain make use of this criteria and therefore this applies to all concepts
3. Hook onto surface irregularities: This criteria especially applies to concepts generated using features that animals use in rocky terrain.
4. Ease of designing: The concepts listed need to still be incorporated into the leg design. Therefore, it is important that it is not difficult to design and implement.
5. Ease of manufacturing: The concepts chosen will be further developed to be manufactured. Therefore, it is important that the materials used and manufacturing processes are not too difficult or time-consuming.

In addition to this, several other pros and cons are listed that are specific to the individual concepts and which can not be used to rate all the other concepts.

From the concepts listed, four concepts will be chosen to be further developed and tested. Two of these concepts will be focused on navigating granular terrain, and the other two concepts will be focused on navigating rocky terrain. These four concepts will be tested along with the original Lunar Zebro leg design (Fig 4.2a) as well as a leg design that is flat and has no grouser features (Fig 4.2b). The results of these tests will then be compared to see if features used in the concepts aid with the trafficability of the legs on the different terrains. Please see Appendix D, for further information on the dimensions of the flat leg.

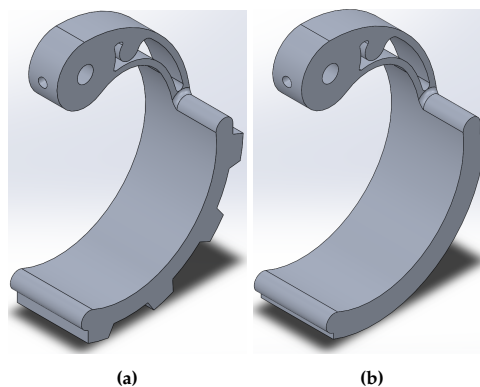


Figure 4.2: (a) Original Leg. (b) Flat Leg

Table 4.3: Concept Description and Scored Pros and Cons

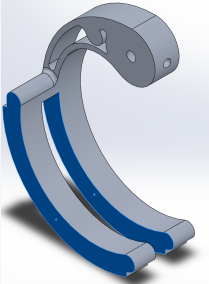
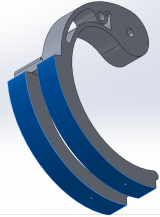
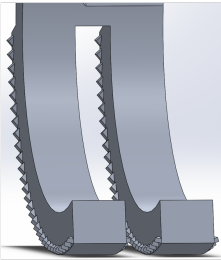
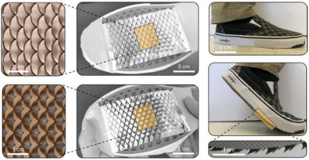
	Feature	Description	Pros	Cons	Score	
Sandy Terrain	Hair		In this design, hair will be located on the side walls and the inner gap of the leg. The hairs will stick out perpendicularly to the wall face. The hair increases the surface area which prevents the leg from sinking into the sand.	<ul style="list-style-type: none"> <li>++ Prevents sinkage</li> <li>++ Relatively easy to Design</li> <li>++ Relatively easy to manufacture</li> <li>+ Lightweight solution to increase ground contact area</li> <li>+ Hairs can flex up and bounce back when pushed by the regolith</li> <li>++ Can be incorporated with other features, such as claws, scales on the bottom of the leg</li> </ul>	<ul style="list-style-type: none"> <li>-- Provides no grip in the regolith</li> </ul>	8
			In this design hair will be placed on the bottom surface of the leg without grousers. The hair should trap regolith in between the hairs and prevent sinkage. In addition to this, the hair should act as a braking mechanism and help with finding grip in the regolith to help propel the leg forward	<ul style="list-style-type: none"> <li>+++ Prevents sinkage</li> <li>++ Relatively easy to Design</li> <li>++ Relatively easy to manufacture</li> <li>+ Lightweight solution to increase ground contact area</li> <li>+ Provides some grip in the regolith</li> <li>++ Can be incorporated with other features, such as claws, scales</li> <li>+ Thermal insulator between the ground and the Lunar Zebro</li> </ul>	<ul style="list-style-type: none"> <li>- Regolith may become trapped in between hairs thereby reducing the effectiveness of the hairs</li> </ul>	11
	Fringes		Like the fringe-toed lizard, this design incorporates small “fringes” which are just triangular protrusion which extend out from the bottom edges of the toes. This helps to increase surface area of the leg.	<ul style="list-style-type: none"> <li>++ Prevents sinkage</li> <li>++ Relatively easy to Design</li> <li>+++ Easy to manufacture</li> <li>+ Lightweight solution to increase ground contact area</li> <li>++ Can be incorporated with other features, such as claws, scales on the bottom of the leg</li> </ul>	<ul style="list-style-type: none"> <li>-- Provides no grip in the regolith</li> <li>- Might cause the leg to dig into the sand when walking, thereby dragging the leg down into the sand and increasing the amount of torque needed</li> </ul>	7
	Scales		This design uses Kirigami – The Japanese art of paper cutting – to create scales by cutting scale-like spikes into a sheet of metal. This material can be applied to the bottom of the Lunar Zebro leg. When the material flexes, the spikes will protrude and dig into the ground surface.	<ul style="list-style-type: none"> <li>+ Flexed scales may help prevent sinkage</li> <li>+ Scales provide some grip in the sand</li> <li>+ Scales only become active when leg is engaged with the ground, otherwise flat</li> <li>++ Scales will act like claws on Rocky surfaces</li> </ul>	<ul style="list-style-type: none"> <li>--- Complex design</li> <li>-- Requires special processes and materials to manufacture</li> <li>-- Rock debris gets stuck in between scales creating high stress points</li> <li>- Legs need to be able to flex to a certain amount to “activate” scales</li> <li>- Only friction in one direction, so will not work when traveling backwards</li> </ul>	-4

Table 4.4: Concept Description and Scored Pros and Cons *continued*

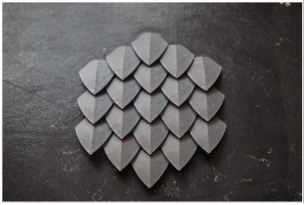
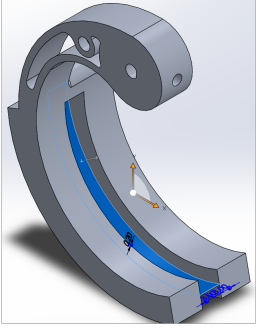
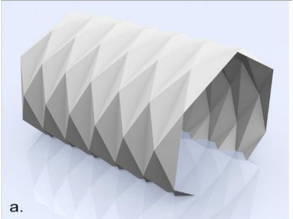
		Feature	Description	Pros	Cons	Score
Sandy Terrain	Scales	3D printed scales on a mesh 	In this design, scales are printed onto a mesh. This mesh can then be attached to the bottom of the leg of the Zebro. Like the Kirigami scales, these scales will also protrude more when the leg flexes when in contact with the ground.	<ul style="list-style-type: none"> <li>+ Flexed scales may help prevent sinkage</li> <li>+ Scales provide some grip in the sand</li> <li>+ Scales only become active when leg is engaged with the ground, otherwise flat</li> <li>++ Scales will act like claws on Rocky surfaces</li> </ul>	<ul style="list-style-type: none"> <li>- Requires some effort to design</li> <li>- Difficult to manufacture</li> <li>- Scales are connected to a mesh, which may easily break, or scales could easily detach</li> <li>-- Rock debris may get stuck in between scales creating stress points</li> <li>- Only friction in one direction Only friction in one direction, so will not work when traveling backwards</li> </ul>	<b>-1</b>
	Webbing	Webbing between toes 	In this a design a flexible mesh structure is connected between the toes of the Lunar Zebro to create a webbing between the toes. When walking on sand, the web prevents the leg from sinking deep into the regolith, while simultaneously pulling the toes together and clamping around the regolith and increase the grip. The mesh allows some sand to escape. When walking on rocky surfaces, any large protrusions on the surface can cause the web to deform up while at the same time pulling the toes together and gripping the protrusion.	<ul style="list-style-type: none"> <li>+++ Prevents sinkage</li> <li>++ Easy to design</li> <li>++ Relatively easy to manufacture</li> <li>+ Lightweight solution to increase ground contact area</li> <li>++ Web can pull toes closer together causing them to clamp around a patch of regolith or a protrusion</li> <li>++ Can be incorporated with other features, such as claws, scales on the bottom of the leg</li> </ul>	<ul style="list-style-type: none"> <li>- Provides no grip in the regolith if toes are not activated</li> <li>- Mesh is vulnerable to perforation</li> </ul>	<b>10</b>
	Webbing	Origami 	This design is based on the Yoshimura origami pattern. When paper is folded in this pattern it is possible to create a C-shaped patten this can expand and contract along the breadth of the paper. This design could be applied to the Lunar Zebro to create a leg that is able to expand and contract depending on the type of surface it is traveling on.	<ul style="list-style-type: none"> <li>+++ Prevents sinkage</li> <li>++ Surface are of the leg can be adjusted depending on the type of surface it is walking on</li> </ul>	<ul style="list-style-type: none"> <li>--- Complex to design</li> <li>--- Complex to manufacture</li> <li>--- Difficult to connect to axle of the Lunar Zebro</li> <li>- Not entirely circular</li> <li>-- Will interfere with spacing of legs from each other and the body</li> <li>-- Provides no grip in the regolith</li> </ul>	<b>-10</b>

Table 4.5: Concept Description and Scored Pros and Cons *continued*


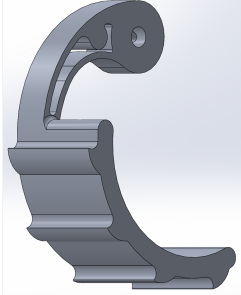
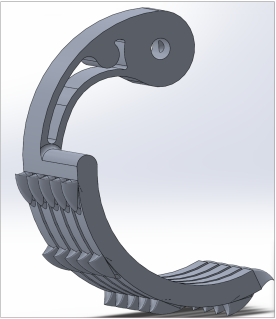
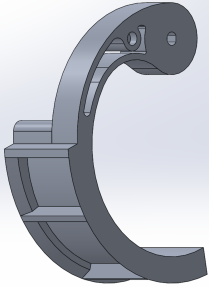

		Feature	Description	Pros	Cons	Score
Sandy/Rocky Terrain	Padding	Shape memory mesh 	The Lunar Environment makes it difficult to use traditional methods to create padding such as using material foam or liquids due to the lack of air and the extreme temperatures. NASA has used shape memory alloy meshes to create tyres. This technology can be used to create padding on the bottom of the legs of the Lunar Zebro. This material is able to deform any protrusion it is placed on and bounce back to its original shape when the protrusion is removed.	<ul style="list-style-type: none"> <li>++ Prevents sinkage</li> <li>++ Provides some grip in the sand</li> <li>+++ Material can mould to surface which enhances its grip</li> <li>++ Can deform to the surface it is on</li> <li>+ Sand can easily escape</li> </ul>	<ul style="list-style-type: none"> <li>--- Difficult to design</li> <li>--- Difficult to manufacture</li> <li>-- Difficult to connect to the leg</li> </ul>	<b>3</b>
		Rocky Terrain	Claws		This design uses the profile of the claws and creates a type of scooping claw. The sharp tips of the claws will be able to hook onto any surface irregularities in the rocky surfaces. The scope type shape may be an advantageous shape for a grouser when traveling on sand.	<ul style="list-style-type: none"> <li>+++ Easy to design</li> <li>+++ Easy to manufacture</li> <li>++ Able to hook onto some irregularities in rock face</li> <li>++ Can act like a paddle in the sand and provide more traction</li> </ul>
Claws				In this design, claws like the ones seen on the left will act as grousers on the toes of the Lunar Zebro. In this design, the leg will be divided into 5 toes. The individual toes will be able to flex upwards when a large protrusion is located underneath it. This means that the toes can “mould” to the surface beneath it and maximises the chance that individual claws are able to hook onto any surface irregularities.	<ul style="list-style-type: none"> <li>++ Relatively easy to design</li> <li>+++ Easy to manufacture</li> <li>+++ Can find very small irregularities and grip onto them</li> <li>++ Toes allow leg to mould to the uneven ground surface</li> </ul>	<ul style="list-style-type: none"> <li>-- Very high stress point at tips</li> <li>- Might rake through sand and not provide a lot of traction</li> </ul>

Table 4.6: Concept Description and Scored Pros and Cons *continued*

		Feature	Description	Pros	Cons	Score
Rocky Terrain	Compartments		This design is based on the hooves of Mountain Goats but without the soft central padding. This design consists of compartments with sharp edges. The sharp edges will be able to lock onto surface irregularities. While the compartments will help with compressing sand thereby prevent sinkage and providing grip	<ul style="list-style-type: none"> <li>+++ Easy to design</li> <li>+++ Easy to manufacture</li> <li>+ Compact sand in compartments preventing sinkage and providing grip</li> </ul>	<ul style="list-style-type: none"> <li>--- Suitable for sandy terrain but not much benefit for climbing rocky terrain without soft pad in between compartments</li> <li>-- The sharp edges may not be able to find many surface irregularities as the Lunar Zebro is not capable of walking sideways and in that way hooking onto surface irregularities</li> </ul>	<b>2</b>
	Rough Surface		This design makes use of sandpaper on the bottom surface of the Leg	<ul style="list-style-type: none"> <li>+++ Easy to design</li> <li>++ Relatively easy to manufacture</li> <li>+++ Will increase friction on solid surfaces significantly</li> </ul>	<ul style="list-style-type: none"> <li>--- Easily worn down</li> </ul>	<b>5</b>



#### 4.1.4. Final Concept Selection

From the above Tables, it can be seen that the concept with the hair located on the bottom of the leg and the leg with the web feature in the middle scored the highest from the granular terrain section. The two concepts that included the claw features scored the highest for the rocky terrain section, therefore, these concepts will be further developed to be manufactured into a prototype.

## 4.2. Concept Development and Manufacturing

The purpose of these designs are to create prototypes of the different concepts selected. While there are many different ways to manufacture and assemble the leg designs, the main focus of these designs are to create simple prototypes which are easy and low-cost to manufacture and assemble. These prototypes will be used to perform simple tests, therefore, they will not experience a lot of wear and so they do not need to be very durable. Thus, these legs will be manufactured using 3D printing methods and will be made from either PLA or resin, depending on the printing resolution needed.

### 4.2.1. Hair Leg

#### Hair Selection:

The first thing that needs to be decided before designing the Hair Leg is the type of hair that should be incorporated into the design. This will affect the design of the Hair Leg, as some features may need to be incorporated into the design to integrate the hairs. Therefore, several hair options were considered:

1. **FDM 3D printed hair:** It is possible to 3D print hair using an FDM printer by bridging the individual strands between two points and then cutting the bridge to free the strands once printing is complete. It would be possible to print these hairs along the bottom of the Lunar Zebro leg using a similar method.

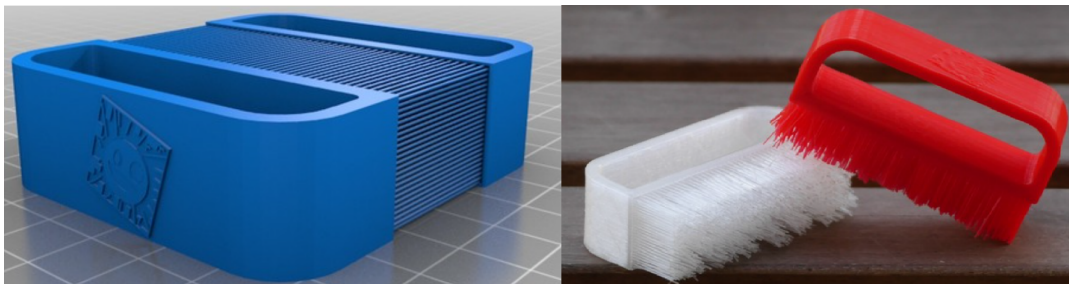


Figure 4.3: FDM 3D Printed Boulder Brush [70]

2. **SLA 3D printer hair:** A research team at MIT developed a method for 3D printing hair-like structures smaller than 100 microns using SLA 3D printers [71]. It is possible to print hair on flat and curved surfaces using this technology and the hair structure can be modified to vary the hair geometry such as height, thickness, angle and profile. This technology was further developed by OTP Industries. It would be possible to use this technology to incorporate hair onto the bottom of the Lunar Zebro Leg.

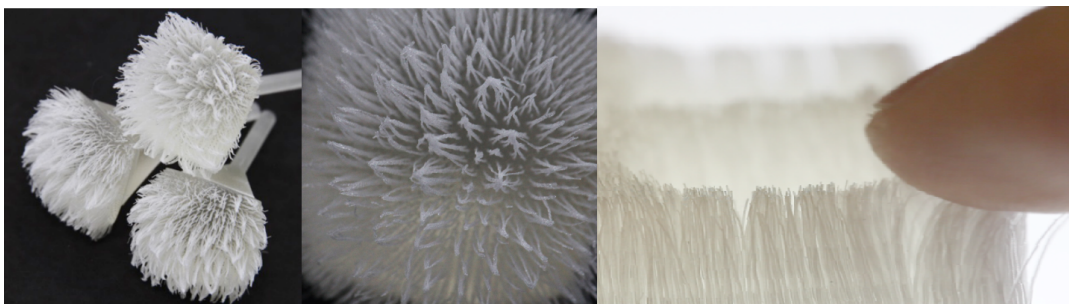


Figure 4.4: Cilia developed by MIT [71]

3. **Long-Haired Fabric:** It is possible to buy hairy fabrics from a fabric store. These fabrics have a range of different lengths, but generally, the hairs are soft and not very dense. An example of this fabrics is shown below. This type of fabric can be cut and glued to the bottom of the Lunar Zebro Leg.

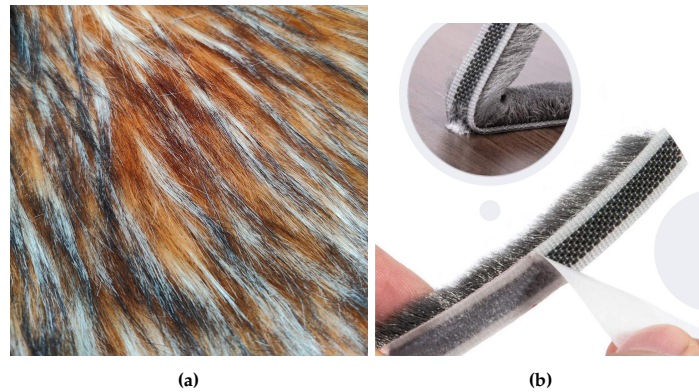


Figure 4.5: (a) Hairy fabric (b) Draft Brush strip

4. **Draft Brush Strip:** Draft brushes have short, densely packed hairs as shown in the Figure above. The density of the hairs aids with making the brush stiff. These strips can be cut to the length of the Lunar Zebro leg and stacked side by side.

Most of these options were created and tested out to get a better understanding of how these hairs would work on the bottom of the leg. An attempt was made to 3D print the hairs using an SLA printer, however, the prints failed. An effort was made to contact MIT and OPT Industries to get a sample of the Cillia hair, however, there was no response. The rest of the options were either made or bought. Several observations were made which helped narrow down the options to one:

1. **FDM 3D printed hair:** The printed hairs were very thick and some of the hairs stuck together during printing. When weight was applied to the patch of hairs, they would either permanently deform or break. In addition to this, it was difficult to cut all the hairs to the same length, making the surface uneven.
2. **Long-Haired Fabric:** The hairs were very thin, soft and a bit too long. In addition to this, the hairs were not densely packed. The worry was that the hairs would fold over instead of digging into the regolith to provide the necessary braking mechanism. Attempts were made to trim the hairs, but it was difficult to trim all the hairs to the same length.
3. **Draft Brush Strip:** The hairs were slightly stiffer than the long-haired fabric and were densely packed. The hairs are sewn into the strip in such a way that the hairs stick straight up, which would aid with the hair digging into the regolith.

From these observations, it was decided that the Draft Brush Strip would be used to add hairs to the Hair Leg Design.



### Final Hair Leg Design:

The Draft Brush Strip is a bit stiff, which makes glueing the strip to the flat bottom of the leg difficult. Therefore, it was decided to add lips to the ends of the length of the leg, under which the edges of the strips can be placed to prevent them from popping up as shown below:

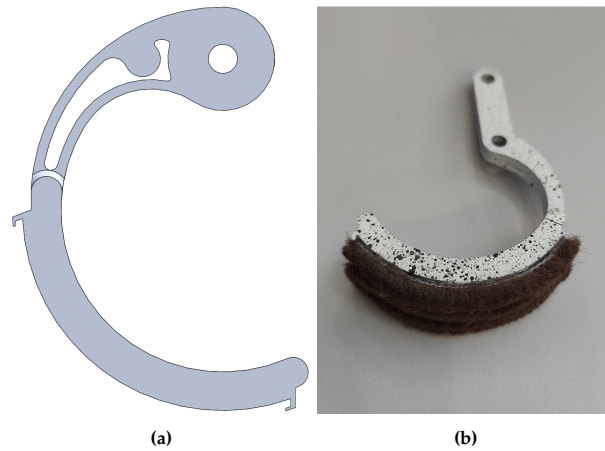


Figure 4.6: (a) Hair Leg Design including Lip feature (b) The final Hair Leg design used during testing

The leg itself is then manufactured using an FDM printer and the hair strips are glued to the bottom. The final manufactured Hair Leg can be seen in Figure 4.6 above.

### 4.2.2. Web Leg

#### Web Selection:

Like the Hair Leg, there are several different options that can be used to make the mesh webbing between the toes of the Web Leg. These options are mentioned below and the reason why they were used or not in the final design is given:

1. **Thin sheet metal which has been laser cut:** A mesh was cut into a 0.5 mm<sup>1</sup> thick piece of sheet metal that would fit between two toes of the leg. The thickness of the sheet metal and the size of the webbing meant that the webbing was not able to bend when a force was applied to the webbing which means that the desirable traits of the webbing were lost. Therefore this option was not considered further.

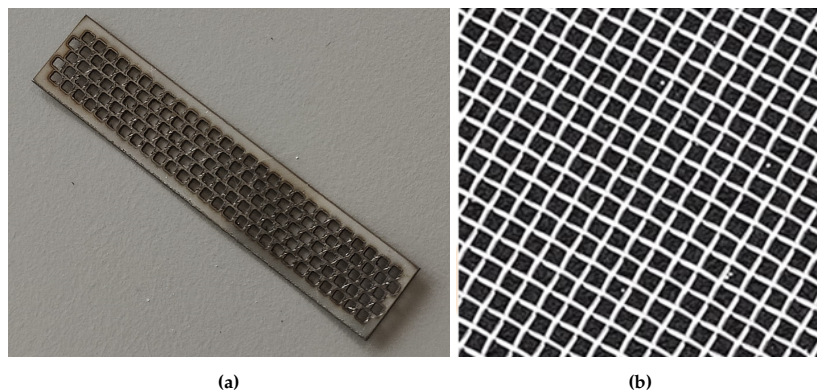


Figure 4.7: (a) Laser cut sheet metal (b) Woven steel wires

2. **Woven steel wires:** Steel wires woven into a mesh were also considered. However, just like the sheet metal, the wires were too stiff and were not able to bend enough when a force was applied to the webbing. Therefore, this mesh was not considered any further.

<sup>1</sup>0.5 mm thick sheet metal was used as it was the thinnest material in the IWM workshop

3. **Hexagonal mesh:** A hexagonal mesh, such as the ones used in mosquito netting was considered. This type of mesh was able to deform when a force was applied to it. However, there was no stiffness in any direction. This means that the mesh did not easily pull the two toes closer together.

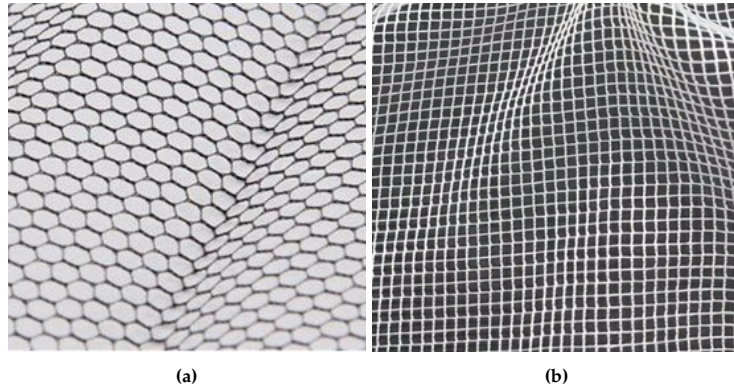


Figure 4.8: (a) Hexagonal Mesh (b) Square Mesh

4. **Square mesh:** A square mesh, such as the ones used in mosquito netting was considered. This type of mesh was able to deform when a force was applied to it and the mesh had a stiffness across the length and width of the mesh which allows it to easily pull the two toes closer together. Therefore, this mesh was used for the final Web Leg design.

#### Final Web Leg Design:

The final design of the Web leg includes two toes between which the square mesh will hang. The mesh will be connected to the leg by glueing it to the bottom of the leg and then glueing a cover (indicated in blue in Figure 4.9a) on top of the mesh. The main body of the leg has a stop (indicated in green in Figure 4.9a) which ensures the mesh cover is located properly. The body of the leg was printed using an SLA printer and it was printed using a tough resin. This printing method and material was used because the joint between the two toes is prone to breakage when it was printed using an FDM printer with PLA.

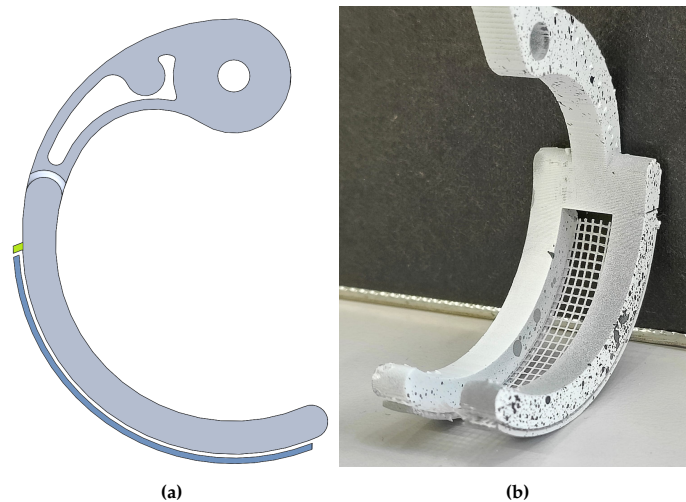


Figure 4.9: (a) Web Leg design (b) The final Web Leg design used during testing

### 4.2.3. Paddle Leg

The Paddle Leg was much more simple to design. For this design, a claw-like grouser with the same height, width and location as the grousers on the Original Lunar Zebro leg was created. Similar to the claws of monitor lizards (as mentioned in Chapter 3), the claw-like grousers are short, thick and have a sharp tip, as seen in Figure 4.10a. The Paddle Leg was printed with tough resin using an SLA printer. This printing method was used to increase the resolution of the print so that the details of the claw grousers are not lost.

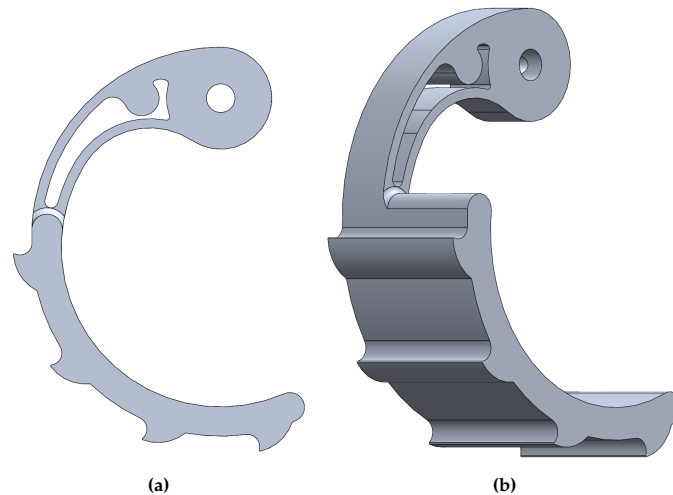


Figure 4.10: The final Paddle Leg design

### 4.2.4. Claw Leg

The Claw leg has been divided into 5 toes as shown in Figure 4.11a. Similar to the Paddle leg, the Claw leg uses the same claw profile, however, these claws have been lofted and converge at a point to make up the tip of the claw. Like the claws of dogs, and other animals, the inner profile of the claw is concave. This feature will allow the claws to scoop regolith and aid with traction. In addition to this, additional claws are located at the tip of the toes. This is to further increase the possibility of the Claw leg hooking onto surface irregularities, especially when climbing. In addition to this, the width of the Claw Leg was increased so that the total contact area with the ground is the same as the other legs. The Claw Leg was printed with tough resin using an SLA printer. This printing method was used to increase the resolution of the print so that the details of the claws are not lost.

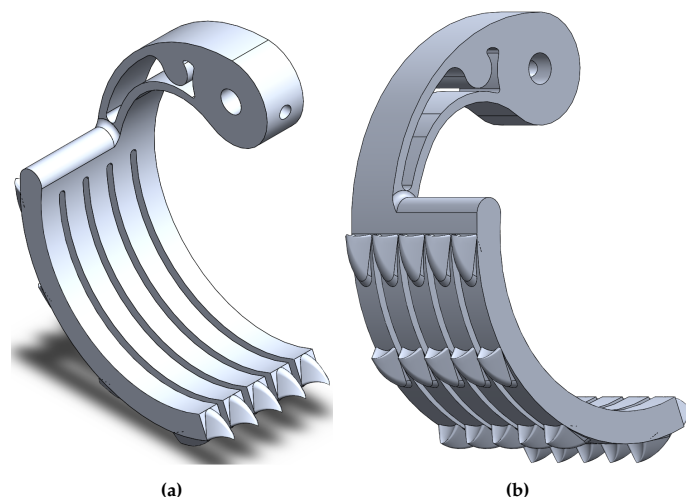


Figure 4.11: The final Claw Leg design

# 5

## Experimental Surfaces

The next step is to test the trafficability of the designed legs individually and all together on the rover. These tests will be performed in a testbed that contains Lunar Simulant, and on various rough surfaces. Before these tests can be designed and performed, it is important to determine the necessary dimensions of the testbed. In this chapter, some information on the Lunar Simulant is provided. In addition to this, the theory used to determine the dimensions of the testbed is described and the results are shown. Furthermore, the procedures used to prepare the Lunar Simulant before every experiment is described. From there, the types of rocky surfaces used for the individual and rover tests are described.

### 5.1. Regolith Surface

The surface of the moon is mostly covered in regolith, therefore, tests will be done to individually measure the performance of each of the legs on a Lunar regolith simulant, as well as the performance of the walking rover with different legs.

#### 5.1.1. Regolith Simulant

The experiments will be performed using LHS-1 Lunar Highlands Simulant from Exolith Lab. When working with the simulant, certain precautions need to be taken as the simulant is classified as a health hazard as it may cause cancer by inhalation through prolonged exposure. For this reason, a risk assessment was performed to determine all the precautionary measures that need to be taken when handling the simulant and when performing any experiments. This risk assessment and the SDS for the Lunar Simulant can be found in Appendix F.

#### 5.1.2. Testbed Dimensions

The dimensions of the testbed are important to ensure that any boundary conditions from the walls and floor of the container do not interfere with the soil disturbance caused by the legs of the Lunar Zebro during experiments. In addition to this, the testbed dimensions must be able to accommodate the size of the rover and allow it to walk the span of its own length. A visual representation of the testbed dimensions is shown below.

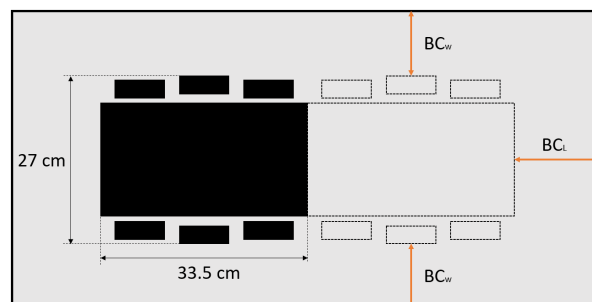


Figure 5.1: Testbed dimensions overview

The length of the rover is 33.5 cm and the width is 27 cm (Appendix E). Therefore the testbed dimensions need to at least be:

$$Length = (2 * 33.5cm) + 2 * BC_L \quad (5.1)$$

$$Width = 27cm + 2 * BC_w \quad (5.2)$$

Where  $BC_L$  is the boundary condition across the length of the foot and  $BC_w$  is the boundary condition across the width of the foot.

In literature, there is no standard method for determining the dimensions of a testbed. In most cases, the dimensions of the testbeds are merely stated without any reason given for the choice of size. However, Meirion-Griffith and Spenko [72], stated in their paper that they used Terzaghi's bearing capacity theory to determine their testbed dimensions, therefore, the same method will be used in this case.

### 5.1.3. Bearing Capacity in the Transition Zone

Terzaghi's bearing capacity theory is dependent on the type of soil used and can be divided into three modes [73]:

1. General shear failure:  $\phi > 36^\circ$
2. Mixed/Transition zone:  $28^\circ < \phi < 36^\circ$
3. Local shear failure:  $\phi < 28^\circ$

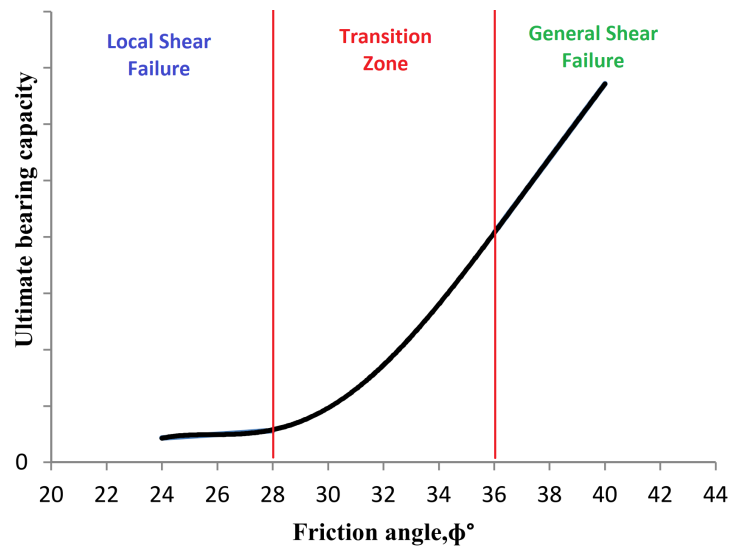


Figure 5.2: Modified Internal friction angle vs Ultimate bearing capacity [73]

For general shear failure conditions, the internal friction angle (IFA) remains the same, and for local shear failure, equation 5.3 is used to adjust the value of the internal friction angle. However, for internal friction angles in the transition zone, there is no equation to adjust the value.

$$\phi' = \arctan(2 \tan(\phi)/3) \quad (5.3)$$

The value of the internal friction angle of the regolith simulant is  $31.49^\circ$ <sup>1</sup> and therefore falls within this transition zone. As a result, any calculation performed using Terzaghi's bearing capacity theory will fall between the results of general shear failure and the local shear failure.

<sup>1</sup>The internal friction angle was ascertained through personal communication with the Exolith Lab team

### 5.1.4. Terzaghi's Soil Bearing Capacity

To determine the testbed dimensions, Terzaghi's shear failure surface (shown below) was used to determine the minimum test bed dimensions. This was done to prevent any boundary conditions created by the wall of the testbed from interfering with the behaviour of the regolith during experiments.

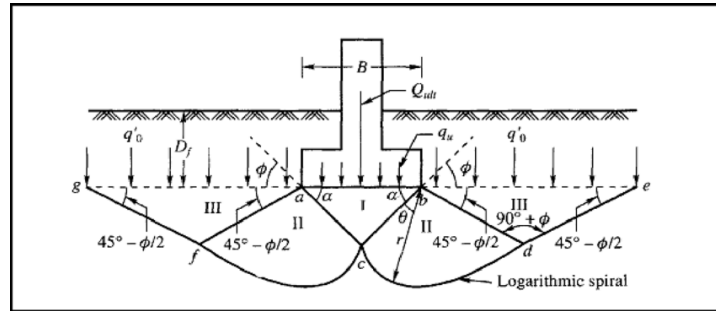


Figure 5.3: General shear stresses based on Terzaghi's soil bearing capacity (Terzaghi 1943)

The three zones indicated in the Figure above are as follows:

- Zone I: Active Zone
- Zone II: Radial Shear Zone
- Zone III: Passive Zone

Calculations were done for the two strips which are created by the foot when interacting with the regolith. The first is across the length of the foot,  $L_i$ , which is dependent on the amount the leg sinks. The second is across the width of the foot,  $b$ , which always remains constant no matter what the sinkage is. These strips are visually represented in the figure below.

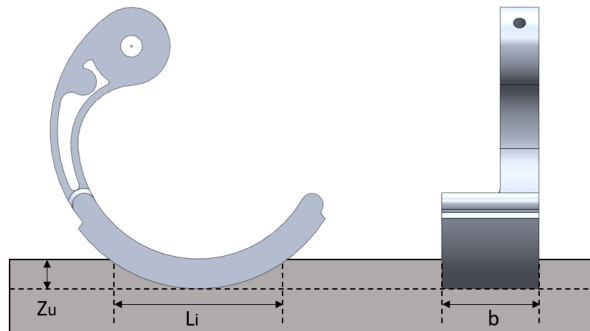


Figure 5.4: The geometry of the leg contact area during sinkage

#### Determining the contact length across the length of the foot

To determine the contact length,  $L_i$ , across the length of the foot, the sinkage of the leg is needed. This can be calculated using the Bernstein–Goriatchkin model, as seen in equation 2.3 in Chapter 2. Unfortunately, the values of  $k_c$  and  $k_\phi$  are not known and therefore the sinkage cannot be predicted. However, the ultimate sinkage<sup>2</sup>,  $z'_u$ , can be calculated using equations 5.4 and 5.5 [74]. This value will be used to determine the testbed dimensions.

$$z'_u = K_u \sqrt{L_i b} \quad (5.4)$$

Where:

$$K_u = 0.5 - 0.01\phi \quad (5.5)$$

<sup>2</sup>It is assumed that the leg will not sink to the ultimate sinkage point. However, this depth is used to determine the dimensions of the test bed.



As mentioned earlier the internal friction angle of the regolith lies within the transition zones. Therefore, the ultimate sinkage was calculated using both the original internal friction angle and the modified internal friction angle. The actual value of the ultimate sinkage will fall between these two values. These calculations can be seen in Appendix G. The results are as follows:

**Table 5.1:** Ultimate sinkage ( $z'_u$ ) and contact length ( $L_i$ ), for the original and modified internal friction ( $\phi$ )

IFA	$\phi$ (°)	$Z'_u$ (mm)	$L_i$ (mm)
Original	31.49	4.7513	32.9450
Modified	22.2138	8.0084	41.5338

### Results for the Test bed Dimensions

Using the results from Table 5.1, it is now possible to calculate the dimensions of the test bed using Terzaghi's shear stress failure surface. These calculations can be found in Appendix H and the results are shown in the table below:

**Table 5.2:** Testbed Dimensions for the different internal friction angles and contact lengths

	Breath, $b$		Length, $L_i$	
	Depth (cm)	Width (cm)	Depth (cm)	Width (cm)
Original IFA	2.62	41.65	4.31	91.12
Modified IFA	1.90	35.67	3.94	85.01

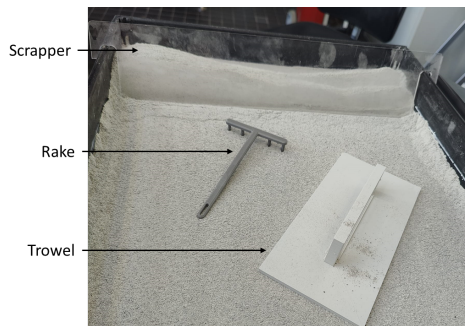
From the results it can be seen that the testbed dimensions will fall within a range of values:

- Length: 85.01 - 91.12 cm
- Width: 35.67 - 41.65 cm
- Depth: 1.90 - 4.31 cm

Therefore, the dimensions<sup>3</sup> of the testbed container were chosen to be 100 cm x 42 cm x 15 cm. The testbed container will then be filled with regolith to a depth of roughly 8 cm. The extra height of the container is to prevent any regolith from spilling over and to try prevent any regolith from flying out during rover tests.

### 5.1.5. Test bed regolith preparation

Before every test, the regolith needs to be prepared. This is done by first raking the regolith, and then smoothing and levelling it with a scraper. The scraper is constrained by the walls of the test bed which will ensure the regolith is level and will prevent the scraper from compressing the regolith too much. This procedure is done to remove any effects/disturbances that previous tests had on the regolith and to prepare the regolith for the next test. A trowel was also made to help flatten and smooth the regolith but it was found to be unnecessary.



**Figure 5.5:** Tools used to prepare the Regolith regolith for tests

<sup>3</sup>An error occurred during the manufacturing of the testbed container, and the dimensions are 98.4 cm x 40.4 cm x 13.4 cm. However, this will have no impact on the single-leg tests and it will have very little impact on the full rover tests as the Terzaghi Method is an overestimation of the soil disturbance zone of the leg



## 5.2. Rocky Surface

Besides regolith, the surface of the moon also consists of a variety of different rock surfaces which vary in size, shape and rock type. For the purpose of this report, tests will be done on flat rough surfaces. The aim of this is to show the performance of the legs and rover on a rough surface with the assumption that these results are relative to the types of rock surfaces found on the moon.

### 5.2.1. Single Leg Tests

For the Single Leg tests, two different surfaces are used with different surface roughness. The first is sandpaper with a surface roughness of 60. The second is a roof tile with an unknown roughness. The roof tile is made up of individual grits and is more rough in comparison to the sandpaper. These surfaces are shown below.

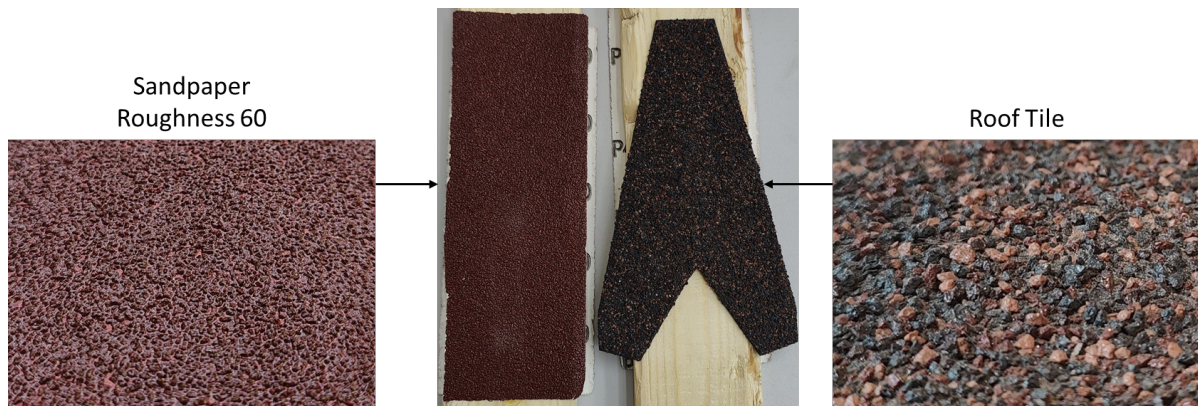


Figure 5.6: The two rough surfaces used for testing: Sandpaper and Roof Tile

The reason two different rough surfaces were used was to see if surface roughness impacts the performance of the individual legs since the moon is covered in rocks of different surface roughness.

### 5.2.2. Rover Tests

For the rover tests, two strips of sandpaper with a surface roughness of 60 were used. The strips of sandpaper were placed parallel to one another with a spacing wide enough so that the legs on each side of the rover will have full contact with one strip of sandpaper as shown in the figure below.

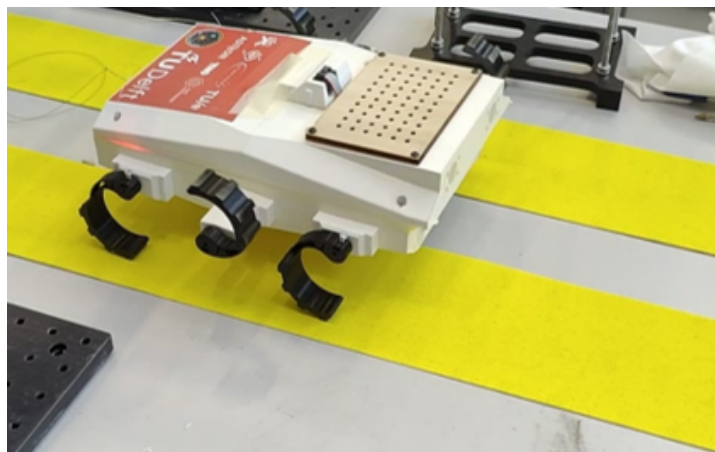


Figure 5.7: Sandpaper strips used for rover testing

# 6

## Single Leg Experimental Set-up

To get a better understanding of the performance of individual legs on different lunar terrains, single-leg tests need to be performed on each of the legs and the results compared.

### 6.1. Measuring Trafficability

From the Terramechanics discussed in Chapter 2, a good indicator of the trafficability of a wheel is to measure its drawbar pull. In literature [75] [76] [77] [78], this is done using a single-wheel test set up as shown in the images below. These test set-ups work by driving the wheel forward using a motor. At the same time, the wheel is attached to a dragging mechanism, which is used to induce slip and control how fast the leg is moving forward. A force sensor is then used to measure the drawbar pull between the rotating wheel and dragging mechanism. In these experiments, the drawbar pull is measured for different induced slips.

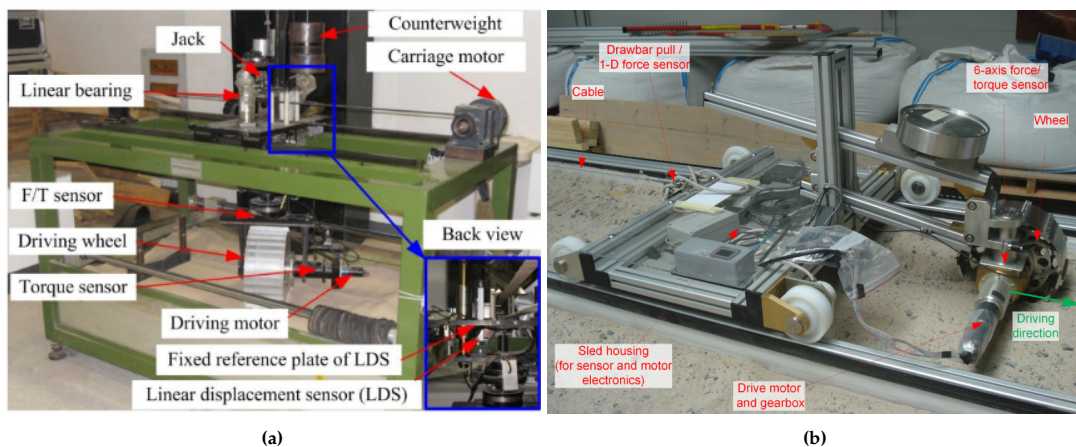


Figure 6.1: (a) Single wheel test bed [79] (b) RUAG Space single-wheel test bed [75]

However, this type of test set up is difficult to apply to the leg of the Lunar Zebra as the ground contact speed is not constant across the bottom of the leg of the Lunar Zebra because the centre of rotation of the leg is not located at the axis of the motor, as illustrated in Figure 6.2a. Therefore, the controlled slip vs drawbar pull test set-ups that are normally performed on wheels would have to be modified to have a specialized motor that rotates the leg at a varying rate to ensure that the ground contact speed is constant, or the dragging mechanism would have to be pulled at a varying rate to induce the necessary slip rates. As a result, a different way of measuring drawbar pull is needed.

Another measure of how well a wheel will perform on granular terrain is to measure how much the wheel sinks into the terrain. In single-wheel test setups, this is normally done by measuring how much

the axis of the wheel sinks as it is driven across the sand. Once again, this is not so simple to do with the leg of the Lunar Zebro as the axis of the leg hops as it walks as shown in Figure 6.2b. Therefore, a different method for measuring sinkage is needed.

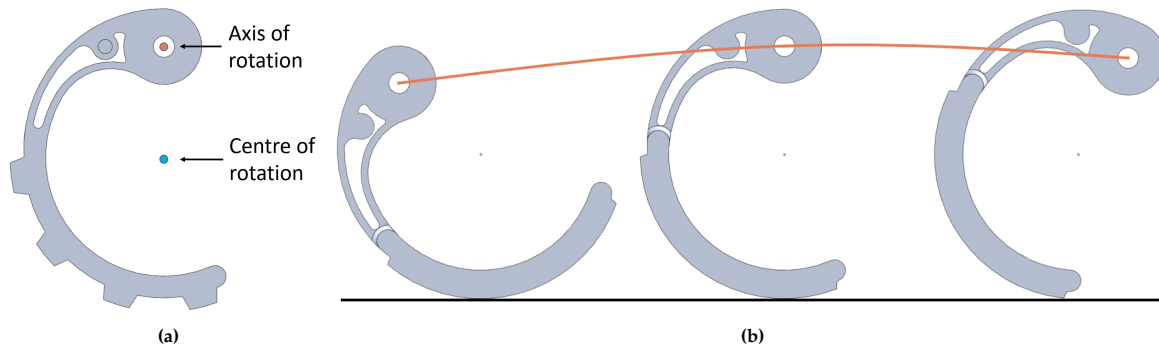


Figure 6.2: (a) Axis of rotation and centre of rotation of the Lunar Zebro Leg (b) Hopping motion of the Lunar Zebro Leg

## 6.2. Test leg

The design of the leg was modified slightly to include a second point of attachment to the test rig as shown in Figure 6.3a. This was done to allow for the option of preventing the leg from rotating during some experiments. As seen in Figure 6.3a, the second attachment point is located in such a way that the leg would be constrained so that the bottom of the C is centred on the ground. In addition to this, the width of the foot protrudes equally from each side of the leg. Normally the foot of the leg is either aligned left or right depending on which side of the rover the leg is positioned on.

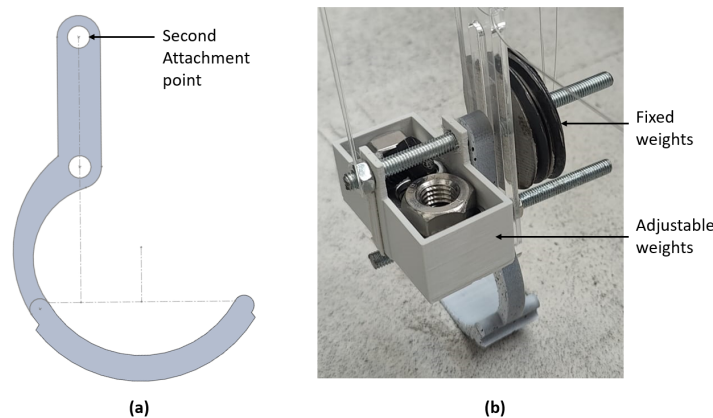


Figure 6.3: (a) Test leg design showing second attachment point (b) Adjustable weight system for the different legs

The weight of the legs used in the experiments will be  $1/6$ th (due to the gravity on the moon) of the weight experienced by the middle legs of the rover. The middle leg carries half the weight of the rover when walking, whereas the front and back legs only carry a quarter of the weight. The rover weighs 2 kg (Appendix E), therefore the weight used for the purpose of the experiment is 167 grams <sup>1</sup>. The six legs all have different weights, therefore, the experimental set up has a fixed weight on one end and an adjustable weight bucket on the other end. This can be seen in Figure 6.3b. Weight can be added or subtracted from the weight bucket to ensure the weight experienced by each leg is within 0.1 grams of one another.

<sup>1</sup>In 2.4 it was noted that the reduced normal load of the wheel is less important than the reduced bearing capacity of the soil in the sinkage and slip performance of a wheel

### 6.3. Measuring Sinkage

For this test, static sinkage tests will be performed on each of the legs. Digital Image Correlation (DIC) software is then used to track the sinkage of the leg. For this software to work, the leg face which is being recorded needs to have a speckle pattern. This was done by spray painting the face of the leg white and then flicking black paint on top. During testing, the leg is slowly lowered onto the regolith simulant using a lowering device. This device consists of a handle which is constrained to slide up and down and two looped ropes that can hook around the bolts carrying the leg. The leg is connected to a slider which allows the leg to slide up and down. The leg is prevented from rolling when coming into contact with the simulant, as the two bolts are constrained by the slider. As the leg is being lowered, a camera is recording a video of the motion of the leg at a frame rate of 30 fps. When the leg has fully sunk into the simulant, the two looped ropes slack off the bolts so that the full weight of the leg is resting on the simulant.

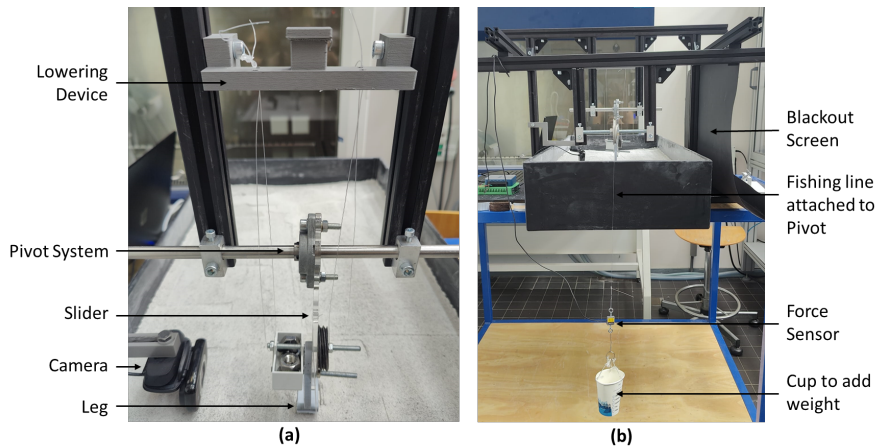


Figure 6.4: Set up used for sinkage experiments and Pivot Thrust experiments

The recorded video is then converted into individual black-and-white frames using *Blender*. These frames are then sorted through manually to find the frame where the leg just touches the simulant and where it is fully resting in the simulant. Using *Ncorr* (an open-source DIC *Matlab* program) these two images are analysed and compared to determine how much the leg sank into the simulant. A step-by-step outline of how the *Ncorr* program is used is shown in Appendix I.

### 6.4. Measuring Drawbar Pull

The drawbar pull of a leg can be broken down into two separate measurements: Thrust and Rolling Resistance. Since the usual methods of measuring drawbar pull are difficult to apply to the leg of the Lunar Zebro, the thrust and rolling resistance of the legs will be measured separately to get a better understanding of the trafficability of the different legs. In addition to this, a simple modified drawbar pull test will be used to show the overall performance of the leg, however, this slip of the leg cannot be controlled and will differ from leg to leg.

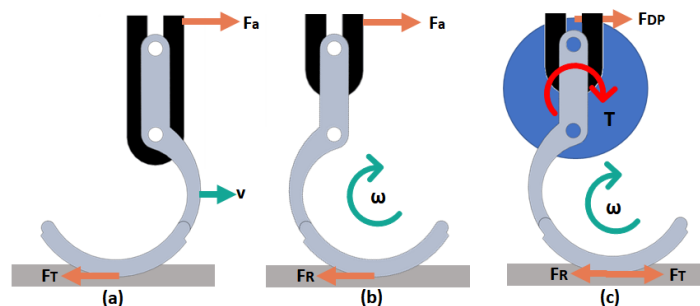


Figure 6.5: Force Diagrams for: (a) Pivot Thrust and Drag Thrust (b) Rolling Resistance (c) Modified Drawbar Pull



Since the rover will be travelling at a very slow speed of 1 cm/s (Appendix E), it is reasonable to consider the leg-soil interaction as a quasi-static problem [77]. Therefore very simple tests can be used to determine the thrust and rolling resistance of the leg. The thrust of the leg can be determined by pulling the leg backwards and determining the force required to make the leg move. The leg can be pulled by pivoting it or dragging it on rollers. For these methods to work, the leg is not allowed to rotate and is constrained by the slider and the two attachment rods. To determine the rolling resistance, the leg is allowed to rotate freely by only connecting the top attachment point to the slider. A force is then applied to the slider causing it to be pulled forward at a certain velocity. The leg is then allowed to rotate, and the force needed to make it rotate freely is the rolling resistance. Lastly, to determine the modified drawbar pull of the leg, the leg is also allowed to rotate freely. A force is applied to a pulley system which in turn applies a torque to the leg making it 'walk' forward a step. The force required to apply the torque is then a modified version of the drawbar pull of the leg as the applied force is also pulling the leg causing it to slip forward. Force diagrams showing the forces acting in the thrust, rolling resistance and modified drawbar pull are shown in Figure 6.5. In subsequent sections, the modified drawbar pull is simply referred to as drawbar pull.

### 6.4.1. Thrust

#### Pivot Thrust

The test set-up as shown in Figure 6.4 was used to measure the thrust when the leg is pivoted. This test set up works by attaching the leg to the pivot system. The pivot system is connected to a force sensor and cup, to which weight can be added. There is also a camera that is used to capture images of the leg so that they can be used to determine the exact moment the leg moves as weight is added to the cup. Using *Labview* the camera and the force sensor are linked so that the camera captures an image at each interval that the force is being measured. These images are then converted into a video, using *Blender* and the video is analysed using the *Kinovea* program to determine the exact moment that the leg moves. A step-by-step outline of how the Kinovea program was used is shown in Appendix J.

#### Drag Thrust

The rest of the tests use a different test set-up to the sinkage and pivot thrust tests. In this test set-up, the vertical sliding device that holds the leg is attached to a drawer rail sliding system which was attached to the test frame as shown in Figure 6.6. The drawer rails allow the leg to move backwards and forwards across the test surface.

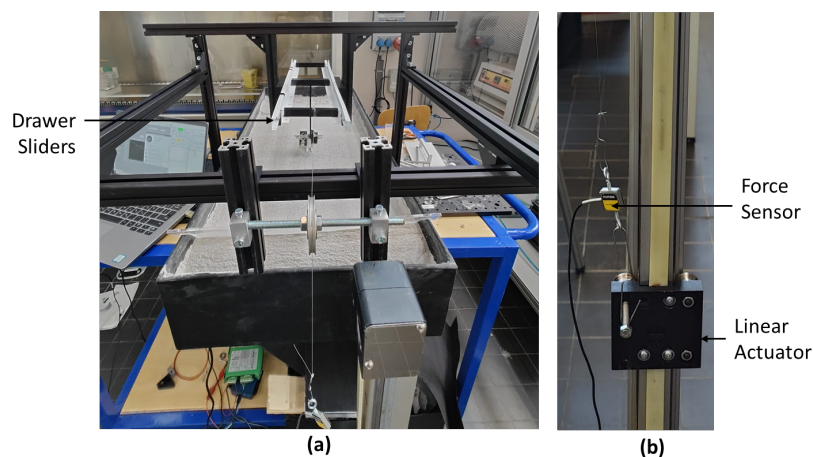


Figure 6.6: General test set up used for the drag thrust, rolling resistance and drawbar pull tests

For the drag thrust test set-up, the leg is constrained like in the pivot thrust test so that it cannot rotate. The sliding device is pulled at a constant rate using a Linear actuator. A force sensor is used to measure the force required to drag the leg across the surface at a constant rate. The resultant soil disturbance is shown in Figure 6.7a.

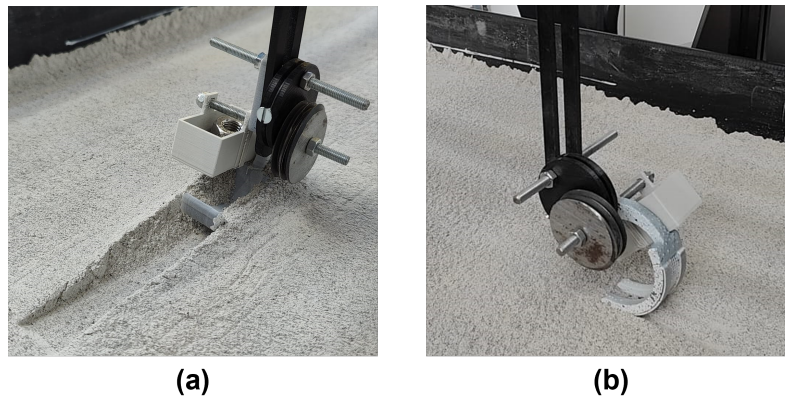


Figure 6.7: (a) Drag Thrust set-up (b) Rolling Resistance set-up

### 6.4.2. Rolling Resistance

This test set up is very similar to the test set-up described in the drag force test, except the leg in the rolling resistance test is able to rotate freely and the leg is attached to the sliding system so that it is facing forward. This test set-up can be seen in Figure 6.7b.

### 6.4.3. Modified Drawbar Pull

For this test, the leg attachment points are connected to a pulley and attached to the sliding device in such a way as to allow the leg to rotate freely. The pulley system consists of a disk with a groove through which a fishing line runs. The fishing line is attached to the pulley through a screw which is screwed into the pulley and around which the fishing line is wrapped. The fishing line is then attached to the linear actuator and pulled at a constant rate, which then causes the pulley disk to rotate. This rotation results in the leg 'walking' forward a step. A force sensor is used to measure the force required to apply a torque to the leg across the step taken. This test set-up can be seen in Figure 6.8.

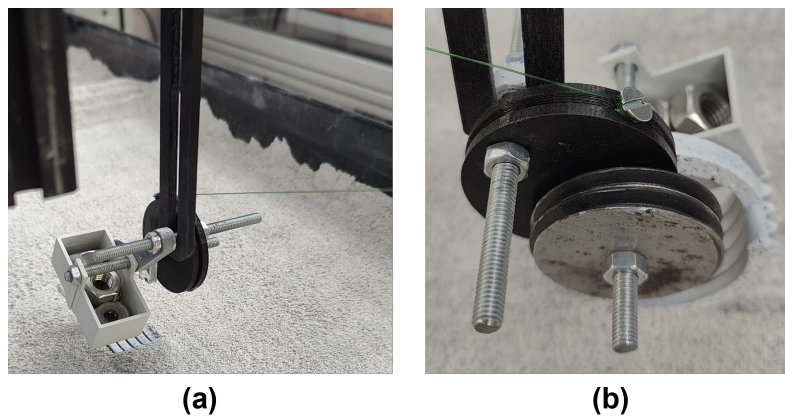


Figure 6.8: Modified Drawbar Pull set-up

## Single Leg Results and Analysis

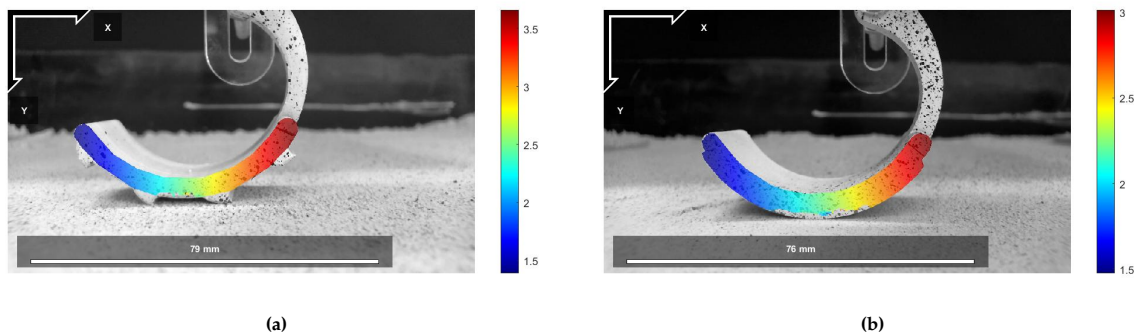
In this chapter, the data obtained from the various single-leg experiments are explained. From this, certain values are recorded and used to compare the performance of the different legs.

### 7.1. Experimental Data

Each experiment was performed three times for each leg. How this data was obtained and what it is showing is explained below using a sample of the data recorded. These samples are indicative of how all the data of the other legs appear and how they were recorded for comparison.

#### 7.1.1. Sinkage

The sinkage of the legs was determined from the moment the grousers of the Original, Paddle and Claw leg touched the regolith and the moment when the flat bottom of the Flat, Web and Hair Leg touched the regolith as shown in Figure 7.1. Liang et al. [80], suggested that grousers have very little influence on sinkage, however, in their study they used much larger wheels, and the width of the grousers was very small in comparison to the wheel contact surface area. In comparison, the grousers of the Lunar Zebro leg are wide with respect to the outer circumference of the legs, therefore, their height will be taken into account when measuring sinkage.



**Figure 7.1:** (a) Starting frame of the Paddle Leg to determine the total sinkage (b) Starting frame of the Flat Leg to determine the total sinkage

Although the legs were constrained to only move up and down the slider, and prevent full rotation during tests, it was found that the leg did rotate slightly as it settled into the regolith during the sinkage tests. As a result, the back of the foot sank lower than the tip as indicated by the gradient in the results in Figure 7.1. Therefore to determine the total sinkage of the leg, the sinkage values at the front and back tip of the legs were determined and the average of their values taken to determine the overall sinkage of the leg, as shown in Figure 7.2. The max and min markers of the images were not used to



determine the overall sinkage because their locations varied from test to test and were dependent on the coefficient correlation cut-off value.

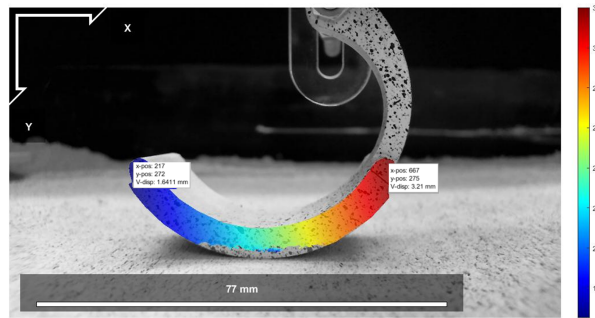


Figure 7.2: Max and Min values used to determine the overall sinkage of the different legs

### Sources of Error in Measurement

During the experiment, there are several ways errors can be introduced into the results. These sources and their values are listed in the table below:

Table 7.1: Sources of error in Sinkage experiment and their values

Sources of error	Value	(±) Value in mm
Starting frame	2 frames	0,05
Soil preparation	Compaction	0,5
Pixel - mm	Calibration	0,001
Point on the image	Pixel position	0,05
		0,601

Where:

- **Starting frame:** The starting frame indicating the moment the leg touches the regolith is manually chosen. There is no way to clearly choose which frame is the correct starting frame, and the starting frame could be between two frames. Therefore the potential error introduced into the measurement is 0.05 mm as this is the difference in distance between two frames
- **Regolith preparation:** Before each test, the regolith is prepared by raking it and then levelling it. Although measures are taken to control the properties of the regolith, exact repetition of the preparation is impossible. Therefore some variation of the regolith properties between tests is expected. As a result, the legs could sink more or less in one test than in other tests due to the compaction of the regolith or unseen air pockets in the regolith. As a result, the added error is 0.5 mm.
- **Pixel calibration:** The size of the pixels are calibrated using the markers on the legs. Some error is introduced when setting the line to calibrate the pixels which can result in an error of 0.001 mm
- **Max/Min point on the image:** The Max and Min points used to calculate the overall sinkage of the legs is manually chosen. This value changes depending on the pixel chosen and therefore an error of roughly 0.05 mm is introduced.

As a result of all these sources of error, the total potential error of the sinkage test is 0.601 mm, with the biggest source being the soil preparation.

### 7.1.2. Pivot Thrust

For this test, the Thrust force is determined at the moment the leg begins to move using the method described in Chapter 6. It was difficult to determine the frame in which the leg begins to move manually, therefore the program *Kinovea* was used to track a line marker in the video to determine the moment at which the leg moved. A result of this analysis is shown below (Figure 7.3), which shows the relative horizontal displacement of the two end points of the line marker that was placed on the images and tracked over time. As can be seen in the figure, the moment at which the program determines the two points move differs slightly as indicated by the green dots. Therefore, the mid point of these two values was used as the time stamp where the leg begins to move and is verified manually by analyzing the video frame by frame around that point. This time stamp is then cross-referenced with the measured force to determine the Thrust force of each leg.

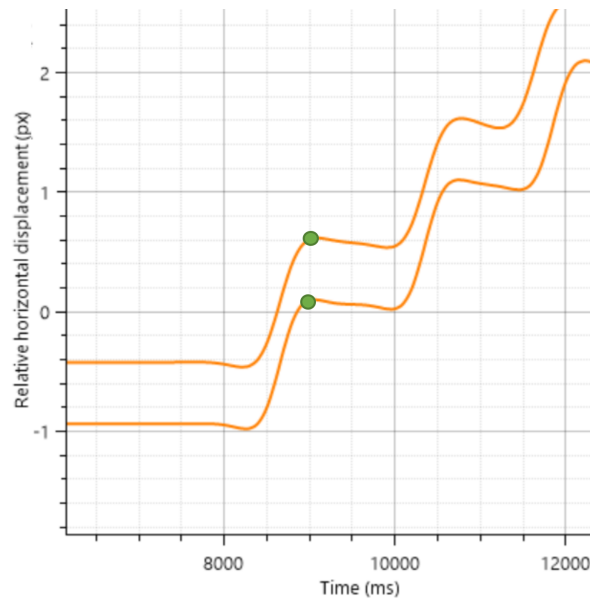


Figure 7.3: An example of the relative horizontal displacement graph of the Paddle Leg to determine the moment the leg moved

#### Sources of Error in Measurement

During the experiment, there are several ways errors can be introduced into the results. These sources and their values are listed in the table below:

Table 7.2: Sources of error in Pivot Thrust experiment and their values

Sources of Error	Value	Regolith	Rocky
		(±) Value in mN	(±) Value in mN
Frame	3 frames	15	15
Weight of the sensor	10,7g +- 5g	49,03	49,03
Force sensor resolution	2.5 N +- 2.5mN	2,5	2,5
Regolith preparation	Compaction	15	
Position on rocky surface	Grit contact		10
		81,53	76,53

Where:

- Chosen Frame:** The frame indicating the moment the leg begins to move falls within a range of frames as indicated by the program *Kinovea*. Although the midpoint of these frames are taken as the moving frame, the correct starting frame could fall elsewhere in this range. As a result, the error introduced into the measurement is on average 15 mN as the difference of force between frames is dependent on the pouring rate of the salt into the cup.

- **Weight of the sensor:** The weight of the force sensor contributes to the force experienced by the leg. This weight of the force sensor is not necessarily constant between measurements as the weight of the cable connected to the sensor may differ slightly depending on how much the cable is drooping. This is estimated to be roughly  $\pm 5$  g which is about 49.03 mN.
- **Force sensor resolution:** A 2.5 N force sensor was used with a resolution of 2.5 mN.
- **Regolith preparation:** Before each test, the regolith is prepared by raking it and then levelling it. Although measures are taken to control the properties of the regolith, exact repetition of the preparation is impossible. Therefore some variation of the regolith properties between tests is expected. As a result, the legs could sink more or less in one test than in other tests due to the compaction of the regolith or unseen air pockets in the regolith. As a result of the sinkage, the value of the force needed to pull the leg is impacted. This is estimated to introduce a difference of 15 mN into the measurement. This is only relevant to experiments performed on regolith.
- **Position on Rocky Surface:** At the start of every test, the legs are placed on the rocky surface, however, this position is not exactly the same every time. As a result, the leg's position in relation to the grits on the rocky surface changes every time, which means the legs may or may not hook onto the surface in the same way every time which will effect the thrust of the leg. This is estimated to introduce a difference of 15 mN into the measurement. This is only relevant to experiments performed on rocky surfaces.

As a result of all these sources of error, the total potential error of the pivot thrust test is 81,53 mN for regolith and 76,53 mN for rocky surfaces.

### Accuracy of this experiment

During the analysis of the results of the Pivot Thrust experiment, it was noticed that these results may not accurately reflect the Thrust of the legs. This experiment assumes that the thrust of the leg occurs when the leg begins to move, however initial movements of the leg in the regolith may be the leg settling into the regolith, and initials movements of the leg on the rocky surfaces may be leg catching onto the grits of the surface after which the thrust values of these legs may increase. Therefore, these results will not be used to compare the performance of the different legs. These results can be found in Appendix K.

### 7.1.3. Drag Thrust

An example of the force graphs of the Drag Thrust experiments performed on regolith and rocky surfaces are shown below. For the experiments done on regolith, it can be seen that the forces measured for the flat leg and paddle leg are both slowly and continuously increasing over time. This is because as the legs are being dragged over the regolith, the legs are bulldozing into the regolith, capturing regolith at the front of the leg while at the same time digging deeper into the regolith as shown in Figure 6.7a in Chapter 6. Therefore, the thrust force is measured at the first peak on the graph.

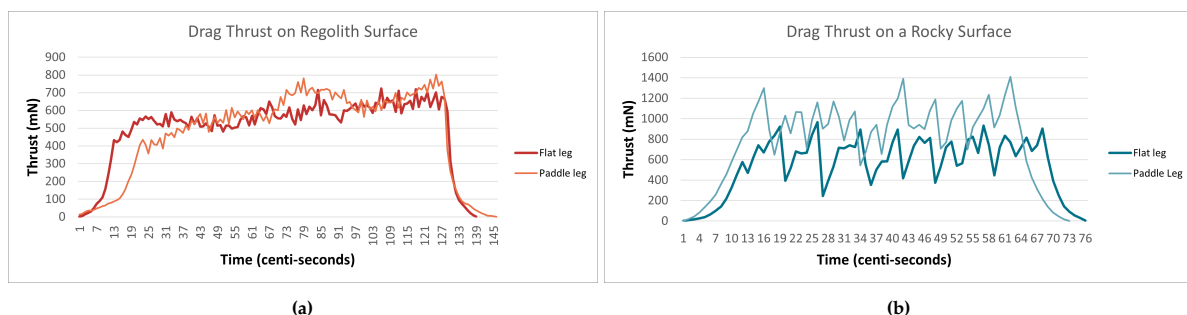


Figure 7.4: Drag Thrust graph of the Paddle Leg and Flat Legs on: (a) Regolith and, (b) Rocky Surface (Sandpaper)

For the experiments performed on the rocky surfaces (either the sandpaper or the roof tile) the bulldozing effect does not occur and therefore the force graph does not gradually increase over time. Instead, what the graph shows is the leg catching onto the rocky surface and then slipping forward before catching onto the surface again. This is evident by the jagged lines on the force graph. Therefore, for this measurement, the maximum force recorded during measurement is used as the thrust force of the

leg. The reason this is done instead of using the first peak value like with the regolith is that the grip of the legs is dependent on their location with respect to the grit on the rocky surface which is difficult to control across all tests.

### Sources of Error in Measurement

During the experiment, there are several ways errors can be introduced into the results. These sources and their values are listed in the table below:

Table 7.3: Sources of error in Drag Thrust experiment and their values

Sources of error	Value	Regolith	Rocky
		(±) Value in mN	± Value in mN
Weight of the sensor	10,7g ± 5g	49,03	49,03
Force sensor resolution	6 N ± 6 mN	6	6
Regolith preparation	Compaction	25	
Position on rocky surface	Grit contact		100
		80,03	155,03

Where:

- **Weight of the sensor:** Same reason as stated in the Pivot Thrust source of error explanation.
- **Force sensor resolution:** A 6 N force sensor was used with a resolution of 6 mN.
- **Regolith preparation:** This is estimated to introduce a difference of 25 mN into the measurement. This is only relevant to experiments performed on regolith.
- **Position on Rocky Surface:** This is estimated to introduce a difference of 100 mN into the measurement. This is only relevant to experiments performed on rocky surfaces.

As a result of all these sources of error, the total potential error of the drag thrust test is 80,03 mN for regolith and 155,03 mN for rocky surfaces.

### 7.1.4. Rolling Resistance

An example of the force graphs of the Rolling Resistance experiments performed on Regolith and Rocky Surfaces are shown below. The graphs show that initially the force needed to roll the leg increased sharply and then gradually begins to decrease.

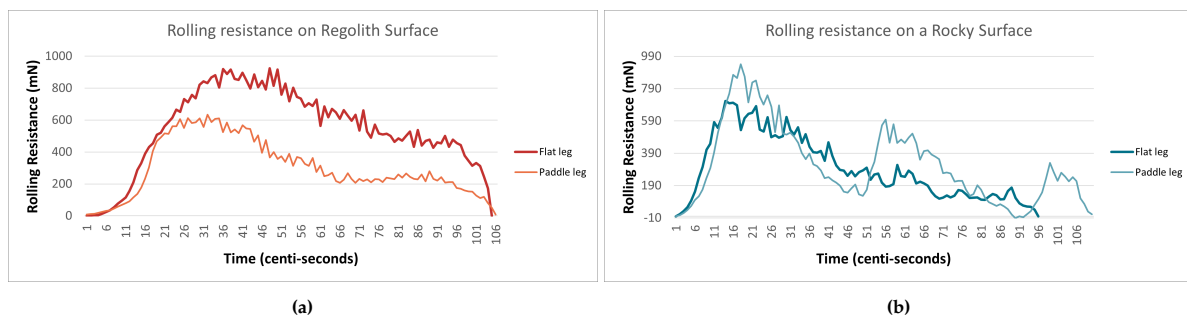


Figure 7.5: Rolling Resistance graph of the Paddle Leg and Flat Legs on: (a) Regolith and, (b) Rocky Surface (Sandpaper)

What this is showing is that initially energy is needed to lift the weight of the added mass up. Once this mass has reached a certain point, the maximum Rolling resistance is reached after which the mass aids with rolling the leg forward. However, why this point occurs so early in the rotation is unknown. It is expected that the peak point would occur when the centre of mass is directly over the centre of rotation on the ground, as this is the highest point the mass is lifted to. If that were the case, the peak force would occur later in the graph. This position and the approximate peak location is shown in Figure 7.6.

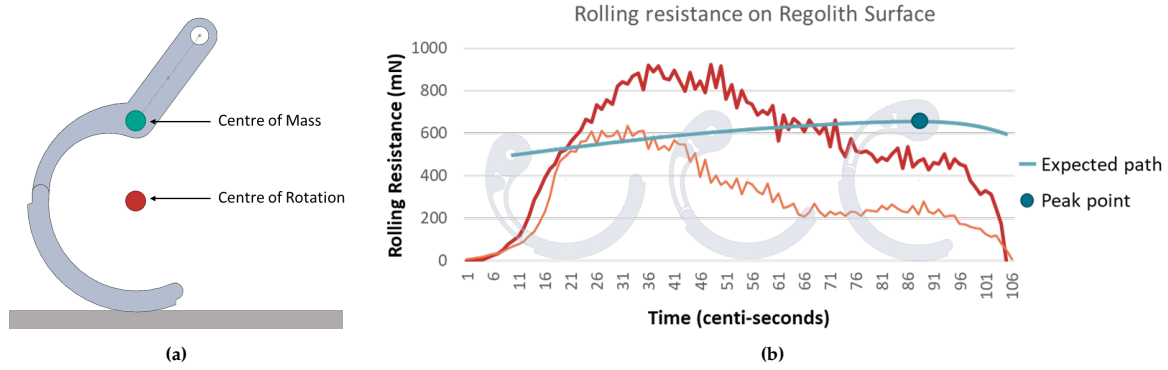


Figure 7.6: (a) Expected position for the occurrence of the maximum force (b) Approximate peak point on the rolling resistance graph

In figure 7.7b, the Rolling Resistance graph of the Paddle leg on a rocky surface shows three descending peaks. What this is showing is the moments the grouzers of the leg are coming into contact with the ground. These 3 peaks do not appear on the regolith tests as the regolith is able to deform and remove this effect from legs with grouzers.

As a result of the constantly changing value of the Rolling resistance, the maximum rolling resistance force experienced by each leg was used to compare the performance of the different legs. However, what is important to note in the Rolling resistance graphs is that the time taken to reach the peak force is longer on regolith then on a rocky surface. This is because, during the experiments, the legs would begin to slip in the regolith, thereby increasing the time taken for the leg to reach the peak.

**Sources of Error in Measurement**

Like with the Drag Thrust Experiments, several sources of error are introduced into the results. These sources are listed in Table 7.3. As a result of all these sources of error, the total potential error of the rolling resistance test is 80,03 mN for regolith and 155,03 mN for rocky surfaces.

**7.1.5. Drawbar Pull**

An example of the force graphs of the Drawbar Pull experiments performed on Regolith and Rocky Surfaces are shown below. Like the rolling resistance tests, the shape of the rolling resistance results are similar for the same reasons given in the rolling resistance graph explanations.

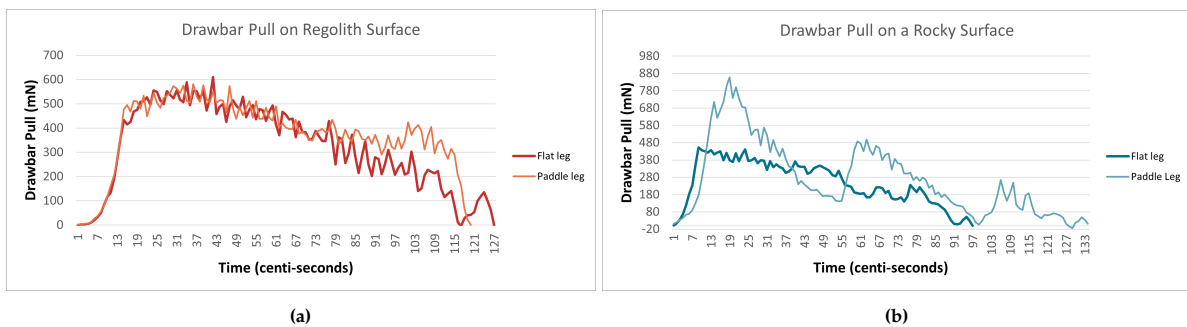


Figure 7.7: Drawbar Pull graph of the Paddle Leg and Flat Legs on: (a) Regolith and, (b) Rocky Surface (Sandpaper)

Like the rolling resistance, the maximum thrust force experienced by each leg was used to compare the performance of the different legs.

**Sources of Error in Measurement**

Like with the Drag Thrust and Rolling Resistance experiments, several sources of error are introduced into the results. These sources are listed in Table 7.3. As a result of all these sources of error, the total potential error of the drawbar pull test is 80,03 mN for regolith and 155,03 mN for rocky surfaces.



## 7.2. Comparison of the performance of the different legs

The results of the different experiments on the different terrains for all six of the legs are shown in the upcoming section. To make it easier to compare, the legs with grousers and the legs without grousers have been grouped together and separated using a dotted line in the graphs. All the legs with grousers are located left of the line, and all legs without grousers are on the right.

### 7.2.1. Regolith

#### Sinkage

The maximum sinkage of the different legs for each of the three tests performed are shown below:

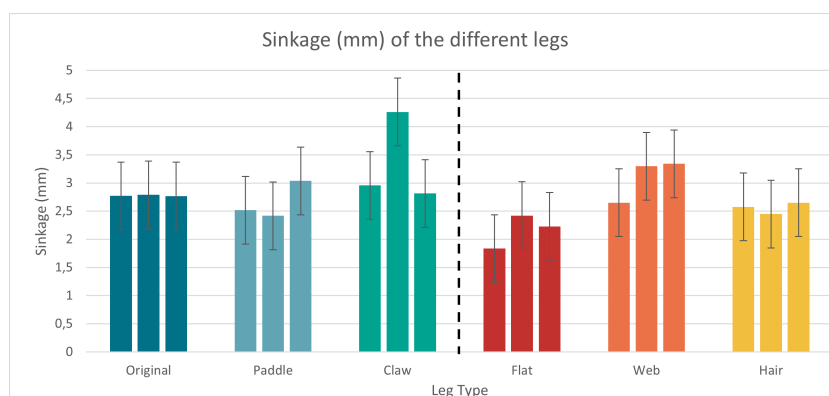


Figure 7.8: Maximum sinkage of the different legs

Excluding some outlier results, the results show that the difference between the maximum sinkage of the different legs between the best performing and worst performing legs differs by less than 1 mm. According to the results, the flat leg performed the best and the web leg the worst. It must be noted that the second result of the claw leg appears to be an outlier and this may be due to the regolith and how it was prepared. It must also be noted that the results of the hair leg do not take into account compression of the hairs which would mean that the amount the hair leg sank into the regolith is less than indicated in the graph.

Observation made during testing indicated that the Hair leg may perform better than the flat leg. To confirm this, the legs were all placed onto the regolith with weights added to the legs so that they all roughly weighed 167 grams and then removed. The imprints of the legs in the regolith were then observed as shown in Figure 7.9 below. From this, it appears that the Hair leg does perform slightly better than the Flat leg, however, this would need to be confirmed with further tests. These tests also do not take into account sinkage as the leg is rolling across the surface and it may be possible that the performance of the legs will differ from their static tests.

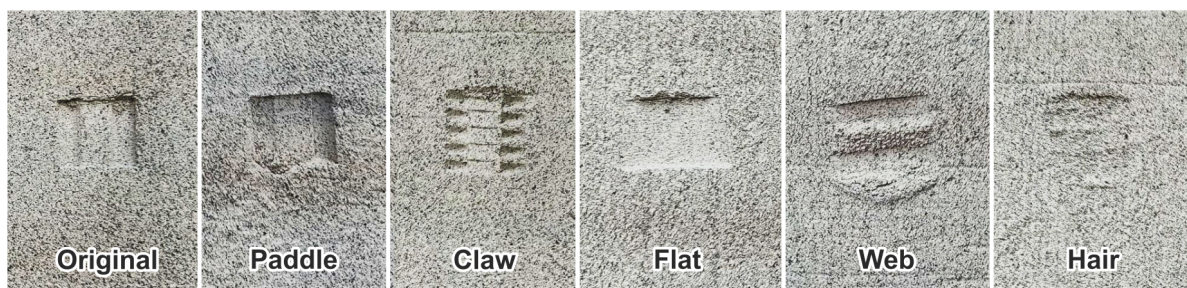


Figure 7.9: Visual Sinkage tests performed on all six legs. The image shows how the Hair leg may sink slightly less than the flat leg

Although the width of the Claw leg was increased so that the total surface area of the leg is the same as the other legs, the Claw leg sank slightly more than most of the rest of the leg - excluding the one outlier

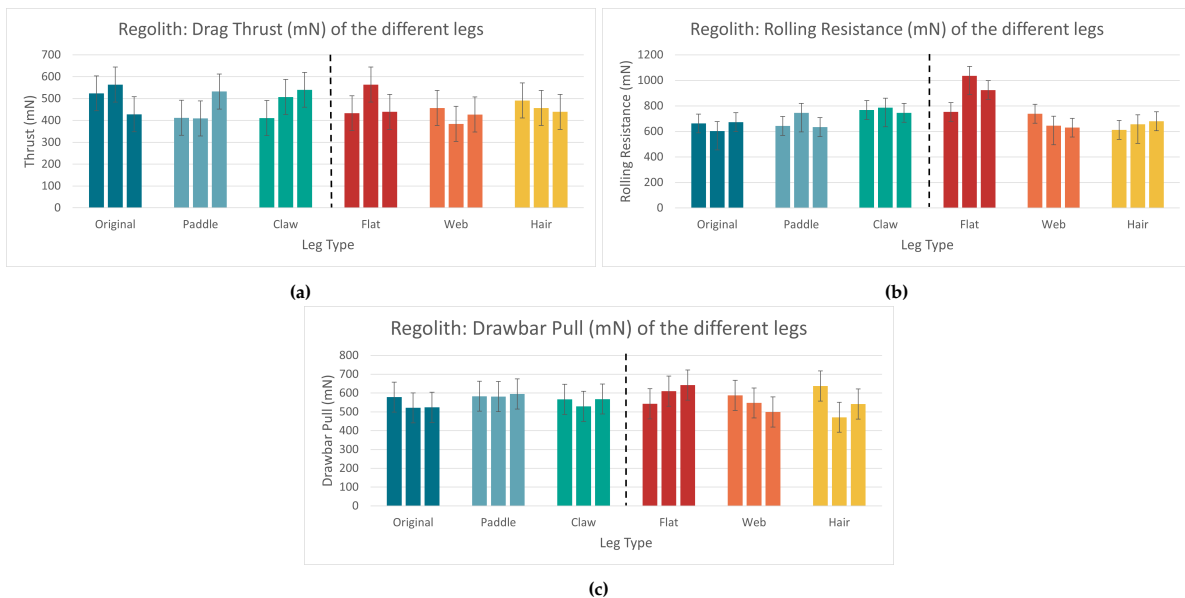


result. In addition to this, the Web leg sank the most which could be due to the fact that most of the weight of the leg is resting on the two toes which have a smaller surface area than the other legs. The webbing between the two toes did appear to catch some of the regolith and prevent the Web leg from sinking further into the regolith. Although a separate test should be performed using the Web leg with webbing and without to see if the webbing does aid with preventing sinkage.

An issue that arose when performing these tests, was whether or not to include the grouser height in the sinkage measurements. As mentioned previously, some studies suggest that the grouser height should not be taken into account, but from observations made during the testing of the legs, the grousers contributed greatly to the amount the legs sank. This is because the width of the grousers were significantly wide in relation to the circumference of the leg. This indicates that grouser width does have an impact on the sinkage performance of the leg.

### Drawbar pull

The results of the different experiments show that the performance of the different legs on regolith does not vary greatly. From the Drag Thrust results seen in Figure 7.10a, it can be seen that the Original leg and Claw leg performed the best, while the Web and Flat legs performed the worst. These results do show that legs with grousers perform slightly better than the legs without grousers.



**Figure 7.10:** Force graphs of each experiment for the different legs on Regolith: (a) Drag Thrust (b) Rolling Resistance (c) Drawbar Pull

The Rolling Resistance results in Figure 7.10b do not show an obvious best performer, with the Original, Paddle, Web and Hair legs displaying similar results. However, the results do show that the flat leg performed the worst out of all the legs. The results also do not show any obvious difference in the performance between the legs with grousers and those without.

The Drawbar Pull results, shown in Figure 7.10c, are very similar for all the different legs, with no clear best and worst performers. There is also no obvious difference between the results of the legs with grousers and those without.

Overall, the results indicate that it would be worth investigating the impact that grouser width and height would have on the sinkage and tractive performance of the leg. The results suggest that perhaps thin grousers would be more advantageous for the Lunar Zebro as the grousers would be able to penetrate deeply into the regolith while the body of the leg would prevent the leg from sinking too deep into the regolith. The results also indicate that hairs may help with preventing sinkage but a more in-depth investigation would be needed to determine this.

## 7.2.2. Rocky Terrain

### Sandpaper

From the Drag Thrust results seen in Figure 7.11a, it can be seen that the Claw leg performed the best, while the Hair leg performed the worst. These results show that legs with grousers perform significantly better than legs without grousers. What is interesting to note is that out of the legs without grousers, the web leg performed better.



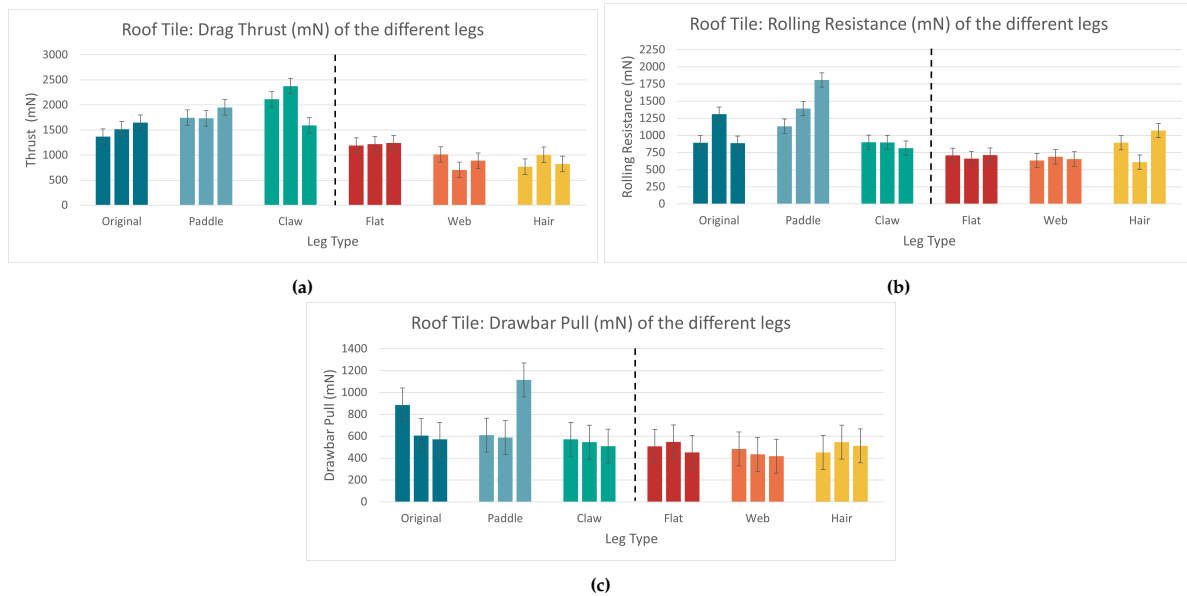
**Figure 7.11:** Force graphs of each experiment for the different legs on the Sandpaper Surface: (a) Drag Thrust (b) Rolling Resistance (c) Drawbar Pull

The Rolling Resistance results in Figure 7.11b show that the Paddle and Claw legs performed the worst, whereas the Original and Web leg performed the best.

The Drawbar Pull results, shown in Figure 7.11c, once again show that the Paddle and Claw legs perform the best with a lot of variation in the value of their results. When it comes to the legs without grousers, the Flat and Web legs performed the worst, while the Hair leg performed better.

### Roof Tile

Like with the Sandpaper results, the Drag Thrust results seen in Figure 7.12a, show that the Claw leg performed the best, while the Hair and web legs performed the worst. These results show that legs with grousers perform significantly better than legs without grousers.



**Figure 7.12:** Force graphs of each experiment for the different legs on the Roof Tile Surface: (a) Drag Thrust (b) Rolling Resistance (c) Drawbar Pull

The Rolling Resistance results in Figure 7.12b show that the Paddle leg performed the worst, whereas the Flat and Web leg performed the best.

The Drawbar Pull results, shown in Figure 7.12c, show that the Original and Paddle leg both display outlier results which are significantly larger than the rest of their values. Overall, these two legs did perform the best out of all the legs. Whereas the Web Leg performed the worst.

### Overall analysis of the experimental results on Rocky Surfaces

The results of both the sandpaper and roof tile experiments both show that the Paddle and Claw legs both performed the best out of all the legs. This indicates that the claw-like grouser profiles of the Paddle and Claw legs are able to hook onto surface irregularities in the ground surface and increase the drawbar pull of the leg as the leg is less likely to slip. The results also show that for legs without any grousers, hair helps to increase the performance of the legs as they increase the grip of the leg on the surface.

These tests were all performed on a flat surface, so it would be interesting to investigate how the performance of the different legs changes when walking up an incline or when walking on loose rocks. It would also be interesting to see how the Claw leg would interact with a surface that is irregular and if it is beneficial for the leg to have toes that can mould to the surface.

## Rover Experimental Set-up

In this chapter, a new hybrid leg is designed based on the results from the single leg test results. This Hybrid leg and the Original Leg will then be used to test the performance of a working model of the rover <sup>1</sup> on regolith and sandpaper. First, some background will be given on how the trafficability of certain vehicles have been measured previously. From there, two experimental setups are described in detail to test the performance of a rover model using the two different leg types.

### 8.1. Hybrid Leg

Using the results shown and analysed in Chapter 7, a Hybrid Leg is designed using features from the individual legs tested that may help improve the performance of the rover compared to the original legs.



Figure 8.1: Standard Set up for measuring the Drawbar Pull of a vehicle [81]

The results indicated that when walking on regolith, grousers do not aid with improving the traction of the leg but that hair may help prevent sinkage. Furthermore, the results of the leg when walking on a rocky surface indicated that legs with claw-like grousers helped to improve the traction of the leg. Therefore, a Hybrid leg was designed, which included the same grouser profile as the Paddle leg but also included hair in between the grousers as shown in the Figure above. The hope is that the claw-like grousers will improve the traction of the rover on rocky surfaces, while the hair will prevent sinkage and slippage when walking on regolith.

In addition to this, the width of the middle legs of the rover was increased from 20 mm to 30 mm while the front and back legs remained the same. This was done because the middle legs support twice the

<sup>1</sup>The weight of the model rover is roughly 1.5 kg which is heavier than the 0.167 kg tested on the single leg tests. It was not possible to lighten the model of the rover

weight of the front and back legs and therefore a larger surface area will help prevent the legs from sinking deeper into the regolith than the front and back legs, thereby preventing the rover from tilting from side to side while walking.

## 8.2. Measuring Trafficability

Like with the single-leg tests, a good indicator of the trafficability of a rover is to measure its drawbar pull. Similar to the way single-wheel drawbar pull tests are done, the standard way of measuring the drawbar pull of a vehicle is to drive the vehicle forward while controlling its slip and measuring the force between the vehicle and the mechanism controlling the slip [81] [82].



Figure 8.2: Standard Set up for measuring the Drawbar Pull of a vehicle [81]

Once again, this is difficult to achieve with the Lunar Zebro for the same reasons as with the single-leg tests. The speed at which the rover travels is constantly changing as a result of the leg, therefore, it is difficult to control the slip of the rover.

Another way to measure the trafficability of vehicles, specifically descendants of the RHex robot, is by measuring the distance the robots travel over a certain time span or over a number of steps. As was briefly discussed in Chapter 3, a technical report published by Roberts et al. [22] measured the performance of two RHex robots with different leg widths by walking both robots for 30 minutes in a single-file line over a desert landscape and measuring the distance both rovers travelled. This is shown in the figure below.



Figure 8.3: Experiment performed by Roberts et al. [21]

### 8.3. Measuring Drawbar Pull

Although it is difficult to measure the drawbar pull at controlled slip rates, it is possible to measure the drawbar pull of the rover at 100 % slip. This is done by hooking the rover to a fixed point and making it walk forward a few steps (in this case 3 steps). A force sensor is located between the rover and the fixed point and this will measure the drawbar pull. The rover will try to walk forward, however, this is not possible, so instead the legs will begin to slip. The force sensor will then measure the force applied by the rover while it experiences 100 % slip. This is only possible as long as the torque of the motors in the rover are large enough to overcome the friction of the surface and induce slippage in the legs. The experimental set-up on sandpaper is shown below. This experimental set-up is also applied to the regolith surface.

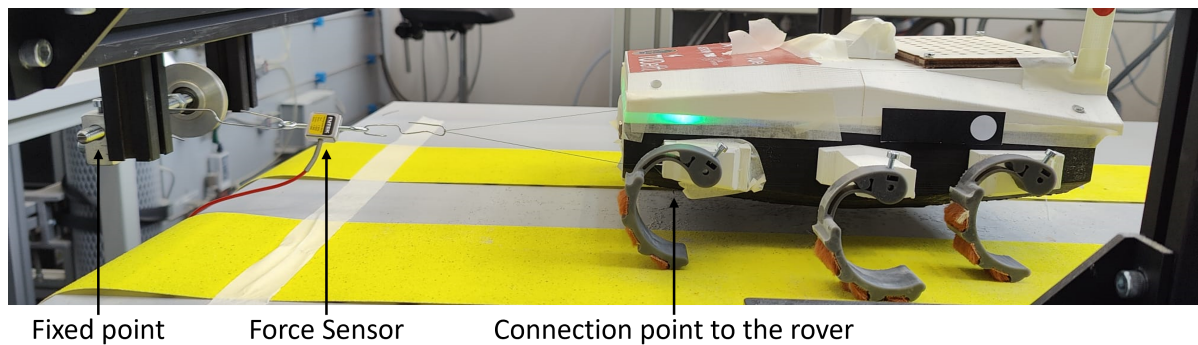


Figure 8.4: Rover drawbar pull experimental set-up on Sandpaper

### 8.4. Measuring Distance Travelled

As mentioned previously, the performance of different leg types on the rover can be determined by measuring the distance travelled by the rover after a certain number of steps. Ideally, when comparing the performance of different wheels on a vehicle, the more steps travelled the more obvious the difference in performance. In this case, the number of steps that can be taken is restricted by the size of the regolith testbed. Therefore, the number of steps that will be taken for comparison is five steps.

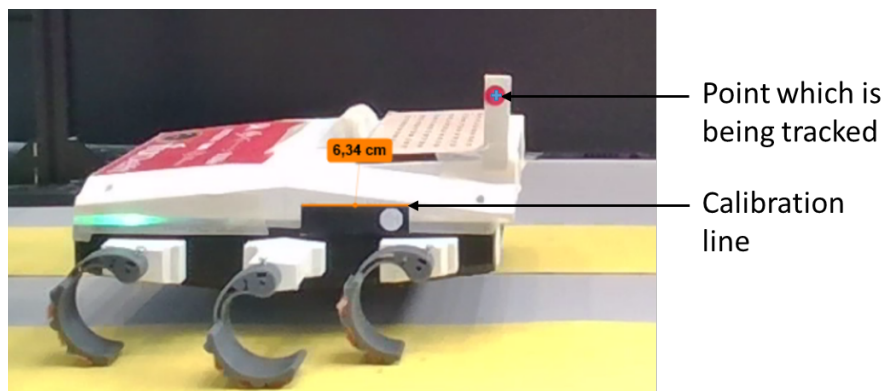


Figure 8.5: Distance Travelled experimental set-up on Sandpaper

The distance that is travelled over the five steps is then recorded using a camera. A red marker has been placed on the rover, as shown in Figure 8.5 above, which will be used to track the distance travelled using *Kinovea*. The program tracks the relative horizontal displacement of the red marker over the span of the recording and this is then used to determine the total horizontal distance travelled. The program has also been calibrated using a known distance marker on the rover so that the pixel size is converted to the relevant distance.



## Rover Results and Analysis

In this chapter, the data obtained from the various rover experiments are explained. From this, certain values are recorded and used to compare the performance of the different legs on the rovers.

### 9.1. Experimental Data

Each experiment was performed three times for each leg type used on the rover. How this data was obtained and what it is showing is explained below using a sample of the data recorded. These samples are indicative of how all the data of the tests appear and how they were recorded for comparison. It is important to note that the mass of the rovers are 1.5 kg which is heavier than the 0.167 kg used in the single leg tests. In addition to this, the weight distribution across the legs differs with the front and back legs experiencing a quarter of the weight and the middle legs experiencing half the weight.

#### 9.1.1. Drawbar Pull

An example of the force graphs of the Drawbar Pull experiments performed on Regolith and Sandpaper for the rover with original legs are shown below.

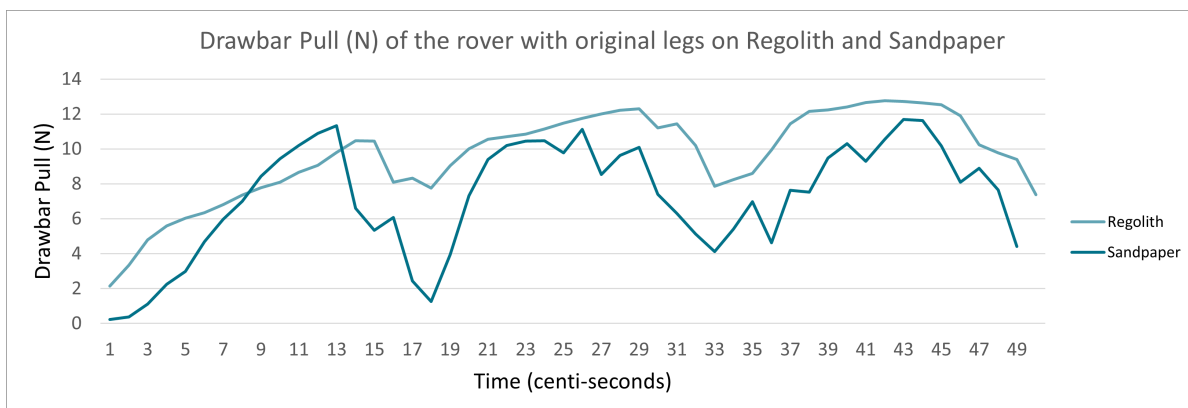


Figure 9.1: Drawbar Pull of the rover with the original legs on the regolith and sandpaper

The results show three peaks which indicate the three steps that the rover is attempting to make. The maximum force measured during the experiments is recorded and used to compare the performance of the rovers with different legs.

The graph also shows that the drawbar pull exerted by the rover on the regolith is higher in regolith than on the sandpaper. This may be due to the stiffness of the surface on which the regolith is walking. The regolith is a deformable surface that can be compressed and pushed to the side, which means that with every step the rover tries to take forward, the deeper it sinks into the regolith. This increases the

amount of regolith that is in contact with the leg which in turn increases its drawbar pull. In contrast, the sandpaper surface is a rigid surface that does not deform when pressure is applied to it. This means that only the edges of the legs of the rover are in contact with the ground which means that the legs are able to slip easier than on the regolith.

### Sources of Error in Measurement

During the experiment, there are several ways errors can be introduced into the results. These sources and their values are listed in the table below:

**Table 9.1:** Sources of error in Drawbar Pull experiment and their values

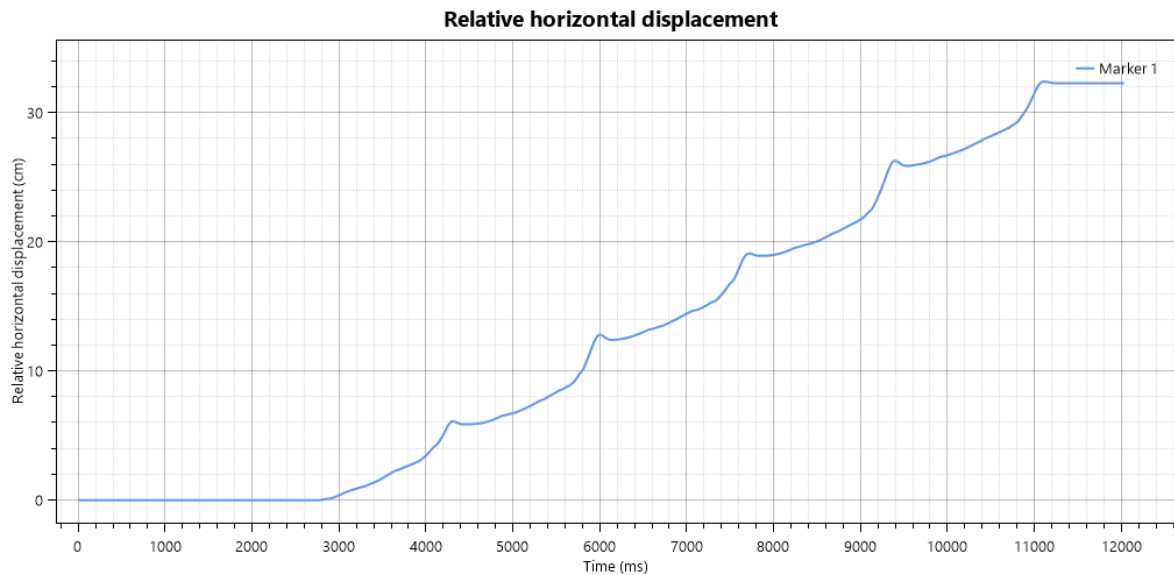
Sources of Error	Value	Regolith	Rocky
		(±) Value in N	(±) Value in N
Force sensor accuracy	22 N +- 22 mN	0,022	0,022
Regolith preparation	Compaction	0,5	
Position on sandpaper	Grit contact		0,5
		0,522	0,522

Where:

- **Force sensor accuracy:** A 22 N force sensor was used with an accuracy of 22 mN.
- **Regolith preparation:** This is estimated to introduce a difference of 500 mN into the measurement.
- **Position on sandpaper:** This is estimated to introduce a difference of 500 mN into the measurement.

### 9.1.2. Distance Travelled

An example of the relative horizontal displacement graph used to determine the total distance the rover travelled over five steps is shown below.



**Figure 9.2:** Drawbar Pull experimental set-up on Sandpaper

The graph shows five peaks which indicate the end of each of the five steps taken by the rover. The horizontal line at the end of the graph indicates the position of the rover after its final step and therefore indicates the total distance travelled by the rover. This value is then used to compare the performance of the rover with different legs.

## Sources of Error in Measurement

**Table 9.2:** Sources of error in Drawbar Pull experiment and their values

Sources of error	Value	(±) Value in cm
Pixel conversion to distance travelled	Calibration	0,6
		0,6

Where:

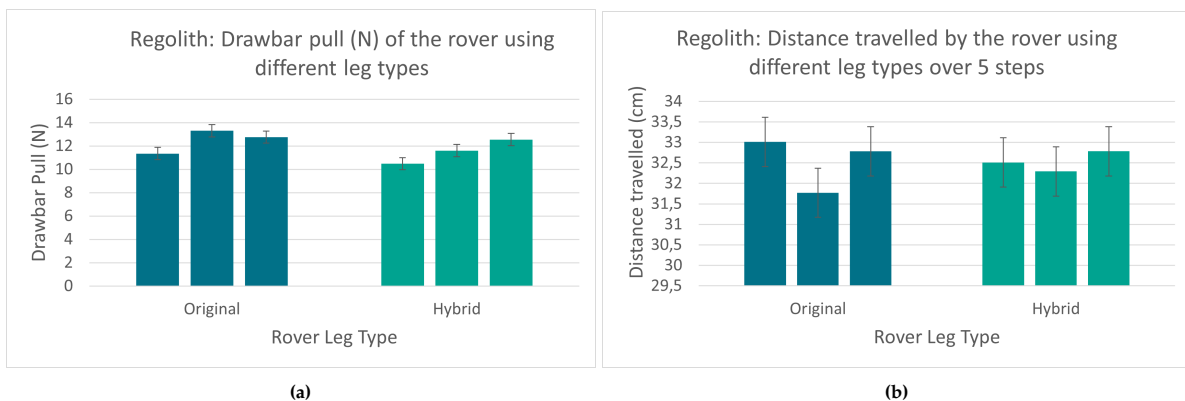
- **Pixel size conversion to distance travelled:** The size of the pixels are calibrated using a calibration line on the rover. The error introduced in the pixel calibration is roughly 0.001 cm. The rover walks around 600 pixels which then as a result of the pixel calibration introduces an error of 0.6 cm into the distance measurements.

## 9.2. Comparison of the performance of the different legs

The results of the different experiments on the different terrains for the two different legs used on the rover are shown in the upcoming section.

### 9.2.1. Regolith

The Drawbar Pull and Distance travelled results for the two different legs used on the rover on regolith are shown in Figure 9.3 below:



**Figure 9.3:** The results of experiments performed on regolith for the original and hybrid legs used on the rover where: **(a)** Drawbar Pull results, **(b)** Distance travelled by the rover over five steps

The results show that the original legs performed marginally better than the hybrid legs for drawbar pull tests while performing the same for the distance travelled.

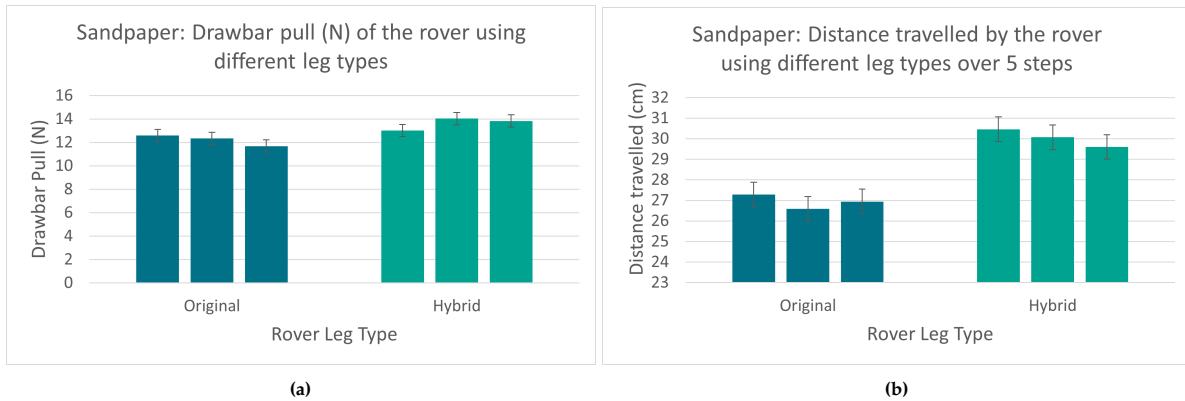
These results are indicating that perhaps the drawbar pull tests at 100% slip rates do not give a good indication on the trafficability of the leg when performed on regolith. The distance travelled test further confirms that grousers on the bottom of the Lunar Zebro leg do not make much of a difference on the performance of the leg on regolith. However, the total number of steps travelled is short and perhaps a better indicator of performance would be observed over more steps and therefore a bigger distance. Unfortunately, this experiment was limited to the size of the testbed and this distance could not be increased.

Another factor that is contributing to the differences between measurements of the legs, is the way the regolith is prepared before each test. As a result, the compaction and therefore the density of the regolith is different for each test. This compaction will impact the way the grousers interact with the regolith and thereby effect the performance of the legs during the different tests.

In addition to this, the Hybrid leg rover with the larger middle legs did not perform better than the rover with the original legs of all the same size. To fully test if changing the leg size impacts the performance of the rover when regolith, separate tests need to be performed where the same leg type with different widths are placed at different locations along the rover and measure the rover's performance.

### 9.2.2. Sandpaper

The Drawbar Pull and Distance travelled results for the two different legs used on the rover on sandpaper are shown in Figure 9.3 below:



**Figure 9.4:** Drawbar Pull graph of the Paddle Leg and Flat Legs on: (a) Regolith and, (b) Rocky Surface (Sandpaper)

The results show that the hybrid legs performed better than the original legs for the two different experiments performed on sandpaper. The reason for this is that the sharp claw-like grouser profile of the hybrid legs are able to hook onto any irregularities in the floor surface created from the grits of the sandpaper whereas the grouser profile of the original legs cannot as easily engage with the grits of the sandpaper.

Like with the tests performed on regolith. The drawbar pull tests do not show a great difference in the performance of the different legs, unlike the distance travelled test. Therefore, the drawbar pull test at 100% slip rate on rocky surfaces is not the best indicator of the performance of the different leg types on the rovers.

# 10

## Conclusion

In this report, a Biomimicry design frame work was used to learn how animals in nature move across terrains similar to those found on the moon. This provided some insight into the working principles behind how these animals thrive in such environments. Using these working principles, new leg designs were created using features that have not yet been explored.

These designs were further developed into prototypes that were tested on both flat regolith and rocky terrains. What the rolling resistance and drawbar pull tests show is that energy is being expended to lift the mass weighing on the legs up over the step cycle of the leg. This is because the centre of rotation is not the same as the axis of rotation. Overall, the results showed that hair has the potential to reduce sinkage in regolith but more research is needed to confirm this. However, the results from the single-leg tests on regolith also indicated that there is not much difference in the drawbar pull performance of the different legs no matter what features were included on the bottom of the leg or if the leg had grousers or not. In addition to this, the results indicated that claw-like grouser features improve the performance of the legs on rocky terrains. Therefore, the results indicate that the legs should be optimized for walking on rocky surfaces rather than on regolith as it has very little impact on the performance of the leg when walking on regolith but has a large impact on the performance when walking on rocky terrain.

From there a new hybrid model was created that included grouser features of the Paddle leg design to increase traction on rocky surfaces. In addition to this, the hybrid leg design included hair in between the grousers to help prevent sinkage when walking on regolith. This leg was then tested on a rover model and the results were compared to the original legs' performance on the rover model. What these results also indicate is that the design of the legs of the rover should focus on improving traction on rocky terrains instead of on regolith as the grouser profile does not impact the performance of the leg greatly when walking on regolith.



## Recommendations for Future Work

Many lessons were learnt from this report, however, it also showed that much more work needs to be done in the future. These recommendations are explained below.

### **Testing on Different terrains**

The experiments done in this report only focused on flat terrains. However, on the moon, this will rarely be the case, especially on rocky terrains. Instead, the rocky terrain will be irregular or consist of loose rocks. Therefore, it would be interesting to see the performance of the rover on such terrains. In particular, the Claw Leg may be ideal for traversing such terrains as the toes of the leg may mould to the rocky surface and find more grip when walking than other leg types.

In addition to this, when on the moon, the rover may have to ascend or descend slopes. It would therefore be beneficial to test the performance of the rover on inclined surfaces both on rocky surfaces and on regolith. Furthermore, the rover may encounter obstacles that it would have to climb. For that reason, it would be helpful to test the performance of the rover with different legs when encountering obstacles.

**Leg Configuration** Currently the leg configuration of the rover consists of six identical legs. But as seen in Chapter 3, six-legged animals make use of different leg types at different positions to aid with mobility. Therefore it would be worth using the information gathered from single-leg tests to change the leg configuration of the Lunar Zebro to maximize performance depending on the location it is being sent to. For example, if the rover is sent to a location consisting mostly out of regolith and very little rocks then the leg configuration should focus on improving traction on regolith. But if the rover is being sent to explore lava tubes, then a leg configuration that focuses on the performance of the rover on rocky surfaces is ideal.

**Investigating the impact of hair features in more depth** The hair leg shows potential in helping prevent sinkage of the leg, however, the test performed in this report were not extensive enough to understand the true impact that hairs have on the leg. Therefore, it would be worth investigating how hair length, type and location impact the performance of the legs.

**Evaluating Against Life's Principles** Evaluating the new leg designs against life's principles was not largely applicable in the context of this report as the focus was on generating new designs and prototyping to see if they made any impact on trafficability. But once a final design is created, it would be worth evaluating it against these principles as it may help make the final design more sustainable. In addition, the entire rover and all its components and process could be evaluated against life's principles with the potential of finding new ways to make the project more sustainable.

**Improved experimental set-up** The experimental set-ups used for the single-leg tests and rover were rudimentary tests set ups that were used to measure and compare the performance of the different legs. As such, the measurements were not accurate and therefore, it would be beneficial to improve the experimental set up to improve the accuracy of the data measured.

### Ideal Grouser Height and Number

It appears that the dimensions of the grousers used in the current leg design were chosen without much reasoning behind them. However, using equations 2.12 and 2.13 in Chapter 2, it is possible to calculate what the ideal grouser height is for a certain number of grousers or what the ideal number of grousers is for grousers with a certain height. Therefore using these equations and the current dimensions of the Lunar Zebro leg design, the ideal height of the grousers if 4 grousers are used is 4.95 mm. Otherwise, if a height of 2.84 mm is used as the grouser height (as is the case with the current design) then the ideal number of grousers is 5.73 which is then  $\approx 6$ . The calculation can be found in Appendix L.

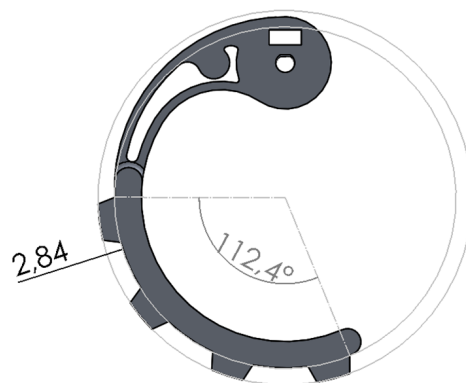


Figure 11.1: Relevant dimensions of the original leg which can be used to determine grouser height or number

### Grouser Width

Although it is possible to calculate the ideal grouser height and number, there is not much information available on grouser width. It would be worth investigating what impact the grouser width has on the performance of a wheel or leg.

### Improving the leg shape

The results of the single-leg rolling resistance and drawbar pull test show that energy is being wasted as the centre of rotation of the leg on the ground is not the same as the axis of rotation. Therefore, it may be beneficial to create a new leg design whose centre of rotation does align with the axis of rotation as shown in the figure below. This design would also prevent the rover from hopping as it walks. This type of leg design has also been suggested by van Rijn and Goosen [83].

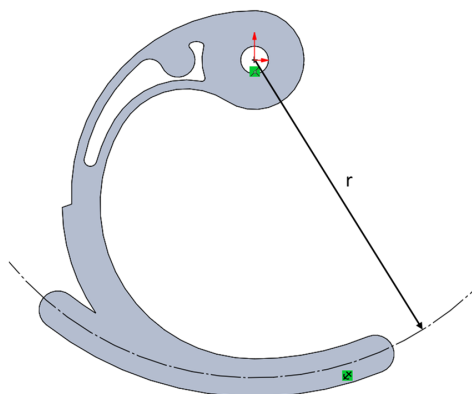


Figure 11.2: Modified Leg Design

# References

- [1] N. Moore and M. Buehler, "RHex : A Biologically Inspired Hexapod Runner," *Autonomous Robots*, vol. 11, pp. 207–213, 2001.
- [2] A. Ellery, *Planetary Rovers*. Chichester Uk: Praxis Publishing, 2016, ISBN: 978-3-642-03259-2 (eBook). DOI: 10.1007/978-3-642-03259-2.
- [3] P. A. Dunker, W. A. Lewinger, A. J. Hunt, and R. D. Quinn, "A biologically inspired robot for lunar In-Situ Resource Utilization," *RSJ International Conference on Intelligent Robot Systems*, pp. 5039–5044, 2009.
- [4] Lunar Zebro, *Lunar Zebro*, <https://zebro.space/>. [Online]. Available: <https://zebro.space/> (visited on 11/04/2021).
- [5] GRASP Laboratory and U. of Pennsylvania, *X-RHex is the new RHex*. [Online]. Available: <https://robots.ieee.org/robots/rhex/?gallery=photo1> (visited on 11/04/2021).
- [6] G. Lopes, *RHex running*, <https://en.wikipedia.org/wiki/Rhex#/media/File:Rhex.jpg>, 2008. [Online]. Available: <https://en.wikipedia.org/wiki/Rhex%7B%5C%7D/media/File:Rhex.jpg> (visited on 12/06/2021).
- [7] NASA, *In Depth | Earth's Moon – NASA Solar System Exploration*, Dec. 2019. [Online]. Available: <https://solarsystem.nasa.gov/moons/earths-moon/in-depth/> (visited on 10/28/2021).
- [8] D. Vaniman, R. Reedy, G. Heiken, G. Olhoft, and W. Mendell, "Lunar environment," in *Lunar Sourcebook: A User's Guide to the Moon*, Cambridge University Press, 1991, pp. 27–60. DOI: 10.1115/1.3120356.
- [9] NASA, *Apollo 11 photograph of footprints in the lunar regolith*. [Online]. Available: <https://www.researchgate.net/figure/Apollo-11-photograph-of-footprints-in-the-lunar-regolith-courtesy-of-NASA%7B%5C%7Dfig1%7B%5C%7D285673299> (visited on 11/01/2021).
- [10] NASA/JSC, *View of Portion of "Relatively Fresh" Crater As Photographed by Apollo 15*, 2018. [Online]. Available: <https://moon.nasa.gov/resources/225/view-of-portion-of-relatively-fresh-crater-as-photographed-by-apollo-15/?category=images>.
- [11] D. S. McKay, G. Heiken, A. Basu, *et al.*, "The Lunar Regolith," in *Lunar Sourcebook: A User's Guide to the Moon*, Cambridge University Press, 1991.
- [12] J. B. Plescia, "Lunar surface environmental conditions: Challenges of developing an outpost and exploiting in situ resources," *47th AIAA Aerospace Sciences Meeting including the New Horizons Forum and Aerospace Exposition*, no. January, pp. 1–13, 2009. DOI: 10.2514/6.2009-756.
- [13] F. Hörz, R. Grieve, G. Heiken, P. Spudis, and A. Binder, "Lunar surface processes," in *Lunar Sourcebook: A User's Guide to the Moon*, Cambridge University Press, 1991, pp. 61–120. [Online]. Available: <https://pdfs.semanticscholar.org/aeef/1404b9cfd5a7d64e131894798cc2f4d2f8be.pdf>.
- [14] S. Matrossov, *LUNOKHOD rover and tire*, <https://www.nasa.gov/specials/wheels/>, 2017.
- [15] Smithsonian National Air and Space Museum, *Wheel, Lunar Rover*, [https://airandspace.si.edu/collection-objects/wheel-lunar-rover/nasm\\_A19750830000](https://airandspace.si.edu/collection-objects/wheel-lunar-rover/nasm_A19750830000). [Online]. Available: <https://airandspace.si.edu/collection-objects/wheel-lunar-rover/nasm%7B%5C%7DA19750830000>.
- [16] Unknown, *Sojourner Wheel*, [https://www.meteorite-times.com/Back\\_Links/2004/February/Accretion\\_Desk.htm](https://www.meteorite-times.com/Back_Links/2004/February/Accretion_Desk.htm). [Online]. Available: <https://www.meteorite-times.com/Back%7B%5C%7DLinks/2004/February/Accretion%7B%5C%7DDesk.htm> (visited on 11/03/2021).
- [17] NASA, *MER Wheel*, <https://mars.nasa.gov/mer/mission/technology/autonomous-planetary-mobility/>. [Online]. Available: <https://mars.nasa.gov/mer/mission/technology/autonomous-planetary-mobility/> (visited on 11/03/2021).

- [18] NASA, *Sol 1471: Mars Hand Lens Imager (MAHLI)*, [https://mars.nasa.gov/raw\\_images/370259/](https://mars.nasa.gov/raw_images/370259/). [Online]. Available: [https://mars.nasa.gov/raw%7B%5C\\_%7Dimages/370259/](https://mars.nasa.gov/raw%7B%5C_%7Dimages/370259/) (visited on 11/03/2021).
- [19] K. Shiflett and NASA, *Perseverance Wheel*, <https://www.bbc.com/news/science-environment-53129281>. [Online]. Available: <https://www.bbc.com/news/science-environment-53129281> (visited on 11/04/2021).
- [20] D. Goldman, H. Komsuoglu, and D. Koditsche, "March of the sandbots," *IEEE Spectrum*, vol. 46, pp. 30–35, 2009, issn: 10210989. doi: 10.1109/MSPEC.2009.4808384.
- [21] S. Roberts, J. Duperret, A. M. Johnson, and T. Zobeck, "Technical Report : Jornada and White Sands Trip," *Technical Reports (ESE)*, no. November, 2014.
- [22] S. F. Roberts, J. M. Duperret, and H. Wang, "Desert Trip Desert RHex Technical Report : Tengger Desert Trip," *Technical Reports (ESE)*, no. November, 2014.
- [23] C. Louth, *6 Reasons Why Rear Wheels on a Farm Tractor are Bigger – Tractor Addict*. [Online]. Available: <https://tractoraddict.com/why-rear-wheels-on-tractor-are-bigger/> (visited on 11/08/2021).
- [24] FarmingUK, *Photo competition celebrates 100 years of blue tractor production inviting New Holland customers to illustrate their part in the brand's heritage story*, [https://www.farminguk.com/news/new-holland-launches-100-year-celebration-photo-competition\\_47262.html](https://www.farminguk.com/news/new-holland-launches-100-year-celebration-photo-competition_47262.html). [Online]. Available: [https://www.farminguk.com/news/new-holland-launches-100-year-celebration-photo-competition%7B%5C\\_%7D47262.html](https://www.farminguk.com/news/new-holland-launches-100-year-celebration-photo-competition%7B%5C_%7D47262.html) (visited on 11/08/2021).
- [25] Rocket Motorsport, *Real American Muscle V8 Automatic Sand Rocket*, <http://www.sandrocket.com/>. [Online]. Available: <http://www.sandrocket.com/> (visited on 11/08/2021).
- [26] TireBuyer, *What's a flotation tire?* <https://www.tirebuyer.com/education/tire-flotation>. [Online]. Available: <https://www.tirebuyer.com/education/tire-flotation> (visited on 11/08/2021).
- [27] Chaparral Motorsports, *Sand (Paddle) Tires 101 – Choosing the Right Tire | ChapMoto.com*, 2018. [Online]. Available: <https://www.chapmoto.com/blog/2018/08/30/sand-paddle-tires-101-choosing-the-right-tire/> (visited on 11/08/2021).
- [28] Lunar Zebro - Structures Department, "Phase B : Body & Thermal (5100),"
- [29] Learn Biomimicry, "Introduction to Biomimicry - What is Biomimicry?" In 6th ed., 2021, pp. 1–48.
- [30] Learn Biomimicry, "Introduction to Biomimicry - How do we do Biomimicry," in 2021.
- [31] N. Patel, G. P. Scott, and A. Ellery, "Application of Bekker Theory for Planetary Exploration through Wheeled, Tracked and Legged Vehicle Locomotion," *A Collection of Technical Papers - AIAA Space 2004 Conference and Exposition*, vol. 3, no. September, pp. 2109–2117, 2004. doi: 10.2514/6.2004-6091.
- [32] M. G. Bekker, *Theory of Land Locomotion: The Mechanics of Vehicle Mobility*. University of Michigan Press, 1956.
- [33] M. G. Bekker, *Introduction to terrain-vehicle systems*. Ann Arbor: University of Michigan Press, 1969.
- [34] E. Karpman, W. Huang, J. Kövecses, and M. Teichmann, "Speed-made-good: Mobility map generation for wheeled vehicles on soft terrain," *Journal of Terramechanics*, vol. 101, pp. 11–22, Jun. 2022, issn: 00224898. doi: 10.1016/j.jterra.2022.01.003.
- [35] H. Inotsume, S. Moreland, K. Skonieczny, and D. Wettergreen, "Parametric study and design guidelines for rigid wheels for planetary rovers," *Journal of Terramechanics*, vol. 85, pp. 39–57, 2019, issn: 00224898. doi: 10.1016/j.jterra.2019.06.002. [Online]. Available: <https://doi.org/10.1016/j.jterra.2019.06.002>.
- [36] R. Bauer, W. Leung, and T. Barfoot, "Experimental and Simulation Results of Wheel-Soil Interaction for Planetary Rovers," *Proceedings of the 2005 IEEE/RSJ International Conference on Intelligent Robots and Systems.*, 2005.
- [37] M. Sutoh, J. Yusa, T. Ito, K. Nagatani, and K. Yoshida, "Traveling Performance Evaluation of Planetary Rovers on Loose Soil," *Journal of Field Robotics*, pp. 1–15, 2012. doi: 10.1002/rob.

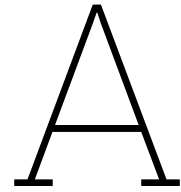
- [38] L. Ding, H. Gao, Z. Deng, K. Nagatani, and K. Yoshida, "Experimental study and analysis on driving wheels' performance for planetary exploration rovers moving in deformable soil," *Journal of Terramechanics*, vol. 48, no. 1, pp. 27–45, 2011, ISSN: 0022-4898. DOI: 10.1016/j.jterra.2010.08.001. [Online]. Available: <http://dx.doi.org/10.1016/j.jterra.2010.08.001>.
- [39] K. Nagaoka, K. Sawada, and K. Yoshida, "Shape effects of wheel grousers on traction performance on sandy terrain," *Journal of Terramechanics*, vol. 90, pp. 23–30, 2020, ISSN: 0022-4898. DOI: 10.1016/j.jterra.2019.08.001. [Online]. Available: <https://doi.org/10.1016/j.jterra.2019.08.001>.
- [40] A. J. Lopez-Arreguin, B. Gundlach, and E. Stoll, "Do lunar rover wheels sink equally on Earth and Moon?" *Results in Physics*, vol. 15, no. August, p. 102617, 2019, ISSN: 22113797. DOI: 10.1016/j.rinp.2019.102617. [Online]. Available: <https://doi.org/10.1016/j.rinp.2019.102617>.
- [41] M. Jiang, F. Liu, Z. Shen, and M. Zheng, "Distinct element simulation of lugged wheel performance under extraterrestrial environmental effects," *Acta Astronautica*, vol. 99, no. 1, pp. 37–51, 2014, ISSN: 00945765. DOI: 10.1016/j.actaastro.2014.02.011. [Online]. Available: <http://dx.doi.org/10.1016/j.actaastro.2014.02.011>.
- [42] Biomimicry 3.8, *DesignLens: Life's Principles - Biomimicry 3.8*. [Online]. Available: <https://biomimicry.net/the-buzz/resources/designlens-lifes-principles/> (visited on 10/04/2022).
- [43] R. E. Ritzmann, R. D. Quinn, and M. S. Fischer, "Convergent evolution and locomotion through complex terrain by insects, vertebrates and robots," *Arthropod Structure & Development* 33, vol. 33, pp. 361–379, 2004. DOI: 10.1016/j.asd.2004.05.001.
- [44] S. Kim, J. E. Clark, and M. R. Cutkosky, "iSprawl: Design and Tuning for High-speed Autonomous Open-loop Running," *The International Journal of Robotics Research*, vol. 25, no. 9, pp. 903–912, 2006. DOI: 10.1177/0278364906069150.
- [45] A. Masterson, *Leg it! Cockroaches change gait for extra speed*. [Online]. Available: <https://cosmosmagazine.com/science/biology/leg-it-cockroaches-change-gait-for-extra-speed/> (visited on 11/10/2021).
- [46] P. Ramdya, R. Thandiackal, R. Cherney, *et al.*, "Climbing favours the tripod gait over alternative faster insect gaits," *Nature Communications*, pp. 1–11, 2017. DOI: 10.1038/ncomms14494.
- [47] J. T. Watson, R. E. Ritzmann, S. N. Zill, and A. J. Pollack, "Control of obstacle climbing in the cockroach, *Blaberus discoidalis*. I. Kinematics," *Journal of Comparative Physiology A: Neuroethology, Sensory, Neural, and Behavioral Physiology*, vol. 188, no. 1, pp. 39–53, 2002, ISSN: 03407594. DOI: 10.1007/s00359-002-0277-y.
- [48] P. Breedveld, J. L. Herder, T. Tomiyama, and F. Mechanical, "Teaching creativity in mechanical design,"
- [49] Felis UK, *A Paws for thought*, <https://felis-uk.com/2017/10/18/felis-paws/>. [Online]. Available: <https://felis-uk.com/2017/10/18/felis-paws/> (visited on 11/10/2021).
- [50] iStock, *Camels Feet Stockfoto en meer beelden van Kameel - iStock*. [Online]. Available: <https://www.istockphoto.com/nl/foto/camels-feet-gm147670445-6753288> (visited on 11/10/2021).
- [51] H. Tributsch and M. Varon, *How Life Learned to Live: Adaptation in Nature*. Cambridge: MIT Press, 1982.
- [52] A. Norris, *8 Fascinating Facts About the Sand Cat*, <https://www.treehugger.com/things-you-didnt-know-about-sand-cat-4864143>, Nov. 2020. [Online]. Available: <https://www.treehugger.com/things-you-didnt-know-about-sand-cat-4864143> (visited on 11/10/2021).
- [53] B. Davis, *Can a camel walk easily on sand but not a horse? - MVOrganizing*, 2021. [Online]. Available: <https://www.mvorganizing.org/can-a-camel-walk-easily-on-sand-but-not-a-horse/> (visited on 11/12/2021).
- [54] Animal Corner, *Grey Wolf - Facts, Size, Diet & Habitat Information*. [Online]. Available: <https://animalcorner.org/animals/grey-wolf/> (visited on 11/12/2021).
- [55] Animalia, *Arabian Oryx - Facts, Diet, Habitat & Pictures on Animalia.bio*, <https://animalia.bio/arabian-oryx>. [Online]. Available: <https://animalia.bio/arabian-oryx> (visited on 11/12/2021).
- [56] Anthropolis, *Caribou and Reindeer Hooves*. [Online]. Available: <https://www.anthropolis.com/arctic-facts/fact-caribou-hoof.htm> (visited on 08/01/2022).

- [57] D. H. Chadwick, "A beast the color of winter : the mountain goat observed," p. 208, 1983.
- [58] CaliforniaHerps, *California species of Fringe-toed Lizards - Uma*. [Online]. Available: <http://www.californiaherps.com/identification/lizardsid/uma.id.html> (visited on 11/12/2021).
- [59] Rumo, *Feet Or Reindeer Stock Photo*, Apr. 2012. [Online]. Available: <https://www.istockphoto.com/nl/foto/feet-of-reindeer-gm176989345-19935653?phrase=reindeer%20hooves> (visited on 08/01/2022).
- [60] C. Barrows, A. Muth, M. Fisher, and J. Lovich, "Coachella Valley Fringe-toed Lizards," in *A Report to the Nation on the Distribution, Abundance, and Health of U.S. Plants, Animals, and Ecosystems*, National Biological Service, 1995, pp. 137–138. [Online]. Available: <https://www.webharvest.gov/peth04/20041028043633/http://biology.usgs.gov/s+t/noframe/d048.htm>.
- [61] A. E. Filippov and S. N. Gorb, "Modelling of the frictional behaviour of the snake skin covered by anisotropic surface nanostructures," *Scientific Reports*, vol. 6, no. March, pp. 1–6, 2016, issn: 20452322. doi: 10.1038/srep23539.
- [62] ValerieVSBN, *Penguin Facts: Things You Never Knew About Penguins | Reader's Digest*. [Online]. Available: <https://www.rd.com/list/facts-about-penguins/> (visited on 08/01/2022).
- [63] C. Li, S. T. Hsieh, and D. I. Goldman, "Multi-functional foot use during running in the zebra-tailed lizard (*Callisaurus draconoides*)," *Journal of Experimental Biology*, vol. 215, no. 18, pp. 3293–3308, 2012, issn: 00220949. doi: 10.1242/jeb.061937.
- [64] S. Childress, W. W. Schultz, and Z. J. Wang, "Comparative Studies Reveal Principles of Movement on and Within Granular Media," in *Natural Locomotion in Fluids and on Surfaces*, IMA, 2012, isbn: 9781461439967.
- [65] N. Mazouchova, N. Gravish, A. Savu, and D. I. Goldman, "Utilization of granular solidification during terrestrial locomotion of hatchling sea turtles," *Biol. Lett.*, no. February, pp. 398–401, 2010.
- [66] S. Pociask, *Why Are Mountain Goats Such Effective Climbers?* 2017. [Online]. Available: <https://www.forbes.com/sites/quora/2017/05/26/why-are-mountain-goats-such-effective-climbers/?sh=4560098e237a> (visited on 12/02/2021).
- [67] S. N. Gorb, "Uncovering insect stickiness: Structure and properties of hairy attachment devices," *American Entomologist*, vol. 51, no. 1, pp. 31–35, 2005, issn: 21559902. doi: 10.1093/ae/51.1.31.
- [68] D. C. D'amore, |. S. Clulow, |. J. S. Doody, D. Rhind, and C. R. Mchenry, "Claw morphometrics in monitor lizards: Variable substrate and habitat use correlate to shape diversity within a predator guild," 6766 | *Ecology and Evolution*, vol. 8, pp. 6766–6778, 2018. doi: 10.1002/ece3.4185. [Online]. Available: [www.ecolevol.org](http://www.ecolevol.org).
- [69] Y. Song, Z. Dai, Z. Wang, A. Ji, and S. N. Gorb, "The synergy between the insect-inspired claws and adhesive pads increases the attachment ability on various rough surfaces OPEN," *Nature Publishing Group*, 2016. doi: 10.1038/srep26219. [Online]. Available: [www.nature.com/scientificreports](http://www.nature.com/scientificreports).
- [70] Unknown, *Nail Brush - Fully 3D printed! by Turbo\_SunShine - Thingiverse*. [Online]. Available: <https://www.thingiverse.com/thing:3355727> (visited on 09/13/2022).
- [71] J. Ou, C.-Y. Cheng, F. Heibeck, and H. Ishii, "Cillia - 3D Printed Micro-Pillar Structures for Surface Texture, Actuation and Sensing," *Designing New Materials and Manufacturing Techniques*, no. c, pp. 184–189, 2016. doi: 10.2307/j.ctt1n7qkg7.29.
- [72] G. Meirion-Griffith and M. Spenko, "A modified pressure-sinkage model for small, rigid wheels on deformable terrains," *Journal of Terramechanics*, vol. 48, no. 2, pp. 149–155, 2011, issn: 00224898. doi: 10.1016/j.jterra.2011.01.001. [Online]. Available: <http://dx.doi.org/10.1016/j.jterra.2011.01.001>.
- [73] S. Ramesh and S. R. V, "Evaluation of Bearing Capacity of ground in Transition Zone," 2021.
- [74] W. H. Perloff and K. S. A. Rah™, "A Study of the Pressure-Penetration Relationship For Model Footings on Cohesive Soil,"
- [75] P. Oettershagen, T. Lew, A. Tardy, and S. Michaud, "INVESTIGATION OF SPECIFIC WHEEL-TERRAIN INTERACTION ASPECTS USING AN ADVANCED SINGLE WHEEL TEST FACILITY,"



- [76] J. Tao, L. Ding, Q. Quan, and H. Gao, "Development and Experiments of a Test-bed for Wheel-Soil Interaction of Lunar Rover," in *Proceedings of the 12th European Conference on Spacecraft Structures, Materials and Environmental Testing*, 2012, p. 202.
- [77] M. Jiang, Y. Dai, L. Cui, and B. Xi, "Soil Mechanics – Based Testbed Setup for Lunar Rover Wheel and Corresponding Experimental Investigations," vol. 1, no. 6, pp. 1–10, 2017. doi: 10.1061/(ASCE)AS.1943-5525.0000782.
- [78] Y. Yang, Y. Sun, and S. Ma, "Drawbar pull of a wheel with an actively actuated lug on sandy terrain," *Journal of Terramechanics*, vol. 56, pp. 17–24, 2014, issn: 00224898. doi: 10.1016/j.jterra.2014.07.002. [Online]. Available: <http://dx.doi.org/10.1016/j.jterra.2014.07.002>.
- [79] J. Guo, W. Li, L. Ding, *et al.*, "Linear Expressions of Drawbar Pull and Driving Torque for Grouser-Wheeled Planetary Rovers Without Terrain Mechanical Parameters," *IEEE Robotics and Automation Letters*, vol. 6, no. 4, pp. 8197–8204, 2021, issn: 2377-3766. doi: 10.1109/lra.2021.3103641.
- [80] D. Liang, H.-B. Gao, Z.-Q. Deng, and J.-G. Tao, "Wheel slip-sinkage and its prediction model of lunar rover," *J. Cent. South Univ. Technol*, vol. 17, pp. 129–135, 2010. doi: 10.1007/s11771-010-0211-7.
- [81] S. Moreland, K. Skonieczny, D. Wettergreen, V. Asnani, C. Creager, and H. Oravec, "Inching locomotion for planetary rover mobility," *IEEE Aerospace Conference Proceedings*, 2011, issn: 1095323X. doi: 10.1109/AERO.2011.5747265.
- [82] S. Michaud, M. Hoepflinger, T. Thueer, *et al.*, "LESSON LEARNED FROM EXOMARS LOCOMOTION SYSTEM TEST CAMPAIGN," 2008.
- [83] J. Van Rijn and H. Goosen, *A system level performance analysis method for the design of a C-shape hexapod leg operating on compactive terrain*, 2022.
- [84] The Tribune, *Why the far side of the Moon so different from near side : The Tribune India*, Jun. 2020. [Online]. Available: <https://www.tribuneindia.com/news/schools/why-the-far-side-of-the-moon-so-different-from-near-side-102715> (visited on 10/06/2021).
- [85] J. Stuby, *Moon Craters*, <https://www.scienceabc.com/nature/universe/why-are-impact-craters-on-the-moon-round-and-not-some-other-shape.html>. [Online]. Available: <https://www.scienceabc.com/nature/universe/why-are-impact-craters-on-the-moon-round-and-not-some-other-shape.html>.
- [86] K. E. Bullen, "Cores of the terrestrial planets," *Nature*, vol. 243, no. 5402, pp. 68–70, 1973, issn: 00280836. doi: 10.1038/243068a0.
- [87] The European Space Agency, *ESA - Highlands and Mare landscapes on the Moon*, 2006. [Online]. Available: [https://www.esa.int/Science%7B%5C\\_%7DExploration/Space%7B%5C\\_%7DScience/SMART-1/Highlands%7B%5C\\_%7Dand%7B%5C\\_%7DMare%7B%5C\\_%7Dlandscapes%7B%5C\\_%7Don%7B%5C\\_%7Dthe%7B%5C\\_%7DMoon](https://www.esa.int/Science%7B%5C_%7DExploration/Space%7B%5C_%7DScience/SMART-1/Highlands%7B%5C_%7Dand%7B%5C_%7DMare%7B%5C_%7Dlandscapes%7B%5C_%7Don%7B%5C_%7Dthe%7B%5C_%7DMoon) (visited on 11/01/2021).
- [88] J. W. Head and A. Gifford, "Lunar Mare Domes: Classification and Modes of Origin," *The Moon and the Planets*, vol. 22, pp. 235–258, 1980. doi: <https://doi.org/10.1007/BF00898434>.
- [89] G. J. Taylor, P. Warren, G. Ryder, J. Delano, C. Pieters, and G. Lofgren, "Lunar Rocks," in *Lunar Sourcebook: A User's Guide to the Moon*, Cambridge University Press, 1991, pp. 183–284. doi: 10.1029/E00531009p00820.
- [90] S. Perkins, "Lava tubes may be havens for ancient alien life and future human explorers," *Proceedings of the National Academy of Sciences of the United States of America*, vol. 117, no. 30, pp. 17461–17464, 2020, issn: 10916490. doi: 10.1073/pnas.2012176117.
- [91] J. 9. NASA, *Sojourner*, [https://www.researchgate.net/figure/Figura-5-Sojourner-NASA-JPL-9\\_fig2\\_33421071](https://www.researchgate.net/figure/Figura-5-Sojourner-NASA-JPL-9_fig2_33421071). [Online]. Available: [https://www.researchgate.net/figure/Figura-5-Sojourner-NASA-JPL-9\\_fig2\\_33421071](https://www.researchgate.net/figure/Figura-5-Sojourner-NASA-JPL-9_fig2_33421071) (visited on 11/03/2021).
- [92] NASA, *Mars Exploration Rover Mission: Spotlight*. [Online]. Available: <https://mars.nasa.gov/mer/spotlight/wheels01.html> (visited on 11/03/2021).
- [93] R. E. Arvidson, P. DeGrosse, J. P. Grotzinger, *et al.*, "Relating geologic units and mobility system kinematics contributing to Curiosity wheel damage at Gale Crater, Mars," *Journal of Terramechanics*, vol. 73, pp. 73–93, 2017, issn: 00224898. doi: 10.1016/j.jterra.2017.03.001. [Online]. Available: <https://doi.org/10.1016/j.jterra.2017.03.001>.

- [94] N. Patel, R. Slade, and J. Clemmet, "The ExoMars rover locomotion subsystem," *Journal of Terramechanics*, vol. 47, no. 4, pp. 227–242, 2010, issn: 00224898. doi: 10.1016/j.jterra.2010.02.004. [Online]. Available: <http://dx.doi.org/10.1016/j.jterra.2010.02.004>.
- [95] P. Poulakis, E. S. Agency, J. L. Vago, *et al.*, "Overview and Development Status of the ExoMars Rover Mobility Subsystem," *Advanced Space Technologies for Robotics and Automation*, no. May, pp. 1–8, 2015.
- [96] K. Iizuka and T. Kubota, "Study of Flexible Wheels for Lunar Exploration Rovers : Running Performance of Flexible Wheels with Various Amount of Deflection," *Journal of Asian Electric Vehicles*, vol. 7, no. 2, pp. 1319–1324, 2009.
- [97] KOD Lab, *The RHex Hexapedal Robot*, <https://kodlab.seas.upenn.edu/past-work/rhex/>. [Online]. Available: <https://kodlab.seas.upenn.edu/past-work/rhex/> (visited on 11/04/2021).
- [98] C. Li, P. B. Umbanhowar, H. Komsuoglu, D. E. Koditschek, and D. I. Goldman, "Sensitive dependence of the motion of a legged robot on granular media," *PNAS*, no. 9, 2009. doi: 10.1073/pnas.0905342106.
- [99] S. F. Roberts and D. E. Koditschek, "RHex Slips on Granular Media," *IEEE International Conference on Robotics and Automation*, no. January, 2016.
- [100] R. D. Maladen, Y. Ding, P. B. Umbanhowar, A. Kamor, and D. I. Goldman, "Mechanical models of sandfish locomotion reveal principles of high performance subsurface sand-swimming," *Journal of the Royal Society*, no. March, pp. 1332–1345, 2011.
- [101] L. Xu, X. Liang, M. Xu, B. Liu, and S. Zhang, "Interplay of theory and experiment in analysis of the advantage of the novel semi-elliptical leg moving on loose soil," *2013 IEEE/ASME International Conference on Advanced Intelligent Mechatronics: Mechatronics for Human Wellbeing, AIM 2013*, pp. 26–31, 2013. doi: 10.1109/AIM.2013.6584063.
- [102] L. Xu, S. Zhang, N. Jiang, and R. Xu, "A hybrid force model to estimate the dynamics of curved legs in granular material," *Journal of Terramechanics*, vol. 59, pp. 59–70, 2015, issn: 0022-4898. doi: 10.1016/j.jterra.2015.03.005. [Online]. Available: <http://dx.doi.org/10.1016/j.jterra.2015.03.005>.



# Lunar Environment

When it comes to the lunar rover, it is very important to take into consideration the environmental conditions that the rover will be exposed to. The lunar environment is very different to that of Earth, with no atmosphere, extreme temperature variations and a terrain that has not yet been fully explored. This chapter will describe the Lunar surface conditions, the types of terrain the rover will most likely encounter and Lunar regolith.

## A.1. Lunar Conditions

As the Earth's constant companion, the Moon has been a source of wonder for mankind for millennia. It is only with recent advances in technology and space exploration that we have been able to explore the Moon and understand its history, conditions and processes. Compared to Earth, the Moon is about 3.7 times smaller with a gravity of  $1.62\text{m/s}^2$  which is roughly 6 times smaller than that of Earth's [8]. The Moon has a synchronous rotation with Earth which means that the Moon is rotating at the same rate that it revolves around the Earth. It also means that the same hemisphere of the Moon is seen from the Earth at all times. These two hemispheres are known as the "light" and "dark side" of the Moon. Unlike Earth, the Moon has a very thin atmosphere also known as an exosphere. This means that it has no protection against the sun's radiation or from meteor impacts [7]. It also means that the atmosphere is unable to insulate the surface of the Moon, nor trap any heat which results in large temperature fluctuations across the Moon's surface depending on the latitude of a location on the Moon and if that location is exposed to sunlight or not. The lowest temperature is experienced at the poles with a minimum temperature of  $-247^\circ\text{C}$  measured at the northern pole, while the highest temperature recorded is  $123^\circ\text{C}$  at the equator [8]. In terms of a magnetic field, it is possible that the early Moon may have had an internal dynamo which is responsible for generating magnetic fields for terrestrial planets, however, this is no longer the case and now the Moon's magnetic field is very weak [7].

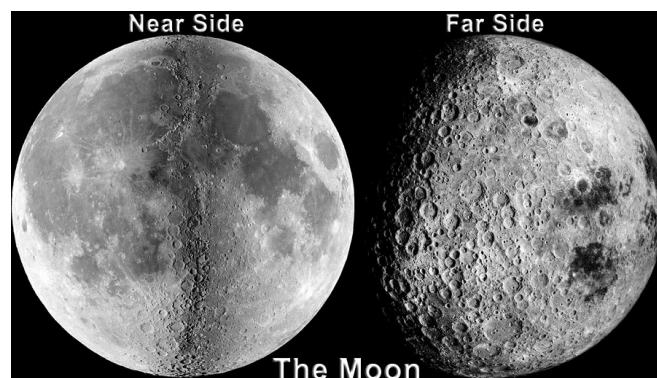
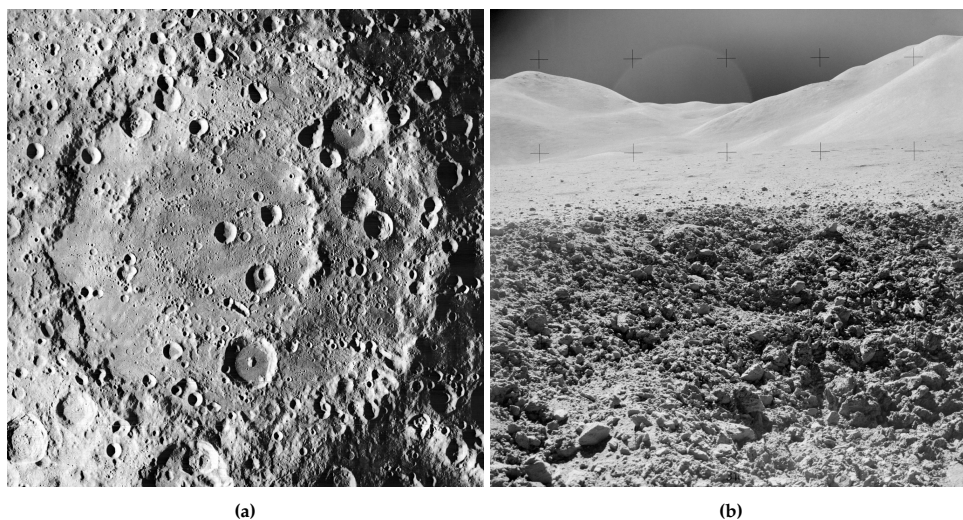


Figure A.1: Near Side and Far Side of the Moon [84]

## A.2. Terrain

The main function of the Lunar Zebro is to traverse the surface of the Moon, therefore, it is essential to understand what types of terrains and obstacles the rover may encounter in its journey. Unlike the Earth, the Moon is not subjected to agents which tend to alter the surface of terrestrial planets such as atmosphere, water or life. Additionally, there have been no recent geological activities on the Moon which means the lunar crust and mantle have remained unchanged for most of the Moon's geological time [13]. However, this does not mean that the surface of the Moon is unchanging. As mentioned previously, the Moon's atmosphere is too thin to be able to prevent impacts from meteors and asteroids. This has resulted in the surface of the Moon becoming riddled with impact craters that vary in size, ranging from a few microns to hundreds of kilometres in diameter [13]. Characteristically, as the diameter of the crater increases, the shallower the depth and the more complex the rims and floor become [13] as illustrated in Figure A.2a. These impacts have also resulted in impact fragments that range from massive boulders to powders [7], some examples of these fragments are shown in Figure A.2b.



**Figure A.2:** (a) Craters on the moon showing how the complexity of the craters increases as the diameter increases[85]. (b) Terrain [10]

The Lunar surface can be divided into two distinct landscapes known as the highlands which are light in colour and heavily cratered, and the lowland maria which are smooth and dark [86]. As seen in Figure A.1 the Maria are more prominent on the near side of the Moon whereas the highlands dominate the rest of the surface of the Moon and are more heavily cratered due to their age which is greater in comparison to the Maria[86]. The Maria was formed after basaltic lava filled up impact craters and then cooled and solidified forming basins rich in iron and magnesium [87]. As this happened fairly recently, between 4.2 and 1.2 billion years ago, the number of impact craters is considerably less than the highland areas [7].

Besides craters, there are other characteristic features on the Moon as a result of volcanic activity, namely, rilles, wrinkle ridges, domes, terraces and lava tubes. Rilles are deep channels that cut the surface of the Moon and were formed by previous volcanic activity [8][13]. Wrinkle ridges, also known as compressional ridges, were created when basaltic lava cooled and contracted causing the surface to buckle [13]. Domes are convex landforms that are a type of shield volcano with gentle slopes [88]. Terraces were created after the withdrawal of lava by draining into vents or by flowing into a lower basin and can be found along the mare-highland boundary [13]. Lastly, lava tubes are hollow underground channels where basaltic lava once flowed [89]. These tubes become visible when a part of the roof collapses revealing a skylight [90]. These lava tubes are of particular interest to researchers as they speculate that lava tubes could become prime locations for colonization [90]. The lava tubes provide an environment that is protected against radiation and meteorites, and which provides relief from the extreme temperature swings experienced on the surface of the Moon [90]. In addition to this, the lava tubes are good sources for geological research as they provide access to subsurface substrates without

the need to drill [90]. The Lunar Zebro is ideal for exploring these lava tubes. However, not much is known about what kind of terrain is in the Lava tubes, therefore Lunar Zebro would have to be able to navigate a wide variety of conditions.

### A.3. Lunar Regolith

The surface of the Moon is covered in a layer of unconsolidated rock fragments, also known as lunar regolith. Unlike terrestrial soils, regolith is created by the continuous impact of meteors as well as the constant bombardment of atomically charged particles from solar wind irradiation [11]. The bulk of lunar regolith is made up of particles that are less than 1 cm in size, although, there are larger boulders and rock fragments spanning several meters across and are more commonly found on the surface [11]. The impact cratering events result in heat, shock and pressure that cause a lot of the pulverized material to melt and join together to produce fragmental rock known as breccias and which makes up a large portion of the Lunar regolith and adds to its complexity [11]. The thickness of the regolith layer varies depending on the location on the Moon with a thickness of roughly 4-5 m on the mare and 10-15 m on the highlands [11]. Beneath the regolith is a layer of fractured rock known as megaregolith and may consist of large rock fragments (>1 m) [11]. However, there is not much known about the detailed properties of megaregolith [11]. The only time regolith does not cover the surface of the Moon is at the location of steep-sided crater walls where only bedrock is visible [11].

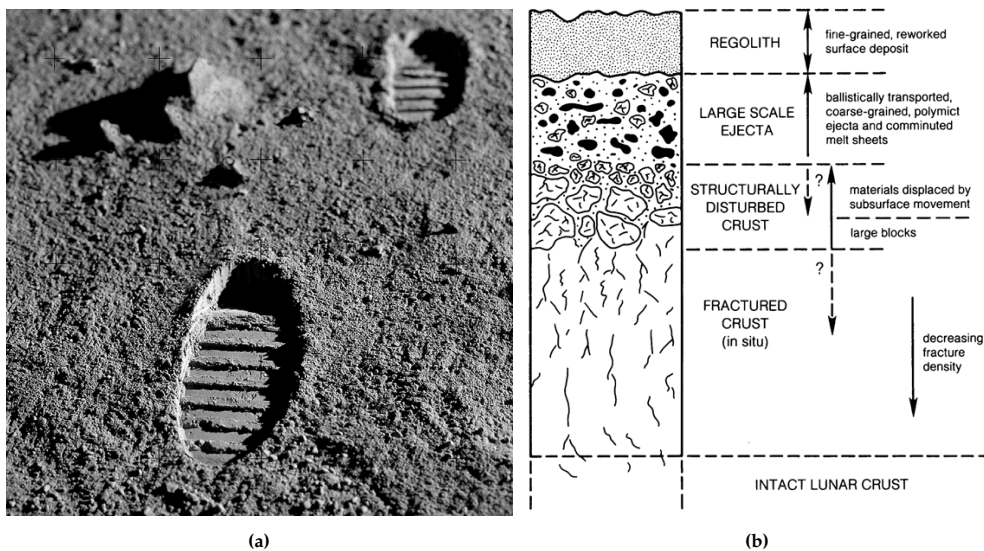


Figure A.3: (a) Regolith [9]. (b) Illustration of the regolith layers [13]

Within the regolith layer itself, the particle sizes vary greatly from microns to tens of meters. As mentioned previously, the bulk of the lunar regolith layer is less than 1 cm in size and can be subdivided into 3 categories: *Dust* (<50  $\mu\text{m}$ ), *soil* (<1 mm) and *coarse fine* (1-10 mm) [12]. Analysis of soil samples taken have found that the majority of the regolith is fined grained meaning that 95% of the particles are less than 1.37 mm in size of which the dust fraction makes up to 40-50% [12]. Lunar regolith also consists to a lesser extent of rocks (<1 cm) and boulders (<10 cm) however their distribution over the lunar surface is variable and largely dependent on the proximity to a fresh impact crater [12].

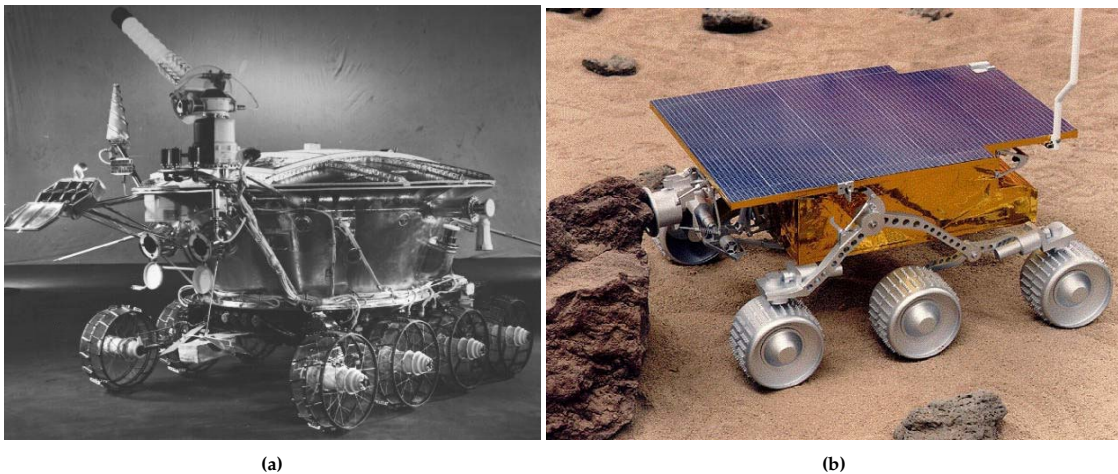
# B

## State of the Art

In this chapter, the state of the art is discussed in which different Planetary rovers are investigated. Special attention will be paid to the wheels or legs of the system and any other features that may improve traction. In addition to this, the RHex and its descendants are discussed as they are the basis on which the Lunar Zebro is designed. Lastly, other vehicles will be discussed whose designs are focused on increased traction.

### B.1. Planetary Rovers

Over the past 50 years many different planetary rovers have been designed with most going on to have successful missions. With each new rover, more and more lessons are being learnt of how to design these rovers so that they can successfully navigate the difficult terrains and conditions that are present on the Moon and on Mars. The figures below shows how much rovers have evolved over the years, with Figure B.1a showing the Lunokhod rover which was the first ever rover on the Moon. While Figure B.1b shows one of the latest Mars rovers, the Sojourner, with its Rocker Bogie suspension system.



**Figure B.1:** (a) The Russian vehicle Lunokhod with a classic wheeled chassis suspension system [14]. (b) Sojourner with a Rocker Bogie suspension system [91]



Figure ?? below gives an overview of the different rovers, showing the location the rovers were sent to, the type of suspension system they used and the the number of wheels they had.

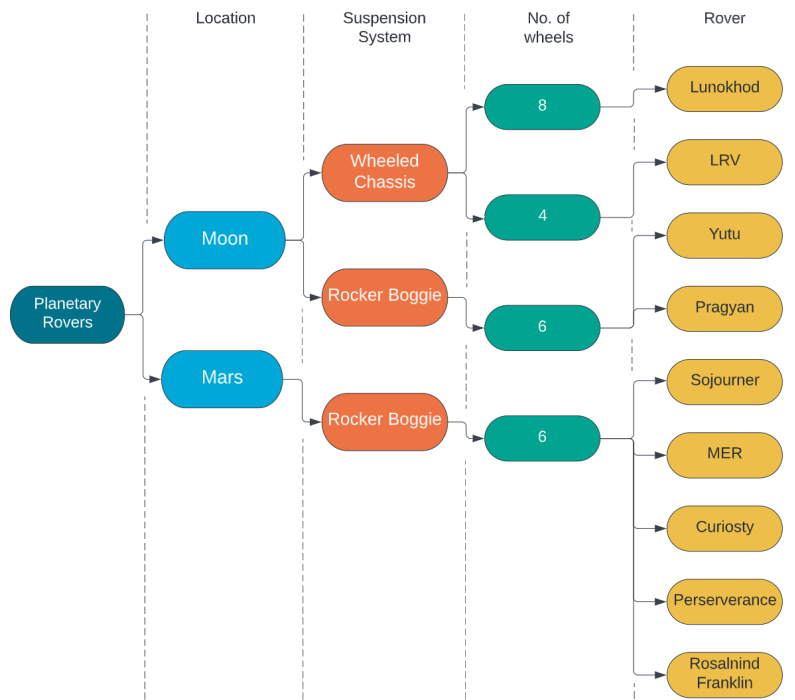


Figure B.2: Overview of the different planetary rovers

Table 3.1 on the next page, gives a more detailed overview of the different rovers and their wheels. It also notes important findings or events that may have occurred during the rovers' missions. In Figure B.2 the Yutu and Pragyan Rovers are listed, however there is very little information regarding the Yutu and Pragyan rovers, therefore they will not be discussed any further in the upcoming table.

From Table 3.1 it is interesting to note that the wheel design and grouser types are constantly changing with every new rover that is designed. This shows that with each new mission and with more research being done, the types of wheels used and their grousers are continuously evolving to have increased traction and more resistance to wear.




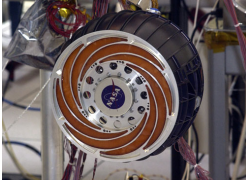


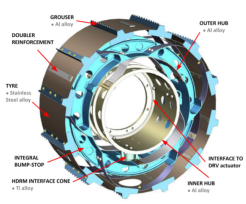
	Rover	Hubs	Grousers	Wheel	Important notes
Moon	Lunokhod [2]	<ul style="list-style-type: none"> <li>• Wire mesh</li> <li>• Titanium helical spring hoop</li> </ul>	<ul style="list-style-type: none"> <li>• Titanium cleats</li> <li>• Corrugated traverse pattern</li> </ul>		
	LRV - Lunar Roving Vehicles [2]	<ul style="list-style-type: none"> <li>• Flexible interwoven Zinc-coated wire mesh</li> <li>• Aluminium hub</li> </ul>	<ul style="list-style-type: none"> <li>• Titanium V/- Chevron pattern</li> </ul>		
Mars	Sojourner [2]		<ul style="list-style-type: none"> <li>• Thick steel cleats, 1cm in length</li> </ul>		
	MER : Spirit & Opportunity [92]	<ul style="list-style-type: none"> <li>• Machined from one piece of aluminium</li> <li>• Consists of spiral flexures to absorb shock</li> </ul>	<ul style="list-style-type: none"> <li>• Straight grousers with end caps to enhance structural strength [35]</li> </ul>		<ul style="list-style-type: none"> <li>• Opportunity got stuck in a sand trap but was able to free itself after a few weeks [2]</li> <li>• Spirit became permanently stuck in a sand trap [2]</li> </ul>
	MSL Rover: Curiosity [35]		<ul style="list-style-type: none"> <li>• W/- Chevron grouser</li> </ul>		<ul style="list-style-type: none"> <li>• The grousers were designed to increase the rover's ability to traverse rocky terrain</li> <li>• Tears formed at the pointed tips of the grousers [93]</li> </ul>
	Perseverance [35]		<ul style="list-style-type: none"> <li>• Sinusoidal grousers with a small curve</li> <li>• Double to number of grousers as the MSL rover</li> </ul>		<ul style="list-style-type: none"> <li>• The shape of the grousers improved the wheel's drawbar pull and durability</li> </ul>
	Rosalind Franklin [94]	<ul style="list-style-type: none"> <li>• Narrow wheel dimension</li> <li>• Flexible</li> </ul>	<ul style="list-style-type: none"> <li>• Straight serrated grousers</li> </ul>		<ul style="list-style-type: none"> <li>• The flexible wheel increases the wheel-soil contact area and reduces the ground pressures [95]</li> <li>• Helpful at preventing sinkage as the wheel flexes and matches the shape of the ground it is travelling on which reduces the overall stress on the wheel [96]</li> </ul>

Table B.1: Overview of the different planetary rovers

## B.2. RHex and Descendants

The Lunar Zebro is a descendant of the RHex, therefore some insight can be provided by looking into how these robots were designed and for what terrain. In this section, the design of the RHex will be discussed as well as some of its relevant descendants.

### B.2.1. The RHex

The RHex is a six-legged robot whose design was inspired by a cockroach as seen in Figure B.3a. One of the most prominent features of the RHex is its C-Shaped legs which are each individually actuated at the hip. The legs are made from a compliant material that aids in producing energy for the running gait [97]. The legs are controlled by a central computer that applies user commands to the system and receives sensor feedback to determine how the legs should move [97].

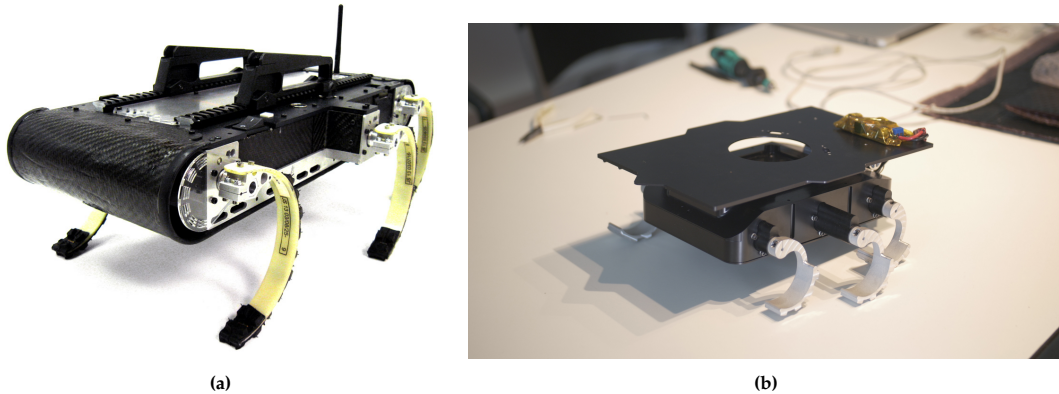


Figure B.3: (a) RHex [5]. (b) Lunar Zebro [4]

Much like a cockroach, the RHex is able to move by rotating the legs in threes with the front and rear legs on the one side rotating in sync with the middle leg on the opposite side as seen in Figure B.4a. When it comes to scaling large objects, the RHex will keep rotating its legs until it can find a perch and lift itself up. However, the RHex is limited in the maximum height that it is able to climb which is determined by the radius of the legs as seen in Figure B.4b.

All of this combined allows the RHex to traverse a wide variety of different terrains including uneven, flat and sandy terrains. It even outperforms other robots with wheels or continuous tracks on rough terrains. Therefore, owing to its versatility in navigating difficult terrains, the RHex has inspired the development of very similar robots such as the Lunar Zebro (Figure B.3b).

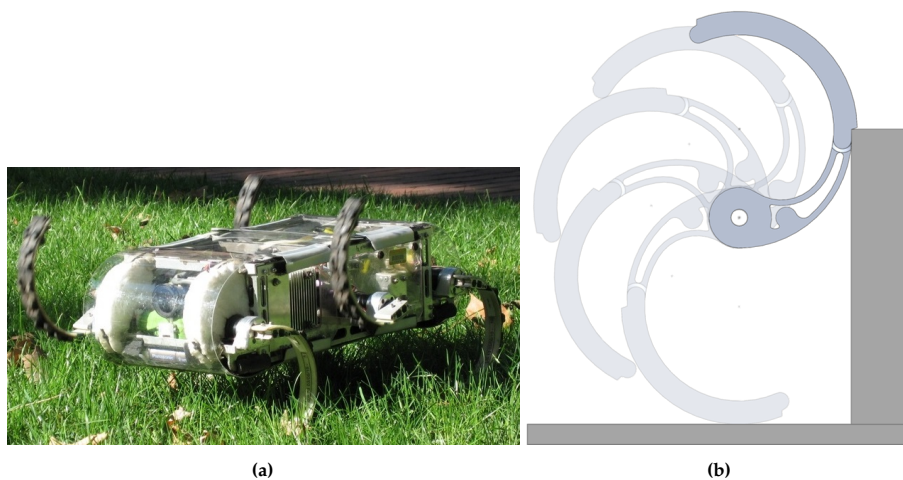


Figure B.4: (a) RHex uses a alternating tripod gait [6]. (b) Climbing Height

### B.2.2. SandBot

Since the RHex performed well on a wide variety of terrains the CRAB Lab (Georgia Institute of Technology) and Kod\*Lab (The University of Pennsylvania) went on to develop the SandBot to walk on sandy terrains (Figure B.5a). Traversing a terrain that consists of granular media is particularly challenging as the ground tends to act like both a solid and a fluid depending on the stresses acting on it [98]. They assumed the robot would perform as well as it did on other terrains, however, the SandBot got stuck after a few steps, with the legs spinning uselessly without propelling the robot forward. They then decided to alter the gait of the robot by modifying the speed of the rotation so that the legs would rotate slower when in contact with the ground and then speed up again when in the air [20]. They found that at low frequencies, the penetration depth of the leg was reduced as the leg is able to enter the material more gently allowing the grains to compact to prevent further sinkage [20]. At high frequencies, this behaviour does not occur and the robot displays swimming like behaviour [20].



Figure B.5: (a) SandBot [20]. (b) Desert RHex [21]

### B.2.3. Desert RHex

Like the SandBot, the Desert RHex was also developed to walk on granular material (Figure B.5b). The purpose of the Desert RHex was to navigate desert landscapes to collect data for research purposes. While testing the suitability and capabilities of the Desert RHex, several observations were made. When ascending dunes, it was noticed that the robot showed signs of obvious slip at the toe which became increasingly obvious as the angle of inclination increased [99]. In addition to this, while testing the robot on dunes with an incline face greater than  $25^\circ$ , the back legs would often hit their thermal limit and the motors would stall [21].

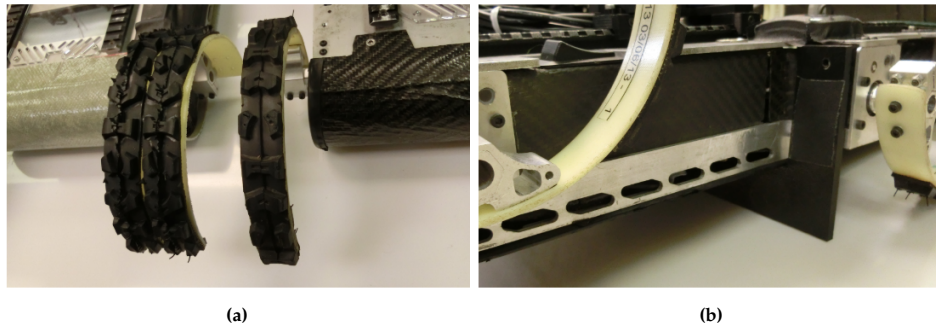
The team also decided to investigate the impact that some morphological changes would have on the performance of the RHex. Some of the changes they investigated were : (1) increasing the width of the leg, (2) moving the centre of mass, and (3) adding a fin to the body of the RHex. However, it must be noted that the experiments that were done were not done in a controlled environment but action was taken to attempt to make the testing conditions as similar as possible.

When increasing the width of the legs, they simply doubled the width as seen in Figure B.6a. It was found that the wide-legged RHex had a specific resistance of 1.1 compared to the specific resistance of 1.3 of the thin-legged RHex [22]. This is evident in the fact that the wide-legged RHex was able to travel further in a single gait cycle than the thin-legged RHex [22]. The difference in specific resistance also means that the wider legs are roughly 20% more efficient than the thinner legs, which increases the range that the robot can travel [22]. When it comes to controlling the RHex while it is walking on the sand, the wide-legs turning performance was greater, making it easier to control [22]. However, it is interesting to note that when ascending a dune with a  $30^\circ$  inclination, the thin-legged robot outperformed the wide-legged robot [22]. The researchers hypothesize that the reason for this is because the thin legs are able to penetrate deeper into the sand and reach more compacted sand underneath [22].

It was noticed in previous experiments that the robot would sometimes fail because the robot would pitch backwards on steep inclines [21]. So to counteract this the centre of mass was moved to the front which resulted in a better performance when ascending inclines [22]. The researchers hypothesize that



having the centre of mass in the front relieves pressure on the rear legs and which subsequently prevents them from stalling [22]. However, it was noticed that when descending an incline the performance of the robot was worse, with the front of the robot often bumping into the ground [22]. This could prove fatal to sensor equipment resulting in poor measurements.



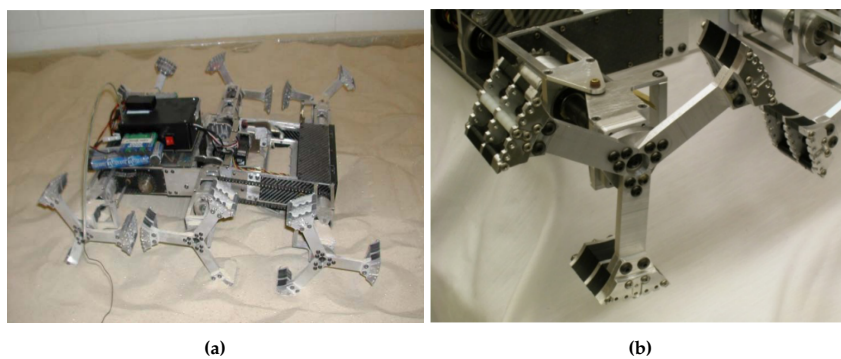
**Figure B.6:** (a) Two robots with two different sizes of legs [22]. (b) The fin used to prevent downward sliding on steep inclines[22]

The last morphological change that was made to the robot was to add a stiff, horizontal strip to the underside of the robot as seen in Figure B.6b. The idea is that the fin will aid the robot when ascending steep inclines to "grip" the sand and prevent the robot from sliding back down [22]. When testing the fin, they found that the Robot was able to ascend slopes 5-7° steeper than without the fin [22].

Besides these changes, the researchers also suggested additional improvements that could be investigated to increase the performance of the RHex. These include using more powerful motors (especially for the rear legs), using bigger treads or cleats as the current treads fill up with sand and become useless [21][22]. Lastly, they also suggested using the middle legs as a source of friction instead of a fin [22].

#### B.2.4. Whegs

Like the RHex, the Whegs is also a six-legged robot inspired by the cockroach as seen in Figure B.7a. However, unlike the RHex, the Whegs uses three-spoke legs that are driven by a single motor. These legs can be seen in Figure B.7b. The feet of the Whegs were designed to have a concave contact area which allows the weight of the robot to be distributed over a larger surface area to prevent the robot from sinking in soft sand [3]. The feet have open compartments which are able to compress the sand and provide the robot with support and traction [3].



**Figure B.7:** (a) Whegs [3]. (b) Whegs Leg [3]

## B.3. Other Vehicles that focus on Traction

There are a number of vehicles that are designed to traverse difficult terrains such as tractors and dune buggies. These vehicles incorporate features that have proven to be successful in increasing their traction and which can also be applied to the Lunar Zebro. These features will be discussed in the following sections.

### B.3.1. Tractors

The wheels of tractors are designed to provide them with traction to prevent slip in terrains where other vehicles are unable to navigate. Tractors normally have large rear wheels which increase the contact area with the ground allowing for increased friction and less slippage [23]. This increased surface area also exerts less pressure on the ground which prevents the tires from sinking into the soil and getting stuck. Furthermore, it also increases the efficiency of the tractor [23]. The larger diameter also increases the maximum torque the wheel exerts on the ground [23]. In addition to this, the rear tires of tractors have very deep treads which increases traction and allows them to navigate difficult and steep terrain [23]. Tractors also have smaller front wheels which allow them to have a smaller steering radius which means they have a higher manoeuvrability [23]. The difference between the two sizes of the wheel does mean that the rate of wear is higher on the smaller front tires than on the larger rear tires [23]



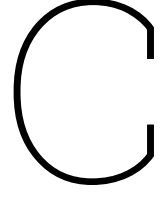
Figure B.8: (a) Tractor [24]. (b) Sandrail [25]

### B.3.2. Sand based Vehicles

There are a few vehicles that have been designed to drive over sand dunes. One of these vehicles is known as the Sandrail (Figure 1.6b). The Sandrail has specialized tires that allow it to drive over sandy terrains. It normally uses flotation tires for the front wheels and paddle tires for the rear wheels. Flotation tires are used to "float" over loose soil, meaning they prevent the tire from sinking into the soft terrain [26]. They are able to do this because these tires are wide and used in combination with a low tire pressure which expands the tire's footprint and increases the ground contact area [26]. In addition to this, the tires do not have deep treads that cut into the ground which means that flotation tires are able to minimize soil disturbances [26]. An example of a flotation tire is shown in Figure B.8b as the front tires.

In contrast, the paddle tires used for the rear wheels are covered in paddles that cover the entire wheel. When driving over loose terrain, the paddles of the wheels are designed to slide into the sand and scoop it up before expelling it which increases the traction of the tire [27]. The more paddles a tire has, the more traction it has, but it also means more torque is required to turn the wheels [27]. The rear tires in Figure B.8b are an example of paddle tires.





# Terramechanics Supplementary

## C.1. Terramechanics of C-shaped Legs in very loose soil

A lot of research has been done into terramechanics to determine how large wheeled vehicles interact with sandy terrains and a set of semi-empirical equations were found by Bekker [32] as shown previously. However, this theory cannot be applied to C shaped legs, which are semi-submerged in granular media. Instead, it was suggested by Maladen et al. [100] to use "Resistive Force Theory" (RFT) to estimate the interaction forces between granular media and submerged locomotors. This theory was further expanded upon by Xu et al. [101],[102] in combination with a failure-based model to create a hybrid model and applied to C-shaped legs.

### C.1.1. Hybrid model

Figure C.1 shows a curved leg with a fixed axle height,  $h$ . This height is assumed to be constant for two reasons: (1) when the granular material is very loose, the leg will sink into the substrate until the body can support the weight of the robot on the surface of the substrate; (2) when the granular material is more densely packed, the height  $h$  will fluctuate, however, the forces acting on the legs at each moment in time can be determined with a certain  $h$  at that moment. As part of the RFT model, the leg can be divided into infinitesimal segments with normal,  $F_{\parallel}$ , and tangential,  $F_{\perp}$ , force components applied by the granular material. Together, these forces contribute to the forward advancing force,  $F_f$ , the supportive force,  $F_s$ , and the Torque,  $T$ , of the leg. This model neglects the internal forces between the infinitesimal segments and it also assumes the packing fraction of the granular material to be constant at all locations on the leg.

The approximate forward advancing force, supportive force and torque of the entire leg can be calculated by integrating the individual force components of each segment over the part of the leg that is submerged in the granular material at any time during the rotation of the leg. These equations are shown in (C.1) below:

$$\begin{aligned}
 F_f(\theta, h) &= \int_{L_s} (F_{\perp} \cos\beta + F_{\parallel} \sin\beta) dl \\
 F_s(\theta, h) &= \int_{L_s} (F_{\perp} \sin\beta - F_{\parallel} \cos\beta) dl \\
 T(\theta, h) &= \int_{L_s} (M_x + M_y) dl
 \end{aligned} \tag{C.1}$$

Where:

$$\begin{aligned}
 M_x &= dF_f(d + h) \\
 M_y &= dF_s(\zeta + \theta - \pi/2)
 \end{aligned}$$

In the above equations,  $L_s$  represents the subsurface edge of the curved leg and  $M_x$  and  $M_y$  are the torques experienced by each element as a result of  $F_x$  and  $F_y$  respectively. Additionally,  $F_{\parallel}$  and  $F_{\perp}$  are

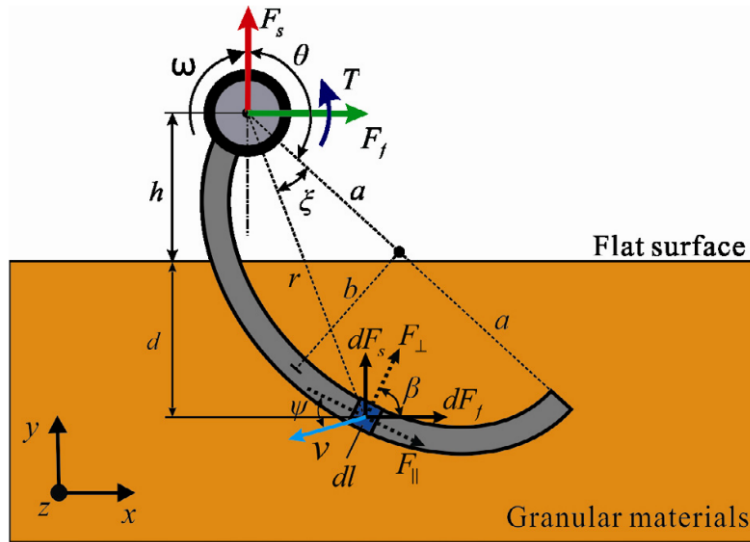


Figure C.1: Resistive Force Theory (RFT) schematic of a curved leg in granular material at a certain depth [102]

dependent on the submerging depth,  $d$ , the velocity,  $v$ , and the tangential direction of the curve,  $\psi$ . But it can also be expressed in terms of the angular position of the leg,  $\theta$ , the angular position of the segment,  $\zeta$ , and the angular velocity of the leg,  $\omega$ :

$$\begin{aligned} F_\perp &= f_1(\psi, v, d) = f_1(\theta, \zeta, \omega) \\ F_\parallel &= f_2(\psi, v, d) = f_2(\theta, \zeta, \omega) \end{aligned} \tag{C.2}$$

The depth has a big impact on  $F_\parallel$  and  $F_\perp$ , which can be explained by Bekker [33] in equation 2.3.

In order to improve the RFT model, Xu et al [102] applied a failure-based model to a bar drag model as shown in Figure C.2. This model takes into account the movement of the sand, as the top surface of the sand bulges in front of the bar and subsides behind it. This model can be used to determine the normal and lateral forces of each segment of the leg as a function of its depth and speed.

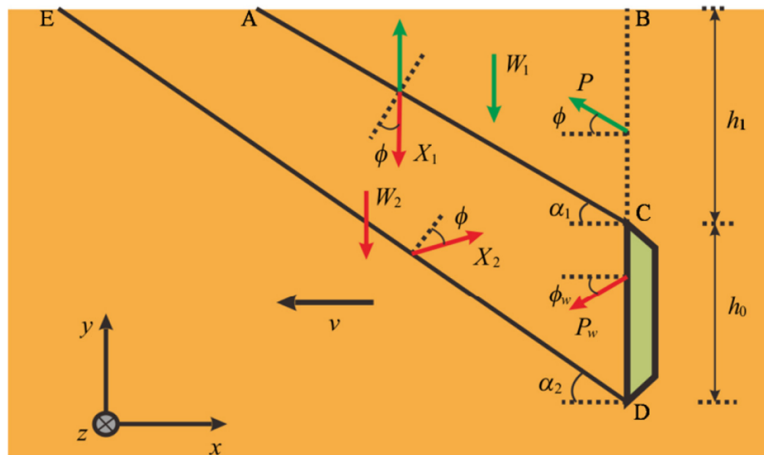
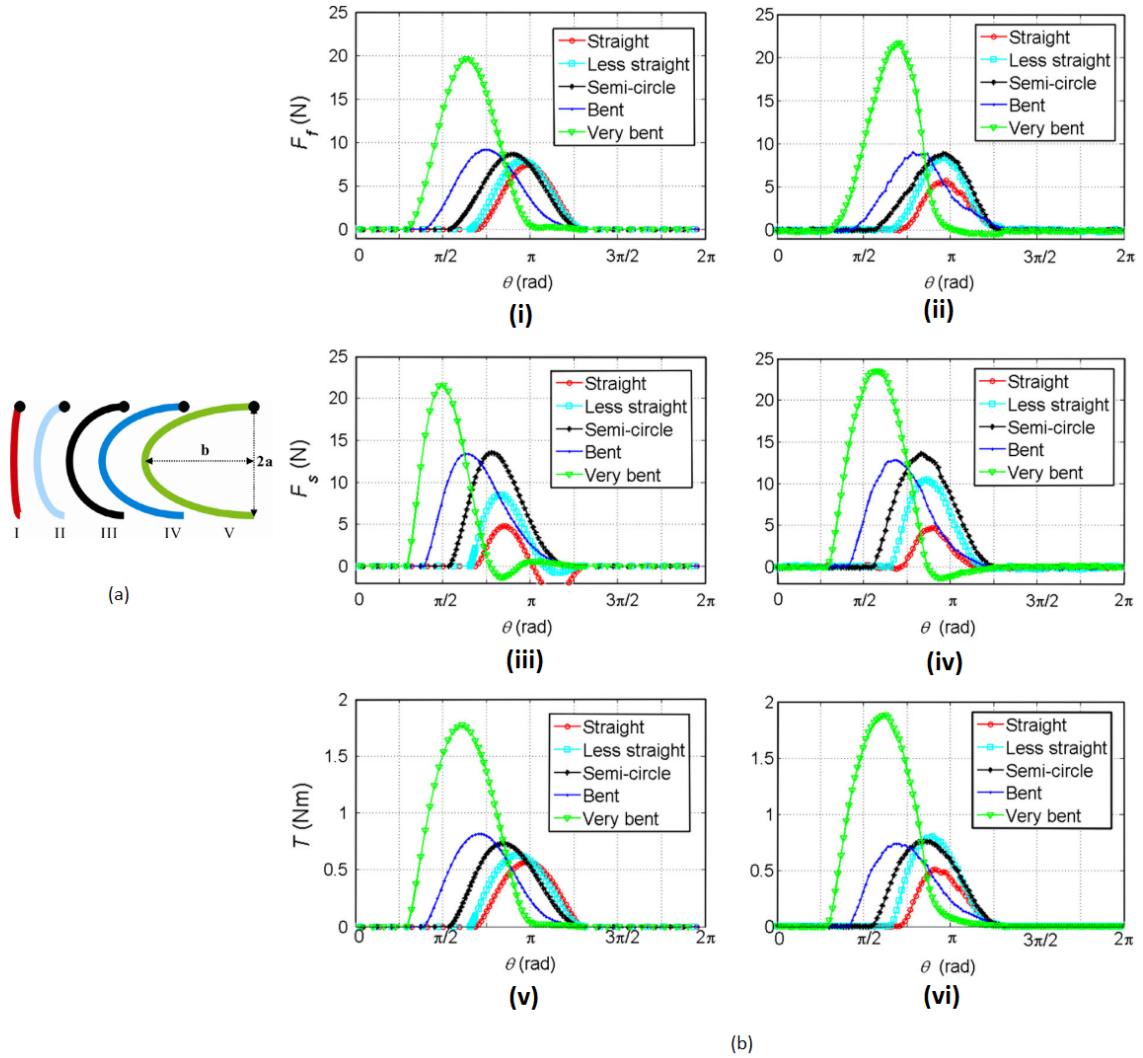


Figure C.2: Failure-based model schematic for a bar in granular media at a certain depth  $h_1$  [102]

The hybrid model was verified using experimental results and it revealed that the model is able to predict with relatively high accuracy the dynamics of complex shapes. However, this model does not take into account different compaction rates and therefore this model can be expanded upon to improve its accuracy.

### C.1.2. Influence of leg shape

Xu et al [102] also investigated the influence of different leg shapes on the dynamic forwarding advancing and supportive forces as well as the torque over a single cycle of a leg penetrating granular media. These different leg shapes and their corresponding simulated and measured forces and torques can be seen in Figure C.3 below.



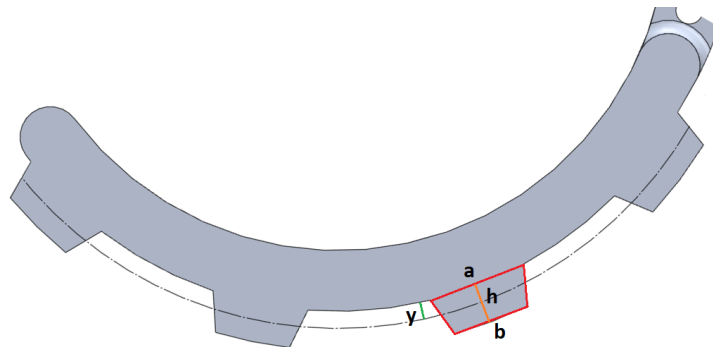
**Figure C.3:** (a) The five different curved leg shapes with variable values of  $a$  and  $b$ [102]. (b) Modelled and experimental Forces and Torque acting on the different leg types during one rotational period[102]

The results show that  $F_f$  and  $F_s$  are relatively small for the straight leg profile but increase monotonically as  $b$  increases until the semi-circle leg profile ( $a = b$ ) is reached. As the leg profile changes from semi-circular to a bent shape ( $a < b$ ), the peak forces remain relatively constant but their angular positions differ. As  $b$  increases significantly, the peak forces and their positions also change significantly. Figure C.3b (v) and (vi) show that as  $b$  increases the amount of torque needed to penetrate the granular material also increases. Analysis of the results by Xu et al. [102] concluded that when the granular media is very loose and energy is not a limiting factor, the very bent leg is the best option. However, if energy is a limiting factor, selecting a semi-circular leg or a bent leg helps to balance the advantages of higher forces to the disadvantages of higher. It also helps with reducing the fluctuations in the position of the centre of mass of the leg. Another suggestion by Xu et al. [102] to increase the performance of the legs is to lower the rotational speed of the leg during the overlapping regions of  $F_f$  and  $F_s$  to reduce the inertial force of the robot and then increases the speed of the leg when regions do not contribute to the forces. This will affect the overall gait of the robot.

# D

## Flat Leg Dimensions

The ground contact area of a leg impacts the amount of traction it has. This area is dependent on the outer radius of the leg, therefore, the outer radius of the leg was chosen to be located along the centre of point of the grousers in the original leg as shown in the figure below:



**Figure D.1:** Grouser dimensions used to calculate the centre for the radius of the flat leg

$$y = h(b + 2a)/3(a + b) \tag{D.1}$$

The Matlab calculations can be found on the next page.

```
close all
clear
```

### Constants

```
a = 7.33;           % trapezium bottom length
b = 5.7;           % trapezium top length
ri = 29.56;        % Original leg grouser inner radius
ro = 32.5;         % Original leg grouser outer radius
```

### Calculating Height

```
h = ro-ri          % trapezium height
```

```
h = 2.9400
```

### Calculating Flat leg Radius

```
y = h*(b+2*a)/(3*(a+b)); % Height of centre of trapezium height
rf = ri + y                % Flat leg radius
```

```
rf = 31.0913
```

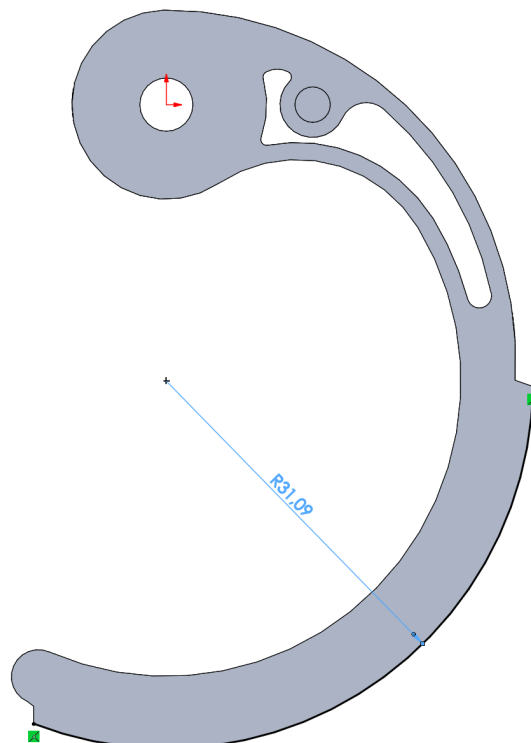
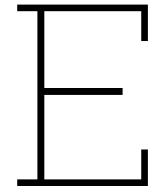


Figure D.2: Flat leg Radius



# Lunar Zebro Dimensions and Requirements

The following information was Ascertained through personal correspondence with the Lunar Zebro team.

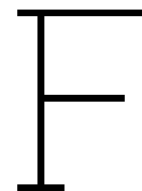
## **E.1. Dimensions**

The Lunar Zebro takes up a space of roughly 335x270x80mm (L x b x h).

## **E.2. Requirements**

- The rover shall be able to traverse obstacles of at least 55 mm.
- The rover shall be able to safely climb a maximum forward gradient of 30 °.
- The rover shall be able to safely climb a maximum sideways gradient of 15°.
- The rover shall have a maximum mass of 2 kg excluding the deployment system.
- The legs shall be able to survive with no plastic deformation a bending moment of maximum 1 Nm.
- The legs material shall allow a maximum of 0.25mm of abrasion by lunar regolith.
- The legs shall have a clearance between each other of minimum 5 mm.
- The legs shall have a clearance between each other of minimum 5 mm when closest between two legs are facing opposite directions aligned.
- The LMS shall enable the rover to propel forward in direction at a maximum speed of 5 cm/s in flat terrain and with the solar panel stowed.
- The LMS shall enable the rover to propel forward in direction at a nominal speed of 1 cm/s in flat terrain and with the solar panel stowed.
- The LMS shall enable the rover to propel backward in direction at a maximum speed of 1 cm/s in flat terrain and with the solar panel stowed.
- The legs shall not allow the rover to sink more than 5mm into lunar soil while walking.





# Risk Assessment and SDS

## RISK ASSESSMENT FORM

RISK TYPE *select one*

<input type="checkbox"/>	Financial
<input type="checkbox"/>	Legal / Contractual
<input type="checkbox"/>	Reputation / Customer Relations
<input checked="" type="checkbox"/>	Resources
<input type="checkbox"/>	Operational

RISK DESCRIPTION

Working with a Carcinogenic Material – <ul style="list-style-type: none"><li>• Carcinogen Category 1A</li><li>• Specific Target Organ Toxicity- Repeated Exposure</li></ul>
---

SOURCE OF RISK

<ul style="list-style-type: none"><li>• LHS-1 Lunar Highlands Simulant</li><li>• When transferring the simulant from the original packages to the testbed, significant amounts of dust will be created</li><li>• This experiment involves testing different leg types of the Lunar Zebro by dragging the legs through the simulant</li><li>• During the experimental preparation, the simulant needs to be prepared by raking and then flattening which may kick up some dust</li><li>• When preparing and performing the experiment, all persons will be in close contact with the simulant</li></ul>
--

PERSON(S) IMPACTED *check all that apply*

<input checked="" type="checkbox"/>	Self
<input checked="" type="checkbox"/>	Public
<input checked="" type="checkbox"/>	Other: TU Delft Lab Technicians

**RISK IMPACT** *select one*

	IMPACT LEVEL	DESCRIPTION
	NOT SIGNIFICANT	Negligible injuries not needing medical treatment
	MINOR	Minor injuries causing temporary impairment needing medical treatment
X	MODERATE	Illness and/or injury requiring hospitalization
	MAJOR	Illness and/or injury resulting in permanent impairment
	SEVERE	Fatality

**RISK PROBABILITY** *select one*

	PROBABILITY LEVEL	DESCRIPTION
	HIGHLY UNLIKELY	Rare chance of an occurrence
X	UNLIKELY	Not likely to occur under normal circumstances
	POSSIBLE	May occur at some point under normal circumstances
	LIKELY	Expected to occur at some point in time
	HIGHLY LIKELY	Expected to occur regularly under normal circumstances

**RISK SEVERITY MATRIX** *based on Impact and Probability Levels*

IMPACT x PROBABILITY	NOT SIGNIFICANT	MINOR	MODERATE	MAJOR	SEVERE
HIGHLY UNLIKELY	LOW	LOW	LOW / MED	MEDIUM	MEDIUM
UNLIKELY	LOW	LOW / MED	LOW / MED	MEDIUM	MED / HIGH
POSSIBLE	LOW	LOW / MED	MEDIUM	MED / HIGH	MED / HIGH
LIKELY	LOW	LOW / MED	MEDIUM	MED / HIGH	HIGH
HIGHLY LIKELY	LOW / MED	MEDIUM	MED / HIGH	HIGH	HIGH

**RISK SEVERITY LEVEL** *select corresponding Severity Level from matrix above based upon Impact and Probability Levels*

	SEVERITY LEVEL
	LOW
X	LOW / MED
	MEDIUM
	MED / HIGH
	HIGH

PPE Required

- 1. FFP3 Mask
- 2. Safety glasses
- 3. Gloves

CURRENT CONTROL MEASURES

- 1. When transferring the simulant into the testbed, relevant PPE and a cleanroom gown shall be worn.
- 2. Transferring the simulant into the testbed shall take place outside and away from any persons not wearing the required PPE.
- 3. The experiment shall be performed in an area where there is very little foot traffic and where the air flow is not strong enough to kick up dust from the simulant.
- 4. When performing experiments, all PPE shall be worn
- 5. Clothes worn when performing experiments shall be washed at the end of every day
- 6. When not in use, the testbed shall be enclosed using a lid for the testbed and a warning sign shall be placed on the lid to warn others not to open unless needed

FURTHER ACTION NEEDED? *select one*

<input type="checkbox"/>	YES
<input checked="" type="checkbox"/>	NO

REMARKS

SDS is attached below

# SAFETY DATA SHEET

Compliant with OSHA's Hazard Communication Standard, 29 CFR 1910.1200(g)

## SECTION 1 - CHEMICAL PRODUCT AND COMPANY IDENTIFICATION

**Product Name:** LHS-1 Lunar Highlands Simulant

**Product Use:** Regolith/planetary simulant

**Manufactured by:** University of Central Florida

Office of Research and Commercialization

12201 Research Parkway, 5<sup>th</sup> Floor

Orlando, FL 23826-3246

**Emergency Contact:** 1-800-535-5053

Or contact your regional Poison Control

**MSDS Issue Date:** 10/04/18

## SECTION 2 - HAZARDS IDENTIFICATION

### Hazard Classification:

Physical	Health
Not hazardous	Carcinogen Category 1A Specific Target Organ Toxicity – Repeated exposure

**Signal Word:** Danger

**Hazard Statements:** May cause cancer by inhalation. Causes damage to lungs through prolonged or repeated exposure by inhalation.

### Pictograms:



### Precautionary Statements - Prevention

Obtain special instructions before use

Do not handle until all safety precautions have been read and understood

Use personal protective equipment as required

Do not breathe dust/fume/gas/mist/vapors/spray

Wash face, hands and any exposed skin thoroughly after handling

Do not eat, drink or smoke when using this product

### Precautionary Statements - Storage

Store locked up

**Precautionary Statements - Response**

If exposed or concerned: Get medical advice/attention

**Precautionary Statements - Disposal**

Dispose of contents/container to an approved waste disposal plant

**Carcinogenicity:** Natural terrestrial minerals are commonly contaminated with crystalline silica (quartz). Independent laboratory analyses indicate that crystalline silica is present in one or more of the simulant components. The International Agency on Research for Cancer (IARC) has classified silica dust, crystalline as a Group 1, known human carcinogen.

**SECTION 3 - COMPOSITION/INFORMATION ON INGREDIENTS**

---

Component	CAS Number	Wt. %
Plagioclase	68476-25-5	74.4
Basaltic Glass	Not Listed	24.2
Basalt	Not Listed	0.5
Ilmenite	12168-52-4	0.4
Pyroxene	14483-19-3	0.3
Olivine	10034-94-3	0.2

**SECTION 4 - FIRST AID MEASURES**

---

**Inhalation:** If irritation or discomfort exists, remove the exposed individual to fresh air.

**Eyes:** If irritation or discomfort exists, flush eyes lightly with water to remove dust.

**Skin:** Wash exposed skin if irritation exists.

**Ingestion:** Adverse effects not expected from this product.

**SECTION 5 - FIREFIGHTING MEASURES**

---

**Flashpoint:** Not applicable (solid)

**Flammable Limits:** N/A

**Autoignition Temperature:** N/A

**Extinguishing Media:** Water Spray (Fog), Foam, CO<sub>2</sub>

**Unusual Fire and Explosion Hazards:** N/D

**Special Protective Equipment or Precautions for Firefighters:** N/A

**SECTION 6 - ACCIDENTAL RELEASE MEASURES**

---

**Use of Personal Precautions:** Wear protective equipment including gloves and safety glasses.

**Emergency Procedures:** N/A

**Methods and Materials Used for Containment:** N/A

**Cleanup Procedures:** Spray lightly with water to avoid creating dust and sweep/shovel into suitable container.

**SECTION 7 - HANDLING AND STORAGE**

---

**Precautions for Safe Handling:** Avoid creating dust. Wash exposed skin and clothes daily.

**Recommendations on the Conditions for Safe Storage:** Do not store near heat or open flame. Keep container closed when not in use. Special containers or storage locations are not required. Incompatible with strong oxidizers.

## SECTION 8 – EXPOSURE CONTROL/PERSONAL PROTECTION

---

**Respiratory Protection:** Not required if dust levels are maintained below occupational exposure limits (TLV-TWA of 10 mg/m<sup>3</sup>). For levels above the occupational exposure limits wear an appropriate NIOSH approved respirator.

**Gloves:** None required. For hygiene purposes, chemically compatible gloves are appropriate.

**Protective Clothing:** None required. Confine work clothing to workplace and wash daily.

**Eye Protection:** Safety glasses should be worn.

## SECTION 9 – PHYSICAL AND CHEMICAL PROPERTIES

---

**Appearance:** Light gray powder.

**Upper/lower flammability or explosive limits:** N/D

**Odor:** None.

**Vapor pressure:** N/D

**Odor threshold:** N/D

**Vapor density:** N/D

**pH:** N/D

**Relative density:** N/D

**Melting point/freezing point:** N/D

**Solubility:** Insoluble in water.

**Initial boiling point and boiling range:** N/D

**Flash point:** N/D

**Evaporation rate:** N/D

**Flammability:** N/D

**Partition coefficient (n-octanol/water):** N/D

**Auto-ignition temperature:** N/D

**Decomposition temperature:** N/D

**Viscosity:** N/D

## SECTION 10 – STABILITY AND REACTIVITY

---

**Stability:** Stable.

**Incompatibility (Materials to Avoid):** Strong oxidizers.

**Hazardous Decomposition Productions:** Releases carbon monoxide, carbon dioxide, sulfur monoxide, sulfur dioxide and methane upon combustion.

**Hazardous Polymerization:** Will not occur.

**Conditions to Avoid:** Heat, open flames, sparks.

## SECTION 11 – TOXICOLOGICAL INFORMATION

---

**Likely routes of exposure:** Inhalation, eye contact.

**Symptoms related to the physical, chemical and toxicological characteristics:** None known.

**Effects of Chronic Exposure:** Adverse health effects including silicosis, lung cancer, autoimmune and chronic kidney diseases, tuberculosis, and non-malignant respiratory diseases are attributed to respirable crystalline silica.

**Numerical Measures of Toxicity:** No data available.



**Carcinogen Listings:** The International Agency on Research for Cancer (IARC) has classified silica dust, crystalline as a Group 1, known human carcinogen.

## SECTION 12 - ECOLOGICAL INFORMATION

---

**Ecotoxicity:** No data available.

**Persistence and Degradability:** No data available.

**Bioaccumulative Potential:** No data available.

**Mobility in Soil:** No data available.

**Other Adverse Effects:** No data available.

## SECTION 13 - DISPOSAL CONSIDERATIONS

---

**Waste Disposal Method:** Disposed of in accordance with all applicable local, state, and federal regulations.

## SECTION 14 - TRANSPORTATION INFORMATION

---

**UN Number:** N/A

**UN Proper Shipping Name:** N/A

**Transport Hazard Class:** N/A

**Packing Group:** N/A

**Environmental Hazards:** N/A

**Transport in Bulk:** N/A

**Special Precautions in Connection with Transport:** N/A

## SECTION 15 - REGULATORY INFORMATION

---

**Safety, Health and Environmental Regulations for the Product in Question:** None known.

## SECTION 16 - OTHER INFORMATION

---

**SDS Prepared on:** 10/04/2018

**Last Known Revision:** 10/04/2018

**Note:** N/A or N/D as an information entry means the data is not applicable or determined, respectively. This document has been prepared using data from sources considered technically reliable. It does *not* constitute a warranty, express or implied, as to the information contained within. Actual conditions of use, handling, storage, and disposal are beyond manufacturer's control. User is responsible to evaluate all available information when using the product for any particular use and to comply with local, state, and federal regulations.



## Calculating Ultimate Sinkage

```
close all  
clear
```

### Constants

```
phi = 31.49;           % simulant (deg)  
b = 20;               % width of leg (mm)  
D = 61.86;           % Diameter of leg (mm)  
phix = atand(2*tand(phi)/3) % adjusted internal friction angle local failure  
Ku = 0.5-0.01*phi;   % sinkage coefficient Original IF  
%Ku = 0.5-0.01*phix; % sinkage coefficient modified IF
```

### Calculating Sinkage

```
z(1) = 10;           % initial assumption sinkage (mm)  
Lid(1) = 2*(D*z(1)-z(1)^2)^(1/2) % subsequent contact length (mm)  
A(1) = b*Lid(1);    % subsequent plate area (mm)  
  
for i = 2:10  
    z(i) = Ku*(A(i-1))^(1/2) % ultimate sinkage (mm)  
    Lid(i) = 2*(D*z(i)-z(i)^2)^(1/2) % contact length depending on sinkage (mm)  
    A(i) = b*Lid(i); % Plate area (mm)  
end
```

### Original Internal Friction Angle

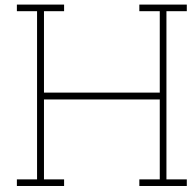
```
z = 4.7513
```

```
Lid = 32.9450
```

### Modified Internal Friction Angle

```
z = 8.0084
```

```
Lid = 41.5338
```



# Terzaghi's shear failure surface calculations

## Constants

```
phi = 31.49;           % Internal friction coefficient simulant (deg)
%phi = atand(2*tand(phi)/3); % Modified internal friction coefficient (deg)
b = 0.02;             % Width of leg (m)
Li = 0.032945;       % Contact Length (m)
%Li = 0.0415338     % Modified contact length
```

## Log spiral method

```
r0f = (Li/2)/(cosd(phi));           % log spiral (Li)
r2f = r0f*exp((((135 - (phi/2))*pi/180))*tand(phi))*100; % length of r at 45 - phi/2
(Li)
wf = 2*r2f*cosd(45-(phi/2));       % width of passive zone in
front of leg (Li)

r0s = (b/2)/(cosd(phi));           % log spiral method (b)
r2s = r0s*exp((((135 - (phi/2))*pi/180))*tand(phi))*100; % length of r at 45 - phi/2
(b)
ws = 2*r2s*cosd(45-(phi/2)) ;     % width of passive zone in
front of leg (b)
```

## Sandbox minimum size

```
lz = 33.5;           % length of zebro
wz = 27.0;           % width of Zebro
st = lz*2;           % length for zebro to walk it's own length

lb = st+ (2*wf);
wb = wz + (2*ws);

%fprintf('Min located at %0.2f\n',y(idx))
fprintf('Min length of sandbox %0.2f cm\n', lb);
fprintf('Min width of sandbox %0.2f cm\n', wb);
```

## Terzaghi Zones

```

phit = phi*pi/180; %internal friction angle (rad)
xc = r0f*cos(phit)*100; % log spiral centre x-cord
yc = r0f*sin(phit)*100; % log spiral centre y-cord

td = ((135 + (phi/2))*pi/180); % angle where passive zone begins (rad)
xb = -(((Li/2)/(cosd(phi)) *exp((td - phit)*tand(phi))*100).*...
      (cos(phit+(td-phit)))); % x-cord start of passive zone on log spiral
yb = -(((Li/2)/(cosd(phi)) *exp((td - phit)*tand(phi))*100).*...
      (sin(phit+(td-phit)))); % y-cordstart of passive zone on log spiral

t = [phit:0.00001:(td)]; % range of angles to create log spiral
x = -(((Li/2)/(cosd(phi)) *exp((t - phit)*tand(phi))*100).*...
      (cos(phit+(t-phit)))); % x-cord on log spiral
y = -(((Li/2)/(cosd(phi)) *exp((t - phit)*tand(phi))*100).*...
      (sin(phit+(t-phit)))); % y-cord on log spiral
idx = islocalmin(y);

figure;
hold on
plot(x,y) % Terzaghi plot
plot([0,-xc], [0,-yc], 'r')
plot([0,-2*xc], [0,0], 'r')
plot([-2*xc,-xc], [0,-yc], 'r')
plot([0,xb], [0,yb], 'g')
plot([0,2*xb], [0,0], 'g')
plot([xb,2*xb], [yb,0], 'g')
plot(x(idx),y(idx), '*r')

title('Terzaghi plot across length of foot')
xlabel('x-coordinate (cm)')
ylabel('y-coordinate (cm)')

fprintf('Min located at %0.2f\n',y(idx))

```

## Terzaghi Zones

```

phit = phi*pi/180;                %internal friction angle (rad)
xc = r0s*cos(phit)*100;          % log spiral centre x-cord
yc = r0s*sin(phit)*100;          % log spiral centre y-cord

td = ((135 + (phi/2))*pi/180);    % angle where passive zone begins (rad)
xb = -(((b/2)/(cosd(phi)) *exp((td - phit)*tand(phi))*100).*...
      (cos(phit+(td-phit))));      % x-cord start of passive zone on log spiral
yb = -(((b/2)/(cosd(phi)) *exp((td - phit)*tand(phi))*100).*...
      (sin(phit+(td-phit))));      % y-cordstart of passive zone on log spiral

t = [phit:0.00001:(td)];          % range of angles to create log spiral
x = -(((b/2)/(cosd(phi)) *exp((t - phit)*tand(phi))*100).*...
      (cos(phit+(t-phit))));      % x-cord on log spiral
y = -(((b/2)/(cosd(phi)) *exp((t - phit)*tand(phi))*100).*...
      (sin(phit+(t-phit))));      % y-cord on log spiral
idx = islocalmin(y);

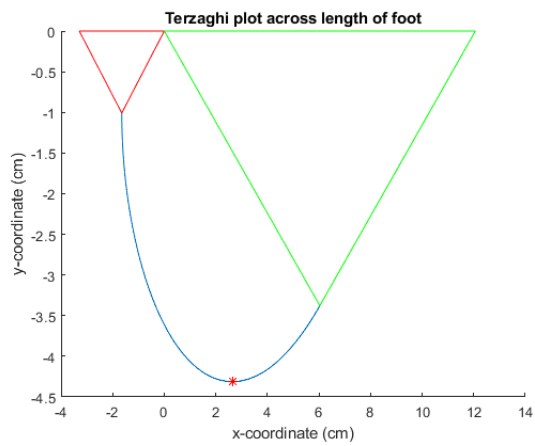
figure;
hold on
plot(x,y)                          % Terzaghi plot
plot([0,-xc], [0,-yc], 'r')
plot([0,-2*xc], [0,0], 'r')
plot([-2*xc,-xc], [0,-yc], 'r')
plot([0,xb], [0,yb], 'g')
plot([0,2*xb], [0,0], 'g')
plot([xb,2*xb], [yb,0], 'g')
plot(x(idx),y(idx),'*r')

title('Terzaghi plot across width of foot')
xlabel('x-coordinate (cm)')
ylabel('y-coordinate (cm)')

fprintf('Min located at %0.2f\n',y(idx))

```

## Original Internal Friction Results



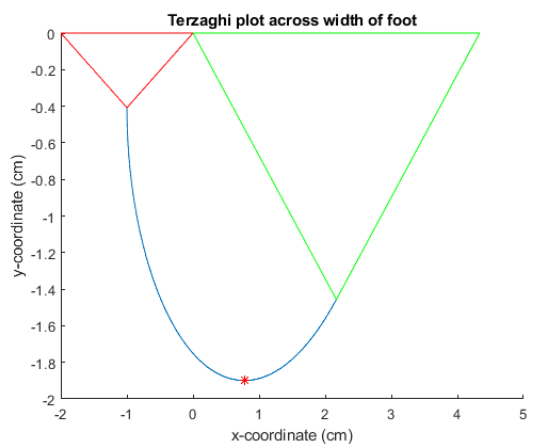
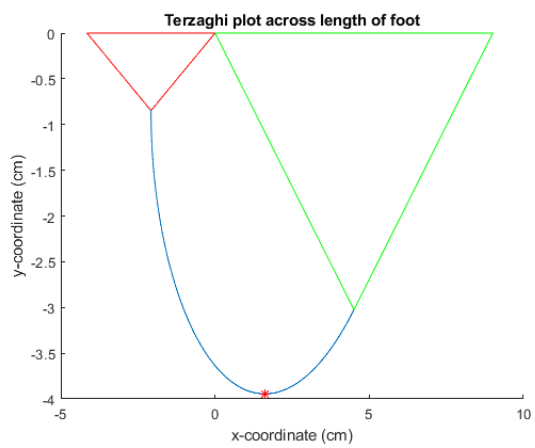
Min length of sandbox 91.12 cm

Min width of sandbox 41.65 cm

Min across length located at -4.31

Min across width located at -2.62

## Modified Internal Friction Results



Min length of sandbox 85.01 cm

Min width of sandbox 35.67 cm

Min across length located at -3.94

Min across width located at -1.90





# Ncorr: Step by Step

## Step 1

1. **Step 1:** The image showing the leg just touching the simulant is added as the reference image and the image showing the fully sunk leg is added as the current image.

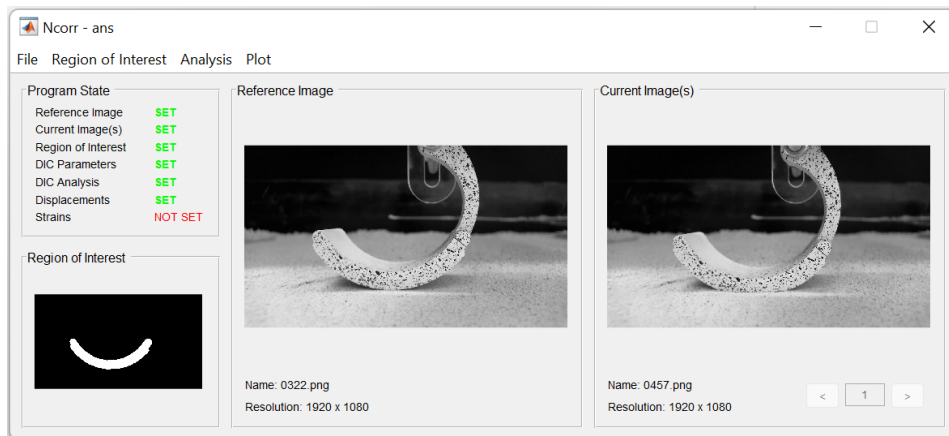


Figure I.1

2. **Step 2:** The Region of interested (ROI) is then drawn onto the reference image. In this case the ROI is the face of the leg closest to the camera.

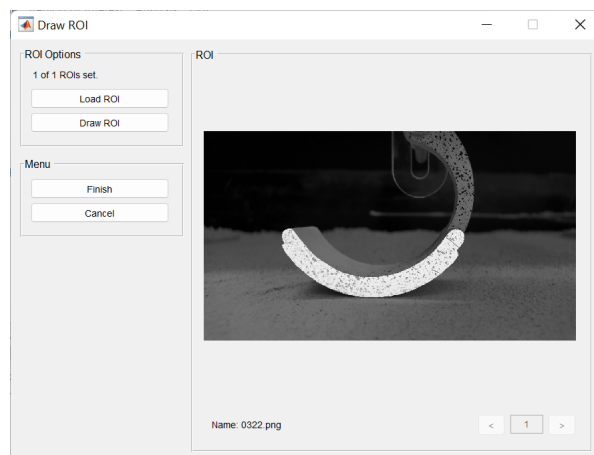


Figure I.2

3. **Step 3:** The DIC parameters are then set using the recommended settings laid out by Ncorr Instruction Manual.

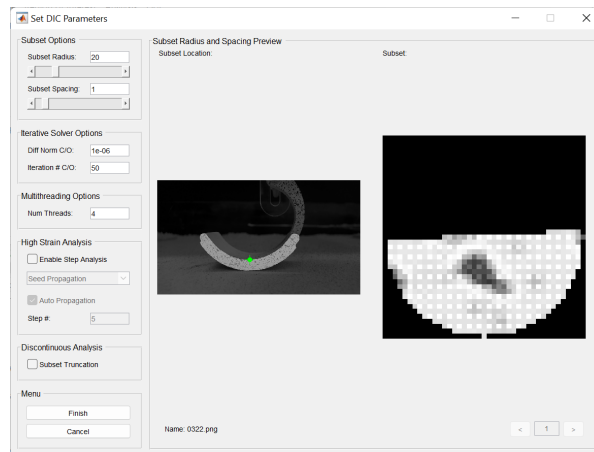


Figure I.3

4. **Step 4:** For the DIC analysis the 4 seeds are set so as to divide the ROI equally.

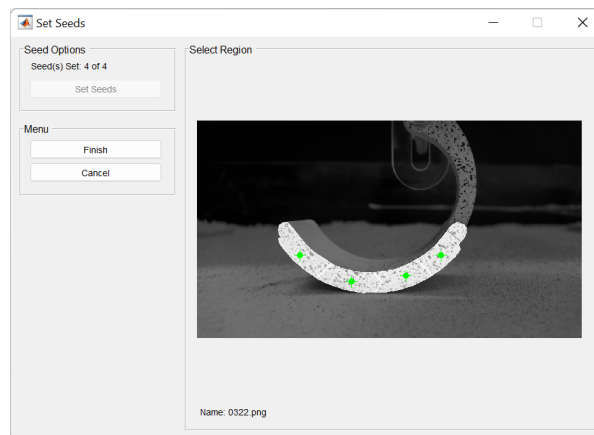


Figure I.4

5. **Step 5:** The Displacement is formatted using the reference image. On each of the legs there is a marker with a known distance (as shown in the table below). This marker is used to determine the dimensions of the pixels which is then used to calculate how much the leg sank into the simulant.

Table I.1: Marker Lengths

Leg	Marker Length (mm)
Original Leg	5.10
Paddle Leg	4.80
Claw Leg	4.80
Flat Leg	4.85
Web Leg	4.55
Hair Leg	4.9

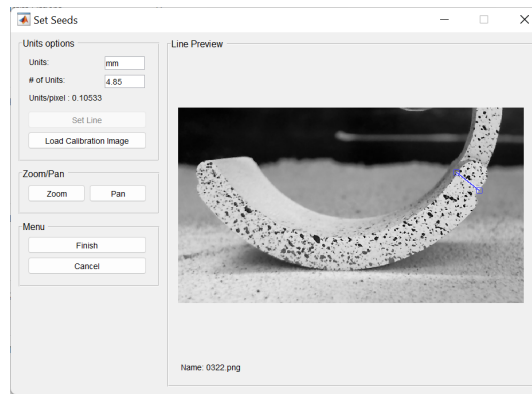


Figure I.5

6. **Step 6:** The displacements are then plotted. From there it is possible to determine the maximum displacements. When the leg sinks into the simulant, it rotates a bit as it settles. this causes the left side of the leg to sink the least and the right side the most. Using the max and min values, it is possible to determine how much the leg sank by averaging them out.

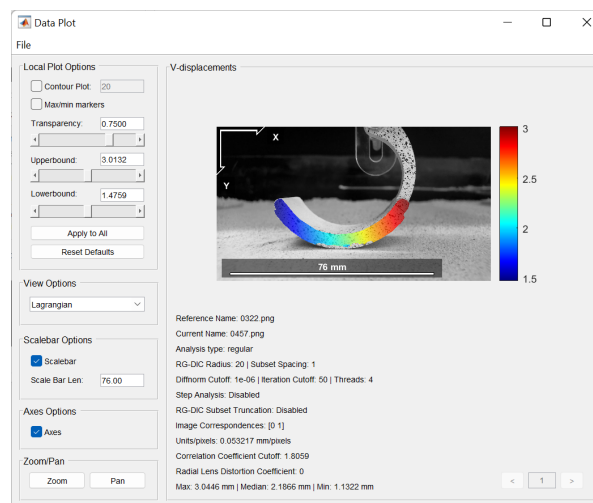


Figure I.6

The max and min spots where chosen as shown below. This was done for consistency across all tests.

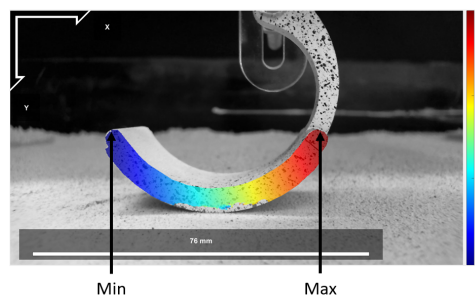


Figure I.7

# J

## Kinovea: Step by step

1. **Step 1:** Add the video to the playback screen
2. **Step 2:** Add a line marker, as shown in orange below, to the slider. This type of marker and location was chosen as the slider is roughly in the same place for each test of each leg. The slider moves the most as it is the point on the pivot. The leg is able to rotate slightly and that is why it does not have the largest displacement.

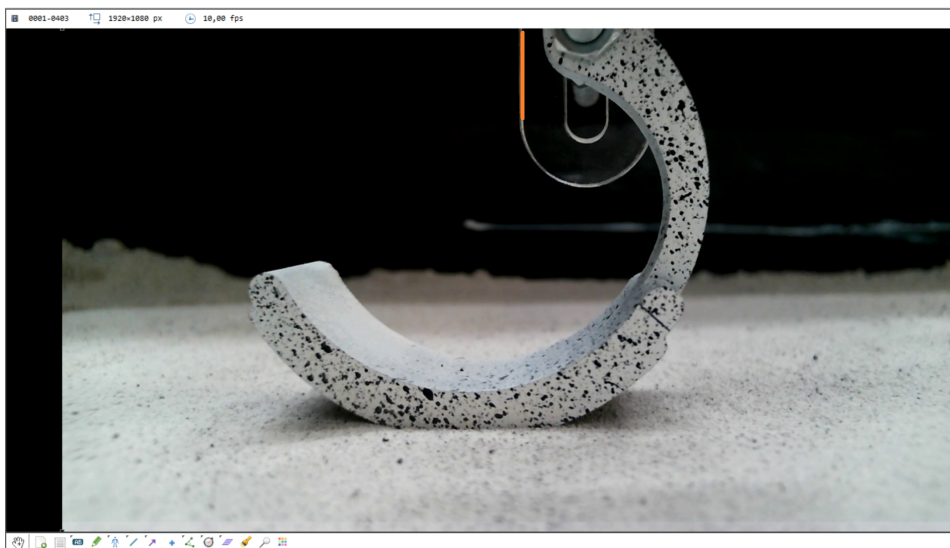


Figure J.1

3. **Step 3:** The program is then run and the relative horizontal displacement graph (shown below) is used to determine the moment the leg moves.

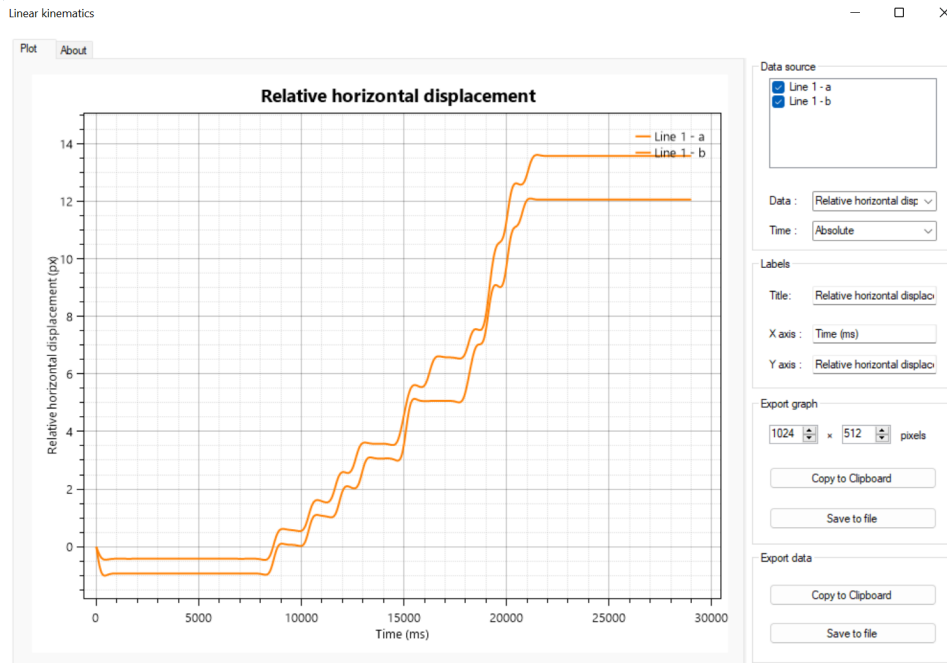


Figure J.2

4. **Step 4:** The time step used to determine the force is chosen to be the value found between the two points indicated in green.

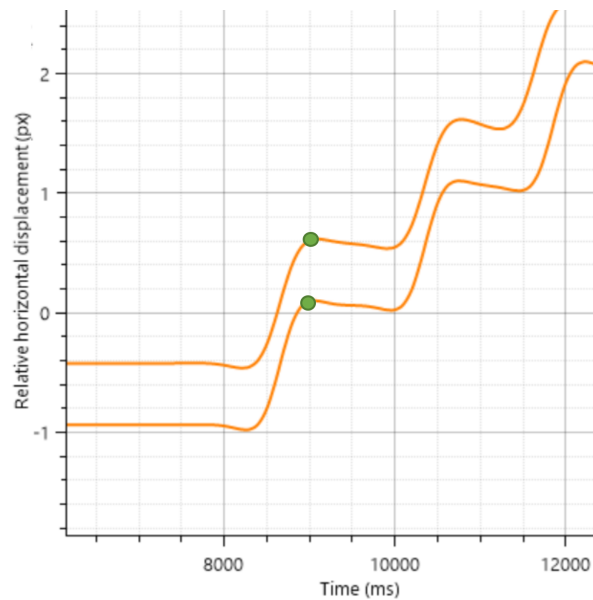
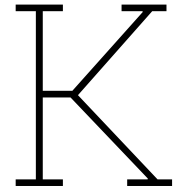


Figure J.3



# Pivot Thrust Results

The results of the pivot thrust experiments on the different terrains are shown below:

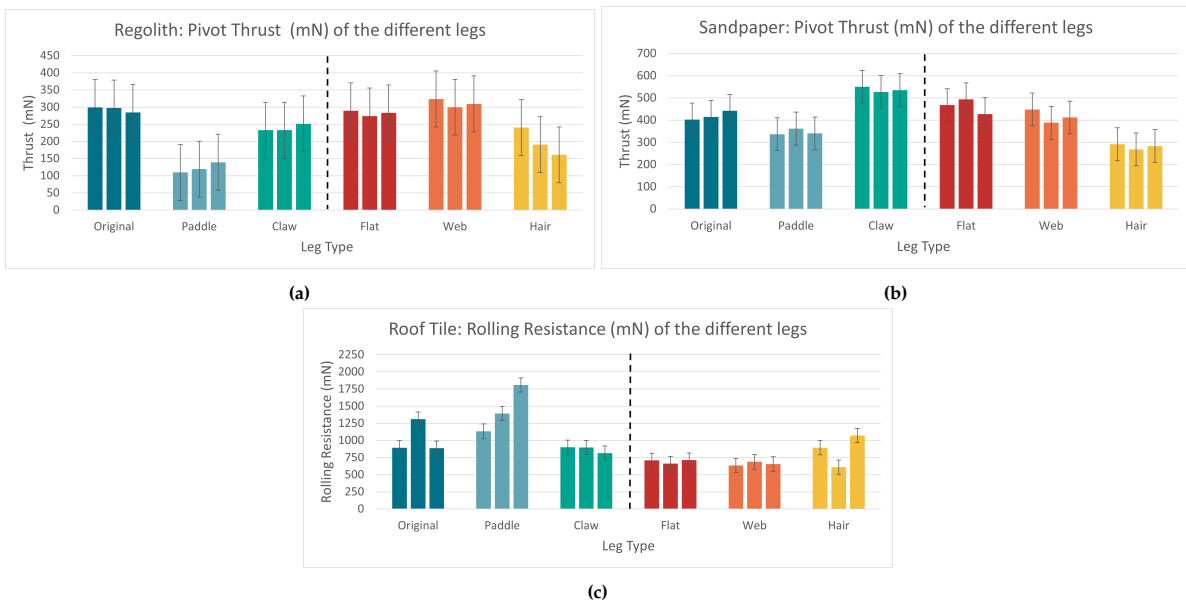


Figure K.1: Results of the Pivot Thrust experiment on: (a) Regolith (b) Sandpaper (c) Roof Tile



# Grouser Calculations

The calculations showing the ideal number of grousers and grouser height based on current leg dimensions are shown below:

## L.1. Grouser Height

```
close all
clear

syms h positive
s = 0.2;           %slip at 20 %
r = 31;           % radius of the leg
z = 2.5;          % approximate sinkage
n = 4;            % number of grousers
phi = (112.4/n) * pi/180; %angle between grousers
eqn = (1/(1-s))*(sqrt((1+h/r)^2 - (1-z/r)^2))-sqrt(1-(1-z/r)^2) - phi==0;
h = double(solve(eqn, h)) % Height of grousrs
```

h =

4.9546

Figure L.1



## L.2. Grouser Number

```
lose all
clear

close all
clear

syms n positive
s = 0.2;           %slip at 20 %
r = 31;           % radius of the leg
z = 2.5;          % approximate sinkage
h = 2.84;         % grouser height
phi = (112.4/n) * pi/180;
eqn = (1/(1-s))*(sqrt((1+h/r)^2 - (1-z/r)^2))-sqrt(1-(1-z/r)^2) - phi==0;
n = double(solve(eqn, n)) %ideal number of grousers
```

n =

5.7315

Figure L.2